MARCH 1961

experimental mechanics

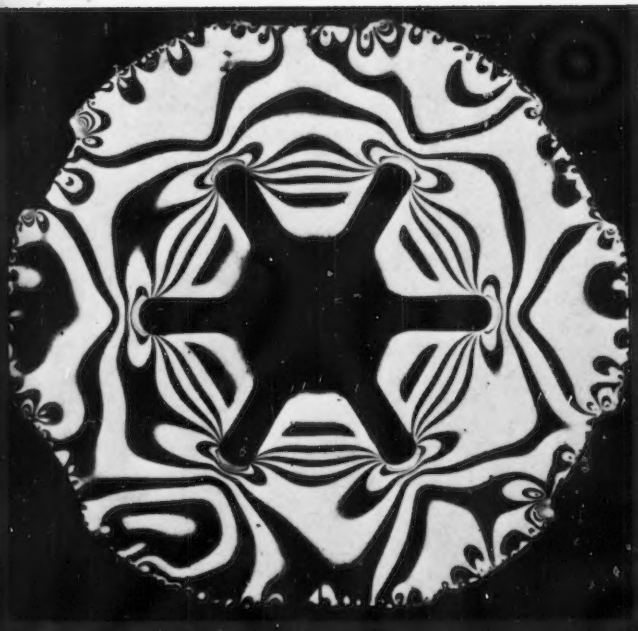

SEE PAGE 88

IN THIS ISSUE

PAGE

65 Photoelastic Strain Gages

74 Effects of the Thickness of Birefringent Coatings

83 Two-dimensional Photoelastic Study of Turbine-shell Flanges

88 Experimental Investigation of the Buckling Instability of Monocoque Shells

97 Photothermoelastic Analysis of Bonded Propellant Grains

SESA JOURNAL OF THE SOCIETY FOR EXPERIMENTAL STRESS ANALYSIS

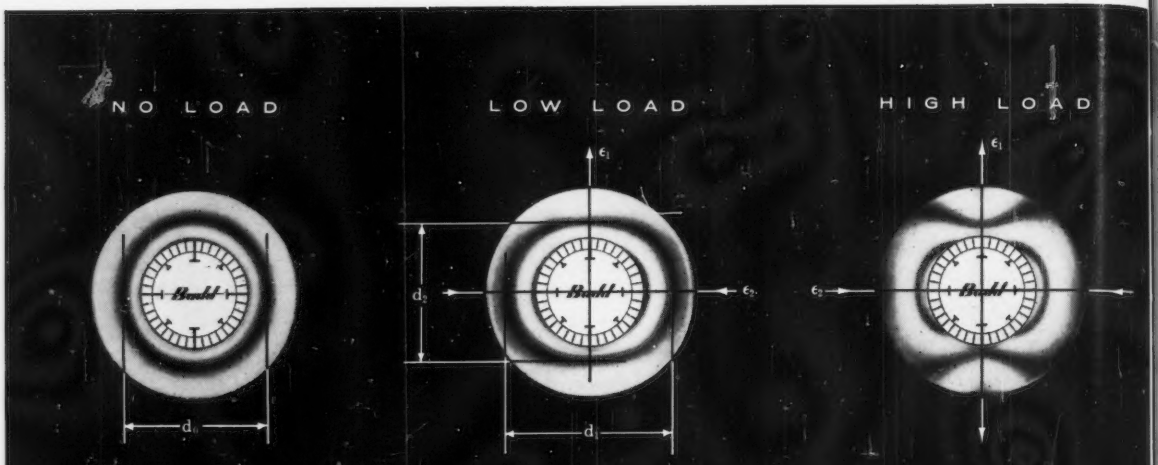

NEW! PhotoStress Rosettes* from Budd

THE ONLY GAGES THAT PROVIDE DIRECTLY BOTH ORIENTATION AND SEPARATE MAGNITUDES OF PRINCIPAL STRAINS

*Developed from original circular photoelastic gage patented in France in 1956 by Dr. G. Golubovic of PhotoStress France, U.S. patent pending.

Gages shown actual size. ϵ_1 and ϵ_2 are principal strains. d_o is diameter of circular fringe for zero strain. d_1-d_o and d_2-d_o give fringe shift along axes of symmetry of patterns, due to strain. Axes of symmetry are principal strain directions. ϵ_1 is a function of d_1-d_o. ϵ_2 is a function of d_2-d_o.

EXCLUSIVE FEATURES:

- Measures principal strain directions for strain levels as low as 50 microinch/inch and up.
- Major and minor principal strain directions obviously apparent.
- Separate magnitudes of strains obtained directly along desired axis.
- High readout sensitivity due to permanent pattern.
- Constant sensitivity for directions and magnitudes for any strain level.
- Proved PhotoStress technique (Zandman method).

GENERAL FEATURES:

- Direct readout, no instruments or connections.
- Static or dynamic (with strobe light) readings.
- Sensitivity and zero stable with time, unaffected by humidity.
- Easily bonded at room temperature to metals, concrete, wood and other materials.

SPECIFICATIONS:

- Directions of principal strains: within ±5° (with care, better accuracies are possible).
- Magnitudes of separate values of principal strains: within ±40 microinch/inch.
- Packaged 5 gages to the package with cement and complete instructions for installation.

LIMITATION:

- Will not perform accurately in areas of high strain gradients. (Use classical PhotoStress or miniature type MetalFilm strain gages.)

WRITE OR CALL FOR FULL INFORMATION OR APPLICATION ASSISTANCE

INSTRUMENTS Budd DIVISION

THE BUDD COMPANY • P.O. Box 245 • Phoenixville, Pa.

Consult your phone book for sales offices in: Atlanta, Ga.; Oak Park, Ill.; Detroit, Mich.; Seattle, Wash.; Dallas, Tex.; Los Angeles, Calif.

In Canada: Budd Instruments, Ltd., 170 Donway West, Don Mills, Ont.

Other countries: Budd S.A., 10 Avenue de la Grande Armée, Paris 17e, France

For details, circle No. 1 on Reader Information Card

AL OF THE SOCIETY FOR EXPERIMENTAL STRESS ANALYSIS

experimental mechanics

VOLUME 1 • NUMBER 3 • MARCH 1961

editor	**B. E. Rossi**
asst. editor	**C. H. Willer**
advertising	**D. L. Vidmark**
art	**Gil Miller**

OFFICERS AND EXECUTIVE COMMITTEE

D. C. Drucker *president*
I. Vigness *vice-president*
W. W. Soroka *vice-president*
W. M. Murray *treasurer*
B. E. Rossi *executive secretary*
F. C. Bailey
B. J. Lazan
J. C. New
C. E. Taylor
E. Wenk, Jr.

JOURNAL ADVISORY COMMITTEE

E. Wenk, Jr. *chairman*
D. C. Drucker
R. Guernsey, Jr.
B. J. Lazan
W. M. Murray
C. C. Perry
F. B. Stern, Jr.
I. Vigness

lished monthly by the Society for Experimental Stress Analysis. blication office, 20th and Northampton Streets, Easton, Pa. Editorial d general offices, 21 Bridge Square, Westport, Conn. Subscription 5.00 per year in the United States and possessions; foreign countries 7.00. Single copies, nonmembers $1.50; members $1.00. Application r mail at second-class postage rates is pending at Easton, Pa.
pyright 1961 by the Society for Experimental Stress Analysis. The ciety is not responsible for any statement made or opinion ex-essed in its publications. Permission is given to reprint any article er its date of publicaton provided credit is given.

this month

TABLE OF CONTENTS

page

65 Photoelastic Strain Gages
by G. U. Oppel

74 Effects of the Thickness of Birefringent Coatings
by J. Duffy

83 Two-dimensional Photoelastic Study of Turbine-shell Flanges
by P. D. Flynn

88 Experimental Investigation of the Buckling Instability of Monocoque Shells
by R. H. Homewood, A. C. Brine and Aldie E. Johnson, Jr.

97 Photothermoelastic Analysis of Bonded Propellant Grains
by I. M. Daniel and A. J. Durelli

3A Experimentally Speaking

4A Tracking Station

6A Personnel in the News

8A New Products

14A New Literature

17A Reader Information Card

18A Index to Advertisers

19A SESA News

22A Section Reports

25A From the Campus

26A Reference Notebook

Strain Gage Techniques

APRIL 17 - 21, 1961

(Monday through Friday)

A Short Intensive Course at the SOUTHWEST RESEARCH INSTITUTE, San Antonio, Texas

Under the Joint Sponsorship of the Society for Experimental Stress Analysis

★ ★ ★

The Program

The program will consist of a series of illustrated lectures which have been arranged to present a broad picture of the theoretical and practical considerations involved in solving industrial problems. Special attention will be paid to high- and low-temperature applications. The lectures have been coordinated to provide an integrated course of instruction dealing with the theory of the strain gage, applied-mechanics aspects of its uses, electric circuits required, instruments, practical techniques employed, and methods for providing automatic computation (direct measurement) of quantities which depend upon the simultaneous observation of strains at several different locations.

Topics to be discussed will include the following.

Basic theory of the wire-resistance strain gage
Semiconductor Gages
Details of gage characteristics
Temperature effects in strain gages
Evaluation of strain gages
Strain-gage installation at normal temperatures
Mechanical and electrical aspects of the gage system
Electric circuits for strain gages
Dynamic and static strain measurements
Computing bridge circuits for direct measurement of quantities depending upon more than one strain
Stresscoat as an auxiliary tool
Measuring systems and instruments
High-temperature strain gages and their installation
Commercial equipment
Rosette analysis and interpretation of observations

Lecturers

W. T. BEAN, JR., *Consulting Engineer*
Detroit, Michigan

W. M. MURRAY, *Professor of Mechanical Engineering*
Massachusetts Institute of Technology
Cambridge, Massachusetts

P. K. STEIN, *Associate Professor of Engineering*
Arizona State University, Tempe, Arizona
Editor, Strain Gage Readings

C. O. VOGT, *Project Engineer*
Century Electronics & Instruments, Inc.
Tulsa, Oklahoma

L. J. WEYMOUTH, *Manager, Strain Gage Application*
Electronics & Instrumentation Division
Baldwin-Lima-Hamilton Corporation
Waltham, Massachusetts

For Whom Intended

This series of lectures has been prepared for the dual purpose of presenting a review of some of the most advanced techniques while at the same time including elementary and fundamental information necessary for the novice who wishes to commence work with strain gages. Each registrant will be provided with a specially prepared set of notes covering the fundamentals.

The program is directed towards laboratory workers, supervisors, designers, metallurgists, theoretical stress analysts, and others who may be interested in obtaining an insight into the operation of the strain gage and the instrumentation associated with it. The academic level is suitable for those with a Bachelor's (or higher) degree in engineering, physics, or metallurgy; however, in certain cases, experienced technicians without degrees can be expected to gain full benefit from the program.

Although the lectures have been prepared largely from the point of view of the mechanical engineer, the topics to be discussed have been selected to provide maximum benefit for those who are already skilled in stress analysis but who possess little experience in electrical instrumentation, and for the electronic experts, who may not be so familiar with the various aspects of stress analysis.

Supplementary Laboratory

For those who desire laboratory work, a separate supplementary program of four sessions can be arranged. (This will only be available to those who register for the lectures.)

Tuition

The tuition per registrant, due and payable in advance to the Southwest Research Institute, will be as follows:

Lecture Program (Alone) . . .	$175.00
Laboratory (Additional) . . .	$100.00
Total for both	$275.00

All applications should be received, and tuition paid, not later than April 10th.

In the event that too few applications are received, the right to cancel the program is reserved.

All Inquiries and Correspondence Should Be Addressed to
Dr. M. M. Lemcoe, Southwest Research Institute, 8500 Culebra Road,
San Antonio 6, Texas

Experimentally Speaking

THE SUM OF THE PARTS

Science and technology, while always a potent factor in our national economy and welfare, have now dramatically emerged to manifest an unprecedented and profound impact on our national security. Not only has scientific achievement itself become an instrument of public policy, with a correspondingly dynamic interplay with political affairs, the quickening pace and expanding scope of technological change have also become significant. More numerous and elaborate research and development programs are being generated, more scientists and engineers are participating, and more private and public institutions have become sponsors. While this sensation of growth is often the subject of comment, the full dimensions and implications of this effort are seldom recognized.

The national budget for R & D now amounts to $13 billion annually, having tripled in just the past ten years. Of this amount, the Federal Government's share for Fiscal Year 1961 will be $8.52 billion, representing over 10% of Federal obligations. In fact, more Federal funds will be spent for science this year than were spent during the entire 169 years from this country's founding through World War II. Corresponding to this support, roughly 160,000 separate R & D tasks will be performed by 360,000 scientists and engineers, in more than 8000 separate establishments. Underscoring this growth in numbers of participants, 80% of those scientists and engineers who have ever lived throughout recorded history are alive today!

With such a maze of interlocking elements, the individual investigator, usually operating in the lower hierarchical echelons of a research organization, can hardly be aware of how massive and complex is this R & D phenomenon. Yet, the scientific contribution of each individual represents an important step toward progress through an aggregation and systematic arrangement of these separate bits and pieces of new knowledge. New information is thus the basic quest and the product of this enormous human activity. The health and vigor of science, and the success with which we compete in a tense international atmosphere place a premium on the effectiveness with which scientific information is developed, screened, disseminated, indexed, abstracted and, finally, used.

It is in this context that the *Journal*, EXPERIMENTAL MECHANICS, may contribute to the flow of information in the multidisciplinary regime that the term "experimental mechanics" implies—a flow that represents the very life blood of science itself.

Edward Wenk, Jr.

CHAIRMAN, JOURNAL ADVISORY COMMITTEE

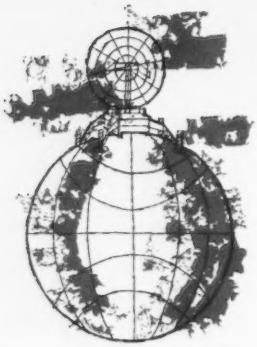

tracking station

the industry in focus

Convair Moves Test-equipment Plant

Convair Division of General Dynamics Corp. has moved its Dynapak facility from Pomona to San Diego. The facility manufactures high-energy-rate metal-forming machines and a line of advanced mechanical test equipment.

Production of Dynapak's machines will be done in an 18,000-sq-ft hangar structure at the seaplane ramp along Harbor Drive.

The move was reportedly made to give Dynapak the added advantage of existing facilities at Convair-San Diego, where up-to-date test equipment and refined data-computing systems will expedite Dynapak's research and development on new high-energy-rate metal-forming devices as well as its work in shock simulation and dynamics loading fields.

Instrumentation Growth Forecast

The U. S. instrumentation industry, which posted record sales during 1960 despite an economic downturn, can look forward in 1961 to continuing growth, according to a prediction by James S. Locke, vice president of Minneapolis-Honeywell Regulator Co.

The extent of this growth will depend on decisions management and government make in the next six months, Mr. Locke explained in a year-end review of instrumentation industry trends.

Centaur in Final Assembly

The booster stage for NASA's Centaur launch vehicle has entered final assembly at the San Diego plant of Convair (Astronautics) Division of General Dynamics Corp. The booster airframe, just beyond the missile in the foreground, is identical to the Air Force Atlas missiles in adjoining docks, except that it is of constant 10-ft diameter, not tapered at forward end. NASA plans to launch the first Centaur flight at Atlantic Missile Range in mid-1961

Research Laboratories Relocated

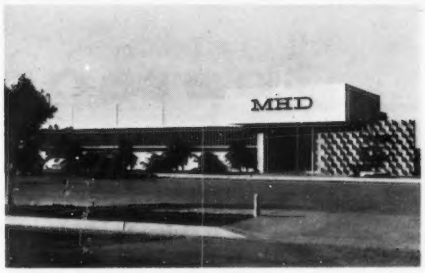

M H D Research, Inc., Newport Beach, Calif., is moving its general offices and primary research laboratories into a new, 10,000-sq ft plant, located at 1535 Monrovia Ave., Newport Beach, according to Donald F. Howard, corporation president. The new facility became essential with the expanded research and development activities in the fields of magnetohydrodynamics, chemical processing, energy conversion, electric propulsion and plasma-jet wind tunnels in which the corporation is engaged.

Automation Purchases Amco Stock

Automation Industries, Inc., Manhattan Beach, Calif., manufacturer of ultrasonic, electronic and magnetic products, recently announced acquisition of Amco Incorporated of Abilene, Tex., an integrated fabricator of aircraft and missile components.

Terms of the acquisition were not disclosed, but Automation President Corwin D. Denney stated that it was accomplished without dilution of equity.

Amco sales during the past 12 months were approximately $750,000. Plant assets are valued at $500,000, and inventory at an additional $250,000. Denney stated that in addition to Amco's $1,000,000 backlog, additional awards of approximately $250,000 are anticipated.

FUTURE MEETINGS

SESA

MAY 10–12. Spring Meeting. Benjamin Franklin Hotel, Philadelphia, Pa.

NOVEMBER 1–3. First International Congress on Experimental Mechanics. Hotel New Yorker, New York, N. Y.

Related Conference:

OCTOBER 29–31. International Symposium on Photoelasticity. Illinois Institute of Technology, Chicago, Ill.

AIP

MARCH 27–31. Symposium of American Institute of Physics. National Symposium on Temperature—Its Measurement and Control in Science and Industry. Columbus, Ohio.

ARS

APRIL 5–7. Conference of the American Rocket Society. Lifting Re-entry Vehicles: Structures, Materials, Design. Palm Springs, Calif.

ASME

JUNE 14–16. Conference of American Society of Mechanical Engineers. Applied Mechanics Conference. Illinois Institute of Technology, Chicago, Ill.

ASTM

JUNE 25–30. Annual Meeting of American Society for Testing Materials. Chalfonte-Haddon Hall, Atlantic City, N. J.

IES

APRIL 5–7. Annual Technical Meeting and Equipment Exposition. Institute of Environmental Sciences. Sheraton Park Hotel, Washington, D. C.

ISA

APRIL 17–19. Symposium on Instrumental Methods of Analysis. Instrument Society of America. Shamrock Hilton Hotel, Houston, Tex.

personnel
in the news

JOHNSON MADE MANAGER

The Systems Division of Beckman Instruments, Inc., Anaheim, Calif., announces the centralization of all customer services activities—field service, technical training, factory maintenance, spare parts provisioning and contracts administration—under a single manager, and the appointment of Arthur R. J. Johnson to this new post.

Frank J. Scheufele, division marketing manager, said the move will enable Beckman to provide better, more efficient service to the company's data processing equipment customers. Mr. Johnson will view service problems from the customers' standpoint, and will, in effect, be the customers' representative within Beckman, Mr. Scheufele said.

ZOPF JOINS BORG-WARNER

David Zopf has joined the Meteorology/Oceanography Systems Engineering group of Borg-Warner Controls. Announcement of the appointment was made by Eugene Bollay, head of this Santa Barbara-based group.

Mr. Zopf will be responsible for systems engineering required for large meteorological and oceanographic data-gathering networks, Mr. Bollay said. Research and development of advanced meteorological and oceanographic instrumentation will also be pursued as required by the demands of systems now under study.

According to Mr. Bollay, the new appointment reflects the increasing scope of meteorological projects undertaken by Borg-Warner Controls, for which the Meteorology/Oceanography group in Santa Barbara performs essential study and research functions.

Mr. Zopf was formerly with the Aerophysics Development Corp. and Curtiss-Wright, where he was section head for Guidance and Control in the Electronics Department. Other employment affiliations include Bell Aircraft Corp., Pt. Mugu (Calif.), where he was in charge of missile guidance systems activities, and Boeing Aircraft Co., as a member of the physical research staff.

He holds B.S., M.S. and E.E. degrees in electrical engineering from Stanford University.

JONCICH NAMED VICE-PRESIDENT

Michael J. Joncich, general sales manager of Datex Corp., has been elected vice-president by the board of directors. Joncich has been with Datex since 1953 as sales engineer, regional sales manager and assistant sales manager. He became general sales manager last January.

Mr. Joncich received his B.S.E.E. from the University of California in 1950. Before coming with Datex he was a sales engineer with Minneapolis-Honeywell and California Electric Power Co.

CARR TO HEAD HUGHES DIVISION

Robert E. Carr has been named manager of rectifier operations for Hughes Aircraft Co.'s semiconductor division, David A. Hill, division manager, recently announced.

Mr. Carr will direct development and production of a complete line of advanced medium power rectifiers with military-approved specifications as part of an over-all technical program emphasizing silicon rectifier product stability, reliability and competitive pricing.

Before joining Hughes, Mr. Carr worked in General Electric's advanced development projects and rectifier department. Previously he managed the silicon division of Bradley Semiconductor Corp., New Haven, Conn. He received a master's degree in mechanical engineering from Carnegie Institute of Technology.

BECK ASSISTANT AT ARMOUR

Niels C. Beck, has been appointed assistant director at Armour Research Foundation, Dr. Haldon A. Leedy, ARF director, announced recently.

Mr. Beck succeeds Dr. Christopher E. Barthel, Jr. who has resigned to become program director for international activities of the National Science Foundation, Washington, D.C.

Mr. Beck has served as director general of the Union of Burma Applied Research Institute, an ARF project, for the past four years. He became associated with the Foundation in 1953 as a staff member of the program development office, and later served as acting manager of it.

He is a former dean of Parks College, St. Louis University. A native of Denver, Colo., he received his A.B. and B.S. degrees in chemistry at Regis College, and did graduate work in geophysics at St. Louis University. He and his wife and two sons reside in Chicago.

WYCKOFF APPOINTED BY ARMOUR RESEARCH

Peter H. Wyckoff has been appointed assistant director of physics research at Armour Research Foundation.

For the past 15 years, Mr. Wyckoff has been chief of the aerophysics laboratory at Air Force Cambridge Research Center, Bedford, Mass. He served as chief scientist for the Air Force International Geophysical Year rocket program at Fort Churchill, and in 1956 successfully directed the launching of the first Aerobee and first Nike Cajun rocket launched from Canadian soil. Currently he is a member of the executive committee of the Rocket and Satellite Research Panel, and a former member of the U. S. Civil Service Board of Examiners.

Mr. Wyckoff received a B.S. degree in electrical engineering at the Carnegie Institute of Technology and his master's in electrical engineering at California Institute of Technology. He also did graduate work in nuclear physics at the University of Pittsburgh.

ROSEN TAKES DATEX POST

Mark Rosen, formerly chief engineer at U. S. Relay-Electronics and earlier development engineer with two English firms, has joined Datex Corp., Monrovia, Calif., as development engineer and will report to Electronic Products section head, Carr Wilson.

Mr. Rosen received his B.Sc. in Engineering and B.Sc. in Mathematics and Logic from London University. He is presently completing requirements for his master's degree in Electrical Engineering at UCLA.

Mr. Rosen's experience in the design of magnetic components, magnetic circuits and logical design will be applied to related product development at Datex.

SOCIETY FOR EXPERIMENTAL STRESS ANALYSIS
21 Bridge Square, Westport, Connecticut

SESA PUBLICATIONS

PROCEEDINGS OF THE SOCIETY FOR EXPERIMENTAL STRESS ANALYSIS

The PROCEEDINGS are a series of bound volumes comprised of the technical papers presented at National Meetings. These contain the results and descriptions of analytical and experimental investigations, as well as techniques for the measurement of mechanical strain. Published twice annually, they include up-to-date information on various phases of instrumentation. Currently available:

Volume III, No. 2
Volume IV, No. 1
Volume IV, No. 2
Volume V, No. 1
Volume XI, No. 2
Volume XII, No. 1
Volume XII, No. 2
Volume XIII, No. 1 (limited)
Volume XIII, No. 2 (limited)
Volume XV, No. 2
Volume XVI, No. 2
Volume XVII, No. 1
Volume XVII, No. 2

CUMULATIVE INDEX—PROCEEDINGS

Thirty-four books of the PROCEEDINGS have been published to date. This Index has been prepared to serve as an easy reference to any one of the 546 papers which have been published in the first thirty books. It consists of three parts: (1) chronological index, (2) author index, (3) topical index. It represents a "master reference file" to all PROCEEDINGS published, from Vol. I, No. 1 through Vol. XV, No. 2.

HANDBOOK OF EXPERIMENTAL STRESS ANALYSIS

This book opens with a thorough presentation of mechanical properties. It presents practical, usable information on: mechanical, electrical and optical gages, brittle coatings, photoelasticity, X-rays, service fractures, analogies, vibration measurements, theory of elasticity and precision of measurements. Stiff cloth binding—contains 1060 pages of text.

MANUAL ON EXPERIMENTAL STRESS ANALYSIS TECHNIQUES

For those who are new to the field of experimental stress analysis, the MANUAL introduces the fundamentals of experimental stress analysis in terms easily understood by the novice. It contains detailed instructions and, with the aid of illustrations and charts, elaborates on the application of three particular methods for determining stress: (1) SR-4 bonded wire strain gages, (2) Stresscoat (brittle lacquer) and (3) photoelasticity.

STRAIN GAGE TECHNIQUES

Twenty-three chapters of lectures and laboratory experiments of special summer programs presented at leading universities, covering such topics as: fundamental concepts, selection of gages, basic considerations in strain-gage instrumentation, electrical and mechanical aspects of the gage system, the potentiometric circuit, the wheatstone bridge, amplitude modulation, fundamentals of measuring systems, some commercial systems and rosette analysis. Approximately 680 pages.

CATALOG OF EQUIPMENT USED IN EXPERIMENTAL STRESS ANALYSIS

The Catalog contains references to manufacturers of equipment, hardware and instrumentation used in the measurement of strain.

EXPERIMENTAL MECHANICS

Official monthly journal of the SESA. Includes technical papers and news items of interest to SESA members and to industry.

ORDER FORM

Publication	Author/s or Editor/s	Members' Price	Bulk Orders*	Price per Copy (Non members)	Postage and Handling (Add for Each Copy) U. S.	Foreign	State Volume Number	Specify Quantity	Total
Proceedings of the Society for Experimental Stress Analysis	Mahlmann, CV and Murray, WM	$ 6.00	$ 6.00	$ 7.00	25¢	50¢	_____	_____	$_____
Handbook of Experimental Stress Analysis	Hetenyi, M.	16.75	15.75	17.75	Included	85¢		_____	$_____
Manual on Experimental Stress Analysis Techniques	Perry, CC and Bean, WT	2.00	1.25	3.00	Included	10¢		_____	$_____
Strain Gage Techniques	Murray, WM and Stein, PK	12.00	12.00	13.00	Included	85¢		_____	$_____
Catalog of Equipment	Hofmeister, WF	2.00	1.25	3.00	Included	10¢		_____	$_____
Cumulative Index		2.00	1.25	3.00	Included	10¢		_____	$_____
EXPERIMENTAL MECHANICS**	Monthly Journal	1.00		1.50	Included	20¢		_____	$_____

*Bulk Orders—10 or more copies of a *single book* (for *PROCEEDINGS*—10 or more copies of a single volume and number).
**Annual Subscription (including postage)—Domestic, $10; Foreign, $12.

Send books to:

_____
_____
_____
_____

Send bill to:

_____
_____
_____
_____

Total.....$_____
Remittance Enclosed ☐ Bill me ☐
PAYMENT MUST ACCOMPANY ORDERS FOR LESS THAN $5.00
Order Number_____
Order Issued by_____
Date_____

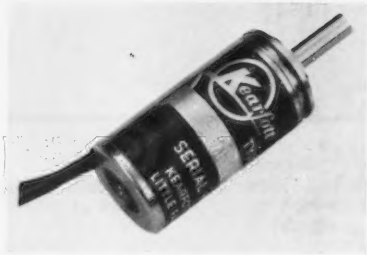

MINIATURE SERVO MOTOR

Kearfott Division, General Precision, Inc., 1150 McBride Ave., Little Falls, N. J., has announced the addition of the J126-06 miniature servo motor to its line of precision components. This high-torque, low-inertia unit has the added advantages of small size and light weight. Only $^1/_2$ in. in diameter and 0.968 in. long, the J126-06 is designed for use in servo systems where instant response is a requirement. This unit is available in a variety of shaft configurations and the control phase is designed specifically for operation by transistorized servo amplifiers such as the Kearfott A3105-02. **61**

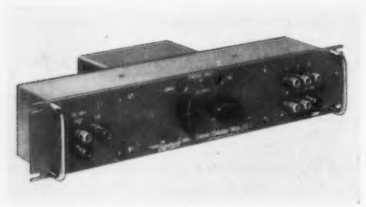

SYNCHRO STANDARDS

A new series of highly accurate test standards designed to simulate the output of a master synchro is announced by Gertsch Products, Inc., 3211 S. La Cienega Blvd., Los Angeles 16, Calif.

These standards, when driven by a suitable signal source, provide stator outputs S_1, S_2 and S_3 corresponding to the outputs of a master synchro as the shaft is rotated in 5-deg increments. Quadrant switching is provided to simulate operation over a full 360 deg.

Designated as Models SS-1, 2 and 3, units feature a low effective series impedance which permits the output to be loaded without introducing stator-output errors. Ratio accuracy is 10 ppm, equivalent to 2 sec of arc absolute angular accuracy, according to manufacturer. **62**

SINGLE-TURN A-C POT

The first of a series of precision potentiometers for a-c excited circuits is now being produced by Helipot Division of Beckman Instruments, Inc., 2500 Fullerton Rd., Fullerton, Calif.

The new a-c pot, a 3-in. diam single-turn designated Model 5803, is reported to be a major improvement over the use of conventional potentiometers in a-c applications. It has high input impedance and low output impedance, thereby substantially reducing quadrature and loading effects. A new design concept also minimizes the chance of catastrophic failure, and provides exceptional linearity that is stable over the entire life of the unit, according to the manufacturer. **63**

A-C/D-C CONVERTER

Non-Linear Systems, Inc., Del Mar, Calif., announces that automatic selection of a-c voltage range is now available with its Model 125E a-c/d-c converter for use with digital voltmeters.

For instance, with an NLS M24 (premium digital volt-ohmmeter), the Model 125E can be used for automatic data logging and system testing jobs where a wide range of a-c voltages are being measured.

Used with a digital voltmeter, the 125E automatically selects the proper range and the instruments display readings of four digits. The input voltage range is 1 mv to 1000 v, in steps of 9.999/99.99/999.9 volts a-c, the manufacturer reports. **65**

new products

For more details regarding these products, circle item number on Reader Information Card.

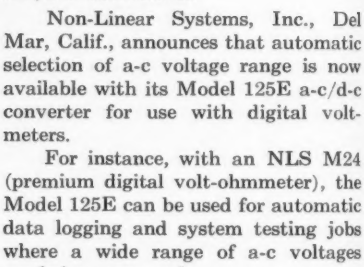

THREE-WAY VACUUM VALVE

A reduction of shutdown time and more positive switching action are said to be the key features of a new three-way vacuum valve now being made for high-vacuum systems by Central Scientific, a division of Cenco Instruments Corp., 1700 Irving Park Rd., Chicago 13, Ill.

This valve is designed to be the master control in a high-vacuum system using a diffusion pump and a mechanical fore pump. It replaces

ALL-METAL DELAY LINES

Helipot Division of Beckman Instruments, Inc., 2500 Fullerton Rd., Fullerton Calif., announces the introduction of a full line of 2 in. diam Helidel all-metal delay lines.

The new 8810 Series delay lines are continuously variable, distributed constant units that afford precise selection of extremely short time intervals. Delay times of 1 microsec to 0.1 microsec are provided, with rise times less than 10% of total delay time.

All models have an ambient temperature range of −55 to +80° C, and life expectance of one million or more shaft revolutions. **66**

the roughing, foreline and high-vacuum valves usually assembled and built into conventional systems.

With this valve, an evacuated chamber may be quickly isolated from, and connected back into, a pumping system without shutting down either diffusion or fore pump, according to the manufacturer. **67**

TRANSISTORIZED DIGITAL CLOCK

A new transistorized digital clock which operates from a 100-kc input and provides an output in hours, minutes and seconds on a 24-hr basis is available from Datex Corp., 1307 S. Myrtle Ave., Monrovia, Calif.

Called the DC-116, it contains a counter and a frequency divider. Circuitry is on standard Datex CM-100 modules, mounted in a standard chassis, 7 x 19 x 11 in.

A record-rate interval control enables a pulse to be generated for system control at preset intervals. **69**

MINIATURE ACCELEROMETER

The development of a new miniature accelerometer, Model 504, having an acceleration range from 0.03 to 40,000 g with a flat frequency response within ±5% from 0.2 cps to 12 kc, has just been announced by Columbia Research Laboratories, MacDade Blvd. & Bullens Lane, Woodlyn, Pa. A special isolated case design makes the unit particularly suitable for applications where unusual stability and accuracy are required in high noise fields, temperature, altitude, humidity and other severe environments, according to the manufacturer.

Sensitivity of the Model 504 is 20/mv/g with an amplitude linearity of ±1%. Resonant frequency is 85 kc and temperature range is from −65° F to +350° F for standard units and from −65 to +500° F for high temperature units, with less than ±10% variation in sensitivity throughout both temperature ranges. **75**

TEMPERATURE METERS

The availability of a new, direct-readout T-meter for remotely reading temperature in the range of 50 to 150° F is announced by MHD Research, Inc., 1535 Monrovia Ave., Newport Beach, Calif. Model T100-1A, the new instrument, is said to incorporate thermistor probes to provide the rapid response necessary for monitoring critical temperatures. The manufacturer also states that with the new T-meter, systems can be fabricated easily for measuring gas temperature or the surface temperature of solids.

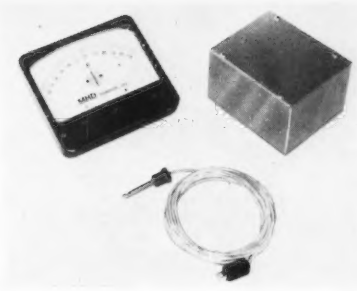

Specifically, the T-meter consists of a compensated d-c bridge with a thermistor as one leg of the bridge. In operation, the thermistor is placed in contact with the substance whose temperature is to be measured. The effect of the change in resistance is read directly on the meter that is calibrated in degrees. Other components of the bridge are remotely located. Probes are corrosion resistant for use in extreme environments. **77**

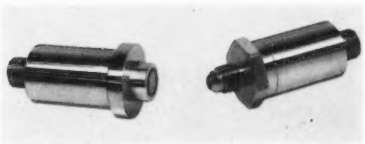

PRESSURE TRANSDUCERS

Two new pressure transducers, Models 538B and 539B, are available from Electro-Mechanical Research, Inc., Sarasota, Fla. The manufacturer states that these transducers feature precycled, prestabilized, standardized operation in temperature environments ranging from −100° to +600° F and are designed to operate in these temperatures during shocks in excess of 100 g for 11 msec in any direction. Performance is said to be standardized to such close tolerances that models covering identical full-scale ranges may be interchanged without recalibrating the measuring system.

EMR Models 538B and 539B are ruggedized miniature transducers of the bonded strain-gage type. The two models are identical except for pressure fitting: the 538B has a flush-mounting diaphragm; the 539B a threaded fitting for quarter-inch flared tubing. **78**

Quick -- Reliable STRESS ANALYSIS

Quantitative -- Qualitative
Dynamic -- Static
Laboratory and Service Tests

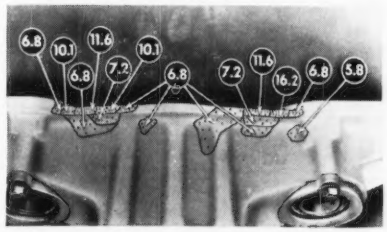

STRESSCOAT®

Stresscoat spray-on brittle coating stress analysis shows distribution, direction and stress level in simple or complex shapes over the entire part. Sharply defined stress indications on the part itself make evaluation with any of numerous coatings quick and positive. New ceramic All-Temp Stresscoat can be used on parts immersed in oil or tested at temperatures to 600° F. Used by leading laboratories and manufacturers to reduce costs, build better, stronger products that weigh less.

COMPLETE LOW-COST KITS – READY TO USE

AFTER ANALYSIS—TEST
As a stress engineer you must depend upon the integrity of materials and parts in relation to stress levels. After evaluation, suggest areas where cracks or laps are most serious. One or another of these Magnaflux Test Systems can help you assure the serviceability of your designs.

MAGNATEST®
Nondestructive electronic eddy current testing instruments for cracks, seams, coating thickness, alloy, etc.

SONIZON®
Ultrasonically determines thickness from one side or discovers sub-surface defects.

MAGNAFLUX-MAGNAGLO®
Magnetic particle testing to find and mark surface and subsurface defects in magnetic parts or assemblies.

ZYGLO®
Fluorescent penetrant marks cracks or pores in nonmagnetic materials.

MAGNAFLUX MATERIALS TESTING SERVICE
From 15 principal cities. Let us test your pilot runs for cracks or suspected cracks due to fatigue in service units. Write for details.

MAGNAFLUX CORPORATION
Subsidiary of General Mills
7356 West Lawrence Avenue
Chicago 31, Illinois

For details, circle No. 2 on Reader Information Card

Deflection Measuring Devices

R-I Potentiometric Displacement Transducers provide a wide range of deflection measuring capability. Designed for measuring displacement during aircraft structural loading tests, they may also be used in other static and dynamic applications.

Model 4040 (illustrated above) has a constant-force reel spring. Responds up to 50 ft./sec.^{2} with accuracy better than ±1%. Maximum displacement range: 10 ft. Shorter ranges available. Cable tension 9-20 ounces. Weight: 2.1 lbs.

Model 4046 has a maximum range of 3½", accuracy is ±1% of range. Cable tension: 8-12 oz. Response rate: up to 50 ft./sec.^{2} Weight only 9.5 oz. Size: 1½" x 1¾" x 1½".

Model 7100 has detachable cable which separates from reel when fully extended. Range: 12 inches. Cable tension: 16 oz. Max. operating temp: 222°F Size: 3½" x 2¼" x 2".

Model 6704 has 4' range with 6-lb. cable tension. High-temp potentiometer operates from —100° to 400°F without cooling. Response: 10 ft./sec.^{2} Cable tension: 6 lbs. Wt: 4 lbs.

Other configurations and characteristics are offered on special order.

RESEARCH INCORPORATED

Box 6164X Minneapolis 24, Minn.

For details, circle No. 9 on Reader Information Card

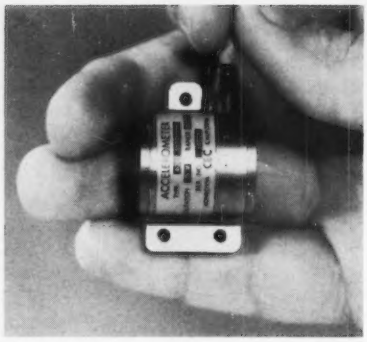

MINIATURE STRAIN-GAGE ACCELEROMETER

Low cross-axis response, minimum damping change with temperature, and high resonant frequency are the significant features of the new Type 4–203 strain-gage accelerometer reported by its manufacturer, Consolidated Electrodynamics Corp., a subsidiary of Bell & Howell Co., 360 Sierra Madre Villa, Pasadena, Calif.

Designed to measure accelerations parallel to mounting surfaces, the instrument is available in ranges from ±5 to ±500 g. Operable temperature range is −70 to +300° F. Sensitivity to acceleration perpendicular to the sensitive axis is less than 0.01 g/g.

The instrument features provisions for strain gage bridge electrical compensation external to the sealed damping-media-filled chamber. **79**

DITIGAL DISPLAY DEVICE

Kearfott Division, General Precision, Inc., 1150 McBride Ave., Little Falls, N. J., has introduced the Digistrobe digital display which employs the stroboscopic principle to provide an in-line, in-plane, high-definition, white-on-black display. The manufacturer states that, through use of a shutter arrangement, a single diode-encoding matrix is shared by all columns, resulting in substantial savings in electronic components and circuitry. Because of its speed, a single display can be used to sample several inputs on command, thus replacing as many as fifteen individual displays of existing types. **80**

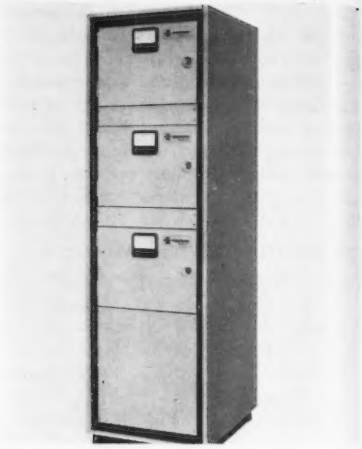

A-C POWER REGULATOR

Absence of power factor, instantaneous response and smooth, proportional power regulation from 5 to 95% of full power are advantages claimed for a new three-phase power regulator offered by Research, Inc., Box 6164, Minneapolis 24, Minn. Using ignitrons for stepless regulation, the equipment accepts either a-c or d-c control signals from an external controller or programmer. Rated output of unit shown is 450 amp in each phase at 230, 460 or 600 v, but overloads up to 100% for 5 min are tolerated.

A primary use is in electric furnace control, but the equipment is applicable wherever smooth regulation of heavy a-c power loads is needed. **81**

D-C AMPLIFIER

Gain of more than 10,000 over a bandwidth of 0 to 10 kc is provided by a new d-c amplifier, according to its manufacturer, Elcor, Inc., 1225 W. Broad St., Falls Church, Va.

Model D441C d-c amplifier is described as being a high-gain direct-coupled differential amplifier suitable for a wide variety of applications requiring amplification of d-c or a-c signals. It is said to be especially well suited for use as a general-purpose operational amplifier in analog computer circuits. Various external or internal feedback arrangements can be employed with the amplifier to accomplish such functions as integration, differentiation, stabilized gain, summing, gating, waveform generation and wave shaping.

The amplifier may be used with either single-ended or push-pull input and either single-ended or push-pull output. **82**

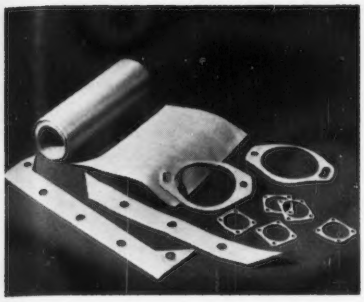

HIGH-TEMPERATURE SEALING GASKETS

COHRlastic conductive gasketing is a silicone rubber and metal material recently developed by the Connecticut Hard Rubber Co., 407 East Street, New Haven 9, Conn., specifically for high-temperature uses. This conductive gasketing conforms easily to irregular surfaces and is impervious to fluids, according to the manufacturer.

COHRlastic silicone-rubber conductive gasketing is available in two types, No. 8516 and No. 8520 which are 30 and 24 mesh aluminum-alloy wire cloth impregnated with a 50 durometer silicone rubber to a thickness of 0.016 and 0.020 in. The aluminum wire cloth meets AMS 4182A and the silicone rubber meets AMS 3302B. This construction is reported to provide a material which will withstand temperatures from −65 to 500° F. **89**

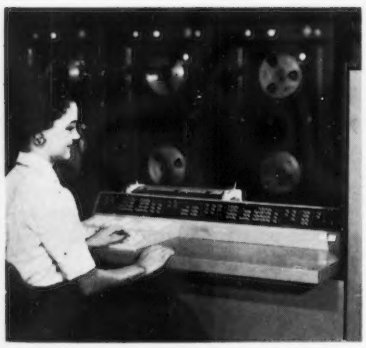

DATA PROCESSOR

The availability of their new Class 315 electronic data-processing system is announced by National Cash Register, Dayton 9, Ohio. This unit is described as being a solid-state, low-cost computer expansible from a basic system of limited capacity to a powerful full-scale system. The computer accepts and delivers large volumes of information in all common business-machine media at high speeds.

The main memory, the magnetic-tape file and the input and output systems are all variable in size or capabilities to fit closely the requirements of the user.

The processor is available with five different memory sizes capable of storing 6000 to 120,000 decimal digits or 4000 to 80,000 alpha-numeric characters. **90**

You'll find
READER INFORMATION CARD
on Page 17A

DATA-LOGGING SYSTEM

An 80-point data-logging system designed and built by Datex Corp., 1307 S. Myrtle Ave., Monrovia, Calif., will scan, measure and record 80 variables at the rate of 1 variable per second or 80 sec per one complete recording cycle, according to the manufacturer. Data are printed on an adding-machine type printer with tape punch, with the tape punch code being suitable for Datatron computer input. **91**

TEMPERATURE CONTROL

Minneapolis-Honeywell, Control Devices Division, 2753 Fourth Ave. South, Minneapolis, Minn., has introduced a low-cost thermocouple-operated potentiometer controller for industrial and laboratory heating operations.

According to the manufacturer, the new electronic control system is designed for a wide variety of temperature-control operations.

Heart of the system is a transistorized amplifier-relay panel containing all necessary operating controls and circuitry. The panel is constructed of heavy-gage metal and is said to be corrosion- and vibration-resistant.

Temperatures are sensed through use of a heat-sensitive thermocouple that is inserted into the medium to be controlled. **92**

DIRECT READING
STRAIN INDICATOR
MODEL DR-20

MINIMIZES TEST TIME
REDUCES OPERATOR ERROR

- WIDE RANGE GAGE FACTOR ADJUSTMENT
- AUTOMATIC POLARITY REVERSAL
- FULL RANGE ZERO
- NO PHASE BALANCING
- STABLE ZERO REFERENCE
- EXCELLENT DAMPING

The Bytrex Model DR-20 packs all the accuracy and versatility of many larger systems into one portable, direct reading instrument weighing but nine pounds.

Strain value for all gage configurations is indicated directly, without manual balancing, to resolutions of from one to one hundred microinches per inch per division. Extreme range and high damping provide excellent characteristics as a transducer indicator.

Write for Bulletin 107

BYTREX®
BYTREX CORPORATION

50 HUNT ST. • NEWTON 58, MASS.

Designers and manufacturers of strain indicators, switching and balancing units, strain gage amplifiers, precision bridges, semiconductor gages and devices, special purpose measuring systems for weight, force, pressure and torsion.

For details, circle No. 3 on Reader Information Card

PLAN NOW TO ATTEND
1961 SPRING MEETING
May 10–12
Benjamin Franklin Hotel
Philadelphia, Pa.

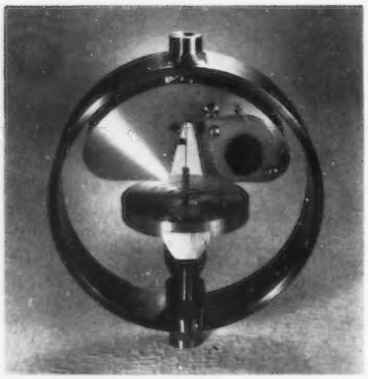

ELECTRICAL VIBRATOR FOR PROVING-RING REEDS

A device which vibrates a proving-ring reed automatically has been introduced by Morehouse Machine Co., 1742 Sixth Ave., York. Pa. It is described as a self-powered unit designed for easy attachment to standard Morehouse proving rings already in the field, or it can be supplied optionally on new proving rings.

According to the manufacturer, the vibrator's action dampens out very easily upon contact thereby increasing the ultimate accuracy of the proving ring through heightened sensitivity. Because of the light pressure required for accurate dampening, wear on the ring's contact points is reduced, assuring maintenance of the proving ring's calibration substantially longer than the normal 3 to 4 years.

The unit is powered by a mercury cell rated at 60 hr. **93**

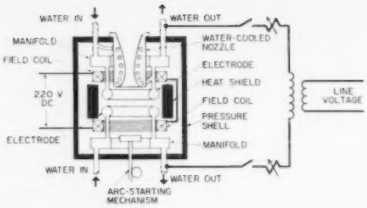

HIGH-ENERGY ELECTRIC-ARC HEATER

A machine with the potential capability to supply a stream of gas at temperatures as high as 20,000°F and pressures as great as 15,000 psi has been devised by the Westinghouse Electric Corp., East Pittsburgh, Pa. The machine, an electric-arc heater, can operate for sustained periods of time and at an extremely low level of gas contamination.

The arc heater has immediate application in a wind tunnel for missile testing. Also, it is said to hold promise as a chemical synthesizer and as a furnace for processing metals with ultra-high melting points. A prototype model of the machine has been operated at a power input of 1700 kw, but a high of 30,000 kw is planned by the company.

Westinghouse credits the new arc heater with being the first to operate continuously and at a low level of gas contamination. **94**

ALLOY FOR TEMPERATURE-SENSITIVE COMPONENTS

LA-685, an alloy suitable for use in microwave cavities, optical structures and other components which are normally temperature sensitive has been developed by General Communication Co., 677 Beacon St., Boston 15, Mass.

The producer reports that the alloy, properly used, has a maximum temperature coefficient of 0.3 part per million per ° C, as compared with a normal practical value of 1.5 ppm/° C for Invar, and compared with the practical value of 0.5 ppm/° C experienced in fused quartz at normal room temperature and above.

Due to the requirement for closely controlled metallurgical processing, it is necessary that the company fabricate the parts in order to assure that they meet the stated performance figures. **95**

COMPUTER DIODES

A gold-bonded silicon diode with a guaranteed recovery time of half a nanosecond is now being produced by the Semiconductor Division, Hughes Aircraft Co., 500 Superior Ave., Newport Beach, Calif.

According to manufacturer, the diode can switch and recover so fast its actual storage time cannot be measured on the finest laboratory traveling wave oscilloscope. The guaranteed recovery time of 0.5 nanosecond is given only to accommodate the measuring limits of standard sampling oscilloscopes. **96**

LABORATORY FURNACES

The availability of custom-built, platinum-wound, high-temperature laboratory furnaces is announced by the Baker Platinum Division of Engelhard Industries, Inc., 75 Austin St., Newark 2, N. J.

These furnaces, the company reports, are intended for use at temperatures up to 1800° C (3272° F) and are supplied with any shape and wall thickness of ceramic muffle up to an inside diameter of 5 in. or more and heat-zone lengths of from a few inches up to 4 ft. Typical applications include high-temperature calibrations, melting-point determinations, creep testing and similar uses. **97**

HARGRAVE CLAMPS — CHISELS — PUNCHES — MASONRY DRILLS

PRO-TECTO-HED PREVENTS MUSHROOMING

FULL RANGE PATTERNS & SIZES

WRITE FOR FREE GENERAL CATALOG

THE CINCINNATI TOOL CO.
4356 Montgomery Rd.
Cincinnati 12, Ohio

CARBIDE TIPPED MASONRY DRILLS

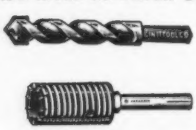

For details, circle No. 4 on Reader Information Card

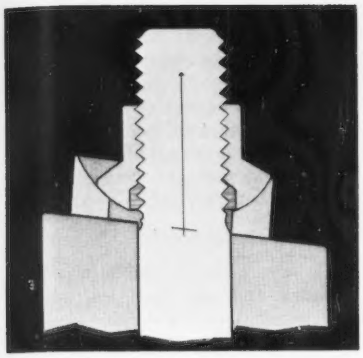

SELF-ALIGNING LOCKNUT

A self-aligning locknut that develops the full-rated strength of aircraft bolts even though the seating surface is as much as 8 deg out of perpendicular to the shank, has been placed on the market by Standard Pressed Steel Co., Jenkintown, Pa.

The compensating fastener (SPS SA16) consists of a hex drive featherweight series self-locking nut which swivels within the spherical seat of a precision-alignment washer.

The design maintains constant bearing area between alignment washer and nut from 0 to 8 deg. Thus full rated strength of 160,000 psi (ultimate tensile of the nut) can be utilized at all angles. **98**

AUTOMATIC BALANCE STRAIN INDICATOR

The availability of Model AS4-FT, a compact portable instrument used as a strain indicator or for the direct indication of the output of strain-gage load cells, pressure cells or torque transducers, is announced by Metrix, Inc., P.O. Box 683, Walnut Creek, Calif. Featuring all transistor circuitry and an automatic null-balancing technique, the unit is operable from self-contained batteries as well as from a 60 cps a-c line. A low-frequency carrier is used to excite the bridge. The bridge connection terminal is arranged to allow the installation of completion resistors for half bridge operation.

The indicator may be used with strain gages having a resistance of 60 ohms or more. Four ranges are provided: 0–200, 0–400, 0–800 and 0–1600 microstrain full scale. Accuracy is 1% of full scale or better and resolution provided by the 100 scale divisions is 2 microstrain per division on the highest sensitivity scale, the manufacturer reports. **99**

PROGRAMMER CHASSIS FOR DATA-SYSTEM CONTROLS

The availability of a new control and programming chassis, primarily designed for data-system controls, is announced by Datex Corp., 1307 S. Myrtle Ave., Monrovia, Calif.

According to the manufacturer, voltage level or contact-closure inputs in any code form may be recorded, serialized and sequenced to output devices such as digital computers, tape punches and typewriters. Special control codes (e.g., carriage return, tab, end code, etc.) may be generated within the programmer.

When used as a system controller, the programmer may be used to initiate "stop" and "start" commands and provide contact closures for control of external equipment. **100**

MEMBERSHIP IN SESA

In the space age, measurements of stresses, forces and accelerations must be made to check calculations and to obtain information that cannot be calculated.

The Society for Experimental Stress Analysis is **the** forum for work and workers in the **experimental mechanics field.**

How you can join the Society and take advantage of its many benefits is explained in descriptive literature available.

For further details write to:

SOCIETY FOR
EXPERIMENTAL STRESS ANALYSIS

21 Bridge Square, Westport, Conn.

PHOTOELASTIC
STRESS ANALYSIS WITH
POLAROID* FILTERS

Standard Equipment or Special
Complete Apparatus or Components

Point Light Sources
White Light and Monochromatic (546 or 589 line)

Matched Quarter Wave Plates to 17″ diameter

Polaroid Polarizers to 17″ diameter
Cemented Glass Laminations #6/006

Straining Frames

Recording Cameras

* *T. M. Reg. U. S. Pat. Off. by Polaroid Corporation*

THE POLARIZING INSTRUMENT COMPANY, Inc.
IRVINGTON-ON-HUDSON, NEW YORK

For details, circle No. 5 on Reader Information Card

To obtain free literature, circle item number on Reader Information Card.

References on Fatigue

The American Society for Testing Materials, 1916 Race St., Philadelphia 3, Pa., has issued a new publication—"1959 References on Fatigue (STP 9-K)." It contains 88 pages, duplicated, $8^1/_2$ x 11 in. $4.00 per copy.

This list of references consists of about 460 entries and provides an extensive source of information on articles published in 1959 dealing with fatigue of structures and materials. An abstract of each reference is included in all but a few cases. The material is so arranged that individual references can be cut apart for filing according to any desired plan.

For additional information, write directly to the ASTM at above address.

Load-measuring Bolt

A 4-page, illustrated bulletin describing the "Strainsert Bolt" has been released by the Strainsert Co., Division of Polyphase Instrument Co., Bridgeport, Pa.

The Standard Strainsert Bolt installation consists of an electric strain gage bonded and sealed in a small hole along the longitudinal neutral axis of the bolt. Thus, the bolt is intended to indicate continuously tensile stress or load induced by either tightening or otherwise loading or unloading it due to shock, vibration, wear, etc.

Bulletin covers general description, mechanical specifications, electrical specifications, calibration, instrumentation, as well as prices. **123**

Testing Equipment

Bulletin 5901 "Facts on Testing," from Thwing-Albert Instrument Co., Penn St. and Pulaski Ave., Philadelphia 44, Pa., is available. This bulletin tells about the combined tensile and tear-tester sample cutter, air operated grips for tensile tester, capstan grips for textile tensile testing, the adhesives tester, the four square cutter, the Spencer impact attachment for the Elmendorf tearing tester, toughness tester attachment for the Elmendorf tearing tester and Elmendorf calibration check weights. **125**

Mounting Sensing Elements

A bulletin describing a technique of mounting sensing elements with "Rokide" ceramic spray coating is available from the Norton Co., Refractory Division, Worcester 6, Mass. It occupies 8 pages and contains a number of illustrations.

The technique discussed is a method for positioning and fastening fine wire and foil sensing elements subjected to elevated temperatures. **127**

Transistorized Null Indicators

Bulletin NI, a two-color catalog sheet showing detailed technical data on small-size, fully transistorized, phase-sensitive null indicators, is offered by Gertsch Products, Inc., 3211 S. La Cienega Blvd., Los Angeles 16, Calif.

Units may be combined with any standard Gertsch RatioTran to form an a-c ratio bridge. Three ranges of sensitivity are provided: 10, 100 and 1000 μv. A maximum sensitivity of 10 microvolts allows proper resolution for bridge circuit operation. A zero-center meter gives the operator "sense" as to being above or below null. Phase-sensitive detector provides quadrature rejection.

Described in the bulletin are two types: Model NI-2, which is battery operated and supplied in a portable carrying case, and Model NI-3, a $3^1/_2$-in. high rack mounted version, containing an internal a-c power supply. **129**

Engineering Data Chart

A catalog is available from M H D Research, Inc., P.O. Box 1815, Newport Beach, Calif., which describes the basic policies and areas of research in which the corporation is engaged, and charts of particular interest to engineers and scientists in the missile and space fields. The brochures and catalog sheets, included, specifically detail several M H D designed and manufactured research "tools" in the field of "Magnetohydrodynamics" and a technical discussion of the field, itself.

This complete catalog is free and will be sent out upon request. **131**

Semiconductor Bases

A line of stud-mounted semiconductor bases and mating caps is reviewed in a four-page technical bulletin (Form 2714) from Standard Pressed Steel Co, Jenkintown, Pa. The bases double as heat sink and electrically conductive mount for transistors, diodes and other types of semiconductors.

The metal bases, available in high-conductivity copper, alloy steel and aluminum, are made by cold heading, a significant departure from conventional machining techniques. **133**

Accelerometer-amplifier System

A new technical bulletin which illustrates and describes the Model 50X2 accelerometer-amplifier system, designed to provide output voltages analogous to shock and vibration data with sufficient amplitude levels to modulate sub-carrier oscillators in a telemetering system, has just been published by Columbia Research Laboratories, MacDade Blvd. & Bullens Lane, Woodlyn, Pa.

According to the manufacturer, the 50X2 system is a miniature solid state package less than 3 cu in. in volume and approximately 4 oz in weight which combines a piezo-electric accelerometer and a transistorized amplifier with high gain and wide frequency response. **135**

Variable-phase Standard

Bulletin VPS-1, a two-color, 4-page brochure describing a variable phase standard, which permits phase between 2 self-generated voltages to be shifted to any desired angle with an accuracy of $\pm 0.05°$ or better, is available from Gertsch Products, Inc., 3211 S. La Cienega Blvd., Los Angeles 16, Calif.

Included in the brochure are technical specifications, a detailed circuitry description, and a simplified block diagram. Unit has an output voltage of 50V rms (reference), and 0–50V rms (vector). The vector output may be attenuated in steps of 50 mv within its range.

Designated as Model VPS-1, this instrument is completely self-contained, requiring no external equipment for operation or calibration. **137**

Micromidget Chopper Specifications

Airpax Electronics, Inc., Cambridge Division, Cambridge, Md., announce the availability of Specification 266 which details characteristics and ratings for "The Smallest Chopper in the World." The Model 30 electromechanical chopper has $^{21}/_{64}$ x $^{21}/_{32}$ x $^5/_8$-in. dimensions and weighs but 9 gm, according to the manufacturer.

Specifications listed include: coil voltage, environmental conditions, construction, contact rating, dwell time, phase angle and chopper noise. Diagrams illustrate: connections, relative phase and typical noise test circuit. **138**

Angle Indicator

Data sheet No. CO2721027, released by Kearfott Division General Precision, Inc., Little Falls, N. J., deals with a high-accuracy two-speed precise angle indicator. **139**

Pocket Guide on Digital Voltmeters

A six-page, two-color folder describing important differences in digital voltmeters is available without charge from Non-Linear Systems, Inc., Del Mar, Calif.

The new folder points out such features as snapout readout, plug-in oil-bath stepping switches, "no-need-less-nines," logic, and 99% plug-in modular construction, the company reports.

The folder also has a section that shows a picture of each NLS instrument and brief specifications. A perforated, prepaid postage card is attached to the folder to facilitate requesting specific information on each model. **140**

Six-channel Hydraulic Force System

A technical reprint, showing schematics, details and applications on their six-channel hydraulic force-control system, has just been released by Gilmore Industries, Inc., 13015 Woodland Ave., Cleveland 20, Ohio.

Used for static and dynamic loading test stands, the system is designed for up to 100,000 lb. force capacity per cylinder and includes a load cell in series with each cylinder to provide the force feedback component to the console. **141**

Test Stands

Bulletin L-2001, an introduction to test stands and their drives, is available from Reliance Electric and Engineering Co., Cleveland 10, Ohio. **142**

Series 50 Voltage Comparators

A new two-color, six-page bulletin on NLS Series 50 transistorized voltage comparators used for critical go/no-go applications is being offered by Non-Linear Systems, Inc., Del Mar, Calif.

The bulletin describes the Model 50 voltage comparator and the Model 51 voltage comparison amplifier, instruments NLS says have the accuracy, speed and reliability of the company's quality digital voltmeters.

Uses of voltage comparators are discussed in the bulletin and series 50 applications are listed. **143**

Batch-weighing Systems

Their new 20-page bulletin on manual and automatic electric batch-weighing systems has just been announced by Gilmore Industries, Inc., 13015 Woodland Ave., Cleveland, 30, Ohio. Bulletin B-100 contains information about six different Gilmore weighing systems. Applications range from low-cost, short-run installations where the formula is frequently varied all the way to complicated production batch-weighing runs.

Details on features, equipment and operation of the various systems are all included, along with diagrams and photos of the systems. **144**

Oscillographs and Amplifiers

Bulletin 210, *Photron Oscillographs and Amplifiers*, is available without charge from Photron Instrument Co., 6516 Detroit Ave., Cleveland 2, Ohio.

This two-color 8-page booklet covers portable as well as mounted oscillographs. It is profusely illustrated. **145**

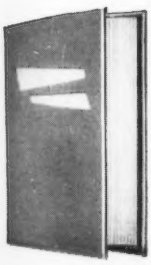

Helpful McGraw-Hill books for your professional library

THEORY OF PLATES AND SHELLS

Covers the general theory of bending of plates under lateral load, with applications to circular and rectangular plates, and with numerous tables simplifying the calculation of deflections and stresses in plates. Provides a treatment of combined bending and tension or compression of plates, with applications to thin plates. **By S. Timoshenko, Stanford Univ.; and S. E. Woinowsky-Krieger, Université Laval, Quebec, Canada, 2nd Ed., 580 pp., 280 illus. $15.00**

THEORY OF ELASTICITY

For engineers concerned with calculating stresses in engineering structures and machine parts—here is essential knowledge of the theory of elasticity, together with the solution of engineering problems of practical importance. The book discusses approximate and experimental methods of solving elastic problems which have proved useful in the study of complicated cases of stress distribution. **By S. Timoshenko and J. N. Goodier, Stanford Univ., 2nd Ed., 506 pp., 266 illus., $11.50**

FORMULAS FOR STRESS AND STRAIN

A compact and readily usable summary of important formulas, facts, and principles pertaining to strength of materials. This reliable reference for engineers provides helpful formulas for stress analysis and elasticity. All experimental data and empirical formulas are in line with current information. New material has been added, ensuring complete coverage of stress and strain. **By Raymond J. Roark, Univ. of Wisconsin, 3rd Ed., 381 pp., $8.25**

THE STRAIN GAGE PRIMER

What the bonded wire resistance strain gage can do in solving problems in experimental stress analysis is explained in this practical book. All phases are covered—from selecting the proper commercial gage through preparing surface of the test member, cementing, damage-proofing, and wiring the gage —to selecting the proper instrument to record the strain gage data, and interpreting readings in terms of significant stresses. **By C. C. Perry and H. R. Lissner, Wayne Univ., 280 pp., 180 illus., $6.00**

THE TESTING AND INSPECTION OF ENGINEERING MATERIALS

A practical approach to the principles and methods of materials testing, with full details on types of tests in use. Describes modern testing equipment and covers effects of variables on test results. Includes information on micro-hardness testers, non-destructive tests, low-temperature impact tests, and more. **By H. E. Davis, G. E. Troxell, Univ. of Calif.; and C. T. Wiskocil, formerly, Univ. of Calif. 2nd Ed., 431 pp., 171 illus., 42 tables, $7.50**

APPLIED ENGINEERING MECHANICS

Emphasizes the use of reasoning rather than complicated mathematics for solving engineering problems. Employing only simple mathematics, the book proceeds from easy to difficult phases of engineering mechanics, clarifying the principles advanced with numerous illustrations. Takes you step-by-step through the solutions of scores of technical problems. **By Alfred Jensen, formerly, Univ. of Washington; assisted by Harry H. Chanoweth, Univ. of Washington. 2nd Ed., 409 pp., 746 illus., $6.50**

SEE THESE BOOKS 10 DAYS FREE

McGraw-Hill Book Co., Dept. EXM-4 327 W. 41st St., N. Y. 36, N.Y.

Send me book(s) checked below for 10 days' examination on approval. In 10 days I will remit for book(s) I keep, plus few cents for delivery costs, and return unwanted book(s) postpaid. (We pay delivery costs if you remit with this coupon —same return privilege.)

- ☐ Roark—**Formulas for Stress & Strain, $8.25**
- ☐ Perry & Lissner—**The Strain Gage Primer, $6.00**
- ☐ Davis et al—**Testing and Inspection of Engr. Materials, $7.50**
- ☐ Jensen & Chenoweth—**Applied Engr. Mechanics, $6.50**
- ☐ Timoshenko & Woinowsky-Krieger—**Theory of Plates and Shells, $15.00**
- ☐ Timoshenko & Goodier—**Theory of Elasticity, $11.50**

Name..... Address.....

City..... Zone.... State.....

Position..... Company.....

For price and terms outside U.S., write McGraw-Hill Int'l. EXM-4

get the size, specs and mobility you need with

SANBORN RECORDERS

2 Channels . . . 35" high mobile cart . . . choice of 4 plug-in preamps

Interchangeable plug-in "850" type preamplifiers in Carrier, DC Coupling, Phase Sensitive Demodulator and Low Level types, for inputs ranging from microvolts to hundreds of volts . . . internal MOPA available when carrier or chopper excitation is required . . . heated stylus, rectangular coordinate recording on 50 mm wide channels . . transistorized circuits . . . frequency response to 125 cps within 3 db, at 10 mm peak-to-peak. Model 297 can also be used in optional portable case or rack mounted in 10½" of panel space.

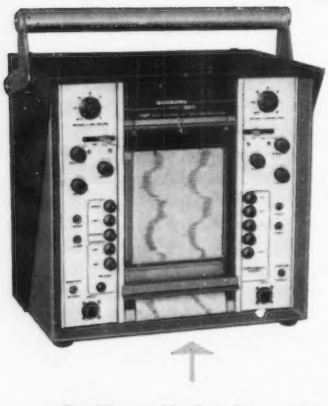

1 Channel . . . 20 lbs., briefcase size . . . 10 mv/div DC Model . . . 10 uv rms/div AC strain gage Model

Extremely compact, highly versatile recorders for general purpose DC inputs (Model 299) and AC strain gage recording (Model 301). Two chart speeds: 5 and 50 mm/sec . . . inkless, rectangular coordinate recording . . . response from DC to 100 cps within 3 db, at 10 div peak-to-peak . . . gain stability better than 1% to 50°C and for line voltage variation from 103 to 127 volts. Model 299 has balanced to ground input, 10 switch-selected sensitivities, calibrated zero suppression. Model 301 has wide sensitivity ranges, can be used with strain gages and inductive transducers, provides excitation voltage of approximately 4.5 volts rms at 2400 cps, and has uncalibrated zero suppression.

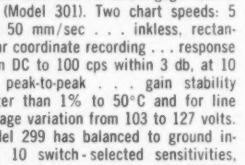

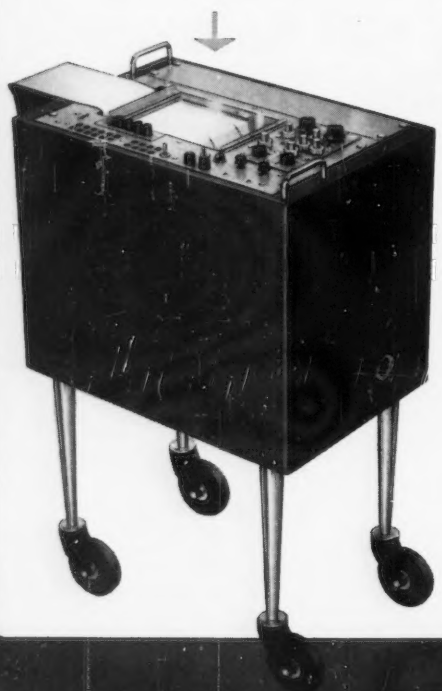

Two 50 mm wide channels . . . separate floating input DC amplifiers . . . 4 chart speeds . . . mv or volt inputs

Operate this 1-cubic-foot recorder vertically, horizontally, or tilted at a 20° angle on carrying handle. Inputs are floating and guarded . . . 12 sensitivities from 0.5 mv/mm to 20 v/cm . . . response DC to 125 cps within 3 db, at 10 div peak-to-peak . : . max. nonlinearity 0.25 mm . . . common mode rejection 140 db min. DC . . . built-in 10 mv calibration signal and electrical limiting . . . internal 1 sec. timer . . . monitor output connectors for each channel. Galvanometers are rugged, low impedance type with velocity feedback damping; most circuitry for each channel is mounted on a single, easily serviced card.

For complete details contact your nearest Sanborn Sales-Engineering representative. Sales representatives are located in major cities throughout the United States, Canada and foreign countries.

SANBORN COMPANY
INDUSTRIAL DIVISION
175 Wyman Street, Waltham 54, Massachusetts

For details, circle No. 6 on Reader Information Card

Photoelastic Strain Gages

Application of photoelastic principle leads to development of new techniques for strain and stress analysis of structural parts

by G. U. Oppel

ABSTRACT—New photoelastic strain gages are described which are self-contained and give an accurate direct indication of magnitudes and directions of principal stresses. Large numbers of gages may be observed simultaneously and critical areas of members may be readily located.

Various types of gages are applicable to high-temperature problems, dynamic measurements or direct photographic recording.

Introduction

Problems arising with the advance of engineering technology require new techniques for strain and stress analysis of structural parts. New applications of the photoelastic principle provide techniques which possess many advantages over other procedures; photoelastic strain gages are in this category.

A photoelastic strain gage consists essentially of a thin, small plate made of an optical strain-sensitive material (for example, epoxy resin) which indicates variations in strain by changes in number and in position of interference fringes. The plate is glued or otherwise rigidly fixed to the surface of the structural part to be tested and then subjected to static or dynamic loading. The fringes in the gage plate become visible when observing the gage in polarized light. For this purpose, a polarizing film is incorporated in the gage or positioned in the path of the light. Therefore, common light is the only power source required for obtaining strain readings.

Various types of photoelastic strain gages are obtained by shaping and preparing the gage plate in different manners; examples are uniaxial strain gages for measuring strain in a particular direction and biaxial strain gages for determining characteristics of biaxial surface strain.[1] These gages are not restricted to room-temperature applications, but they also promise to meet the technical requirements at extreme temperatures.

The Uniaxial Photoelastic Strain Gage

The uniaxial photoelastic strain gage indicates changes in strain by displacements of fringe lines visible in the gage. Figure 1 shows a self-contained gage of the uniaxial type in this final form and also shows the displacement of the fringes caused by changing the load applied to the specimen. The arrows marked in this figure call attention to the displaced fringe line. The gage shown was designed so that a displacement of one full fringe order—i.e., a shift of one fringe line into the exact position previously occupied by the adjacent fringe line—corresponds to a change in strain of 1000 microin/in. The scale which is attached to the top of the gage permits strain readings of fractions of one order. Strains in excess of the amount corresponding to one fringe order are measured by counting the number of

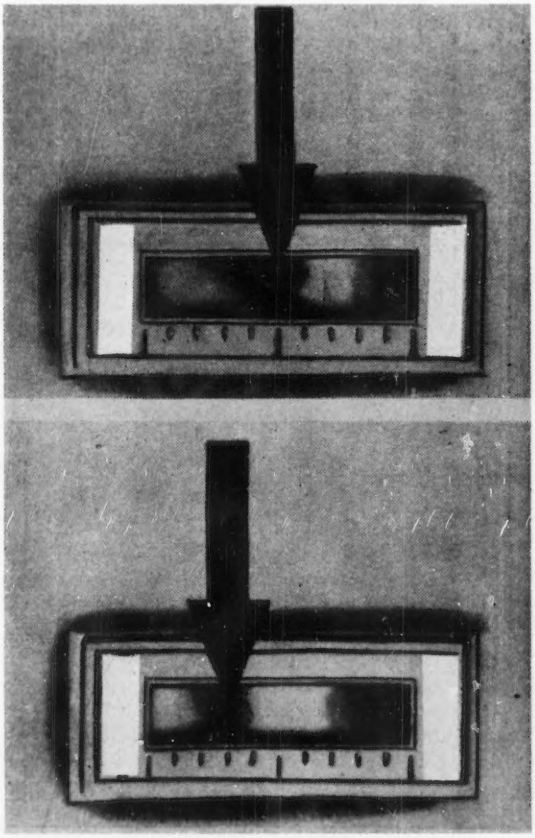

Fig. 1—Self-contained uniaxial photoelastic strain gage

G. U. Oppel is Professor of Engineering Mechanics, Pennsylvania State University, University Park, Pa.

Paper presented at 1959 SESA Annual Meeting held in Detroit, Mich., on October 21–23.

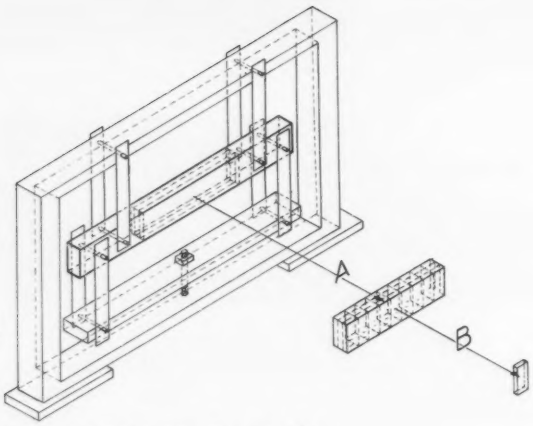

Fig. 2—Uniaxial gage. Diagram of a manufacturing procedure

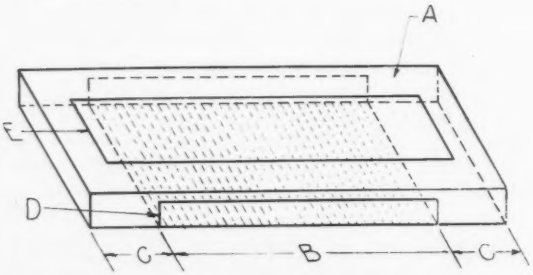

Fig. 3—Uniaxial gage. Schematic design diagram. A—gage plate, B—reflecting rear face, C—gluing area, D—rubber sheet, E—polarizing film

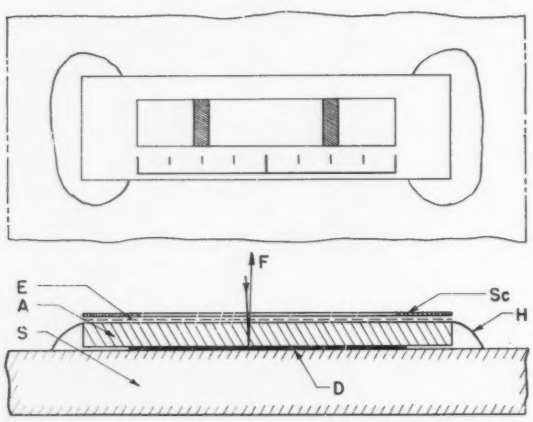

Fig. 4—Schematic diagram of the uniaxial gage bonded to a specimen. A—gage plate, D—rubber sheet, E—polarizing film, F—reflected light, H—glue, Sc—scale, S—specimen

fringes and fractions thereof passing an arbitrarily picked location on the scale.

The dimensions of the gage shown in Fig. 1 are $^5/_4$ x $^1/_2$ in. The uniaxial gage displays a fringe line or a set of such lines in the unstressed state. These lines were obtained by utilizing the frozen-stress method[2, 3] in the manner illustrated in Fig. 2. A beam of epoxy resin is placed into a bending frame

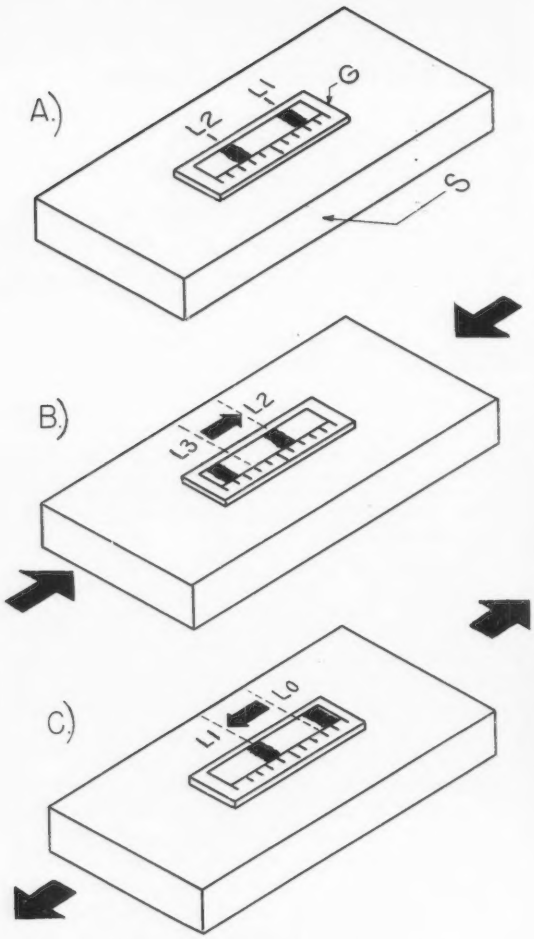

Fig. 5—Uniaxial gage. Schematic diagram of strain indication. L_0, L_1, L_2, L_3—interference lines

and then slowly heated to about 240° F. At this temperature, the beam is subjected to pure elastic bending. The imposed deformations and a photoelastic fringe pattern are retained in the beam after slow cooling to room temperature. The central portion of the beam is then cut into small rectangular plates as shown in this figure. The length of the plates is taken perpendicular to the axis of the beam in order to obtain the desired set of frozen-in fringe lines. These plates then serve as gage plates of uniaxial photoelastic strain gages.

Figure 3 is a schematic design diagram with details of the uniaxial gage. The rectangular gage plate is ground to have plane and parallel faces. The middle portion of the gage is given a reflecting surface by means of an aluminum coating. Plastic tape (*D*) protects the mirror and, at the same time, prevents rigid bonding of the gage to the specimen in this region and at the lateral faces. Firm bond between the gage and the specimen is provided only at the ends of the gage plate in order to avoid lateral

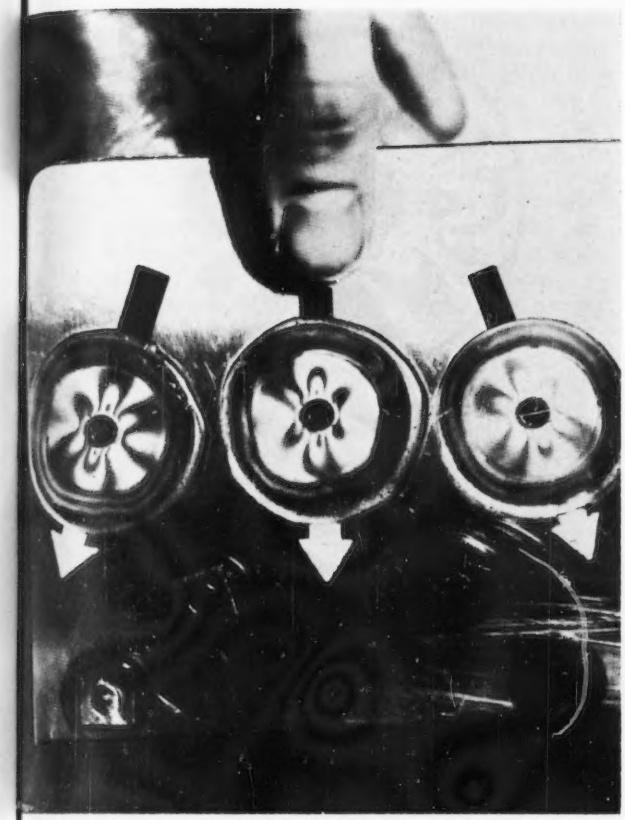

Fig. 6—Self-contained biaxial photoelastic strain gages. Axes of symmetry of the interference patterns (arrows) indicate the directions of the principal strains and stresses

sensitivity of the gage. By covering the front face of the gage plate with a polarizing film (E), the frozen-in fringe lines become visible. From another diagram (Fig. 4), further details of a uniaxial gage as glued to a specimen can be recognized. The diagram shows a top view and a side view of a complete gage.

The gage commonly is attached to the specimen by means of a two-component epoxy glue. In the gluing procedure, the components are well mixed and brushed onto the surface of the specimen. The gage is then pressed lightly into the glue. Gluing of the gage at vertical or sloped surfaces can be facilitated by taping the gage to the surface of the specimen.

Determination of positive and negative strains by aid of the uniaxial gage is illustrated by Fig. 5. In the unstrained condition, the gage displays a set of fringe lines, for example, L_1 and L_2 (Fig. 5A), which were frozen-in by the manufacturing process. When subjecting the gage to a negative strain by compressive stress, the set of fringe lines moves in a certain direction (Fig. 5B), whereas elongations by tensile stresses cause displacements of the fringe lines in the opposite direction (Fig. 5C). In this manner, positive and negative strains are distinguishable. Lines of higher or of lower order may enter the field of observation when increasing the load. However, the distances between the lines remain constant. The fringe movement is directly proportional to the longitudinal deformation of the gage, and therefore to the directional strain of the part to which the gage is bonded.

It has been found, by numerous calibration tests, that the uniaxial photoelastic strain gage is suited as a tool for exact strain determinations and that the gage displays a constant gage factor and a strong linear strain-optical behavior.

Design Conditions for the Uniaxial Gage

Measuring Range. The total amount of elastic strain obtainable with high-strength aluminum alloy (Aluminum 7075T6: s_y = 60,000 psi, E = 10 × 10^6 psi) and with heat-treated medium-strength steel (SAE 4340: s_y = 180,000 psi, E = 30 × 10^6) is in the order of 6000 microin/in. Highest-strength steel as obtained by oil quenching or by case hardening might exhibit a yield-free tensile strength up to approximately 360,000 psi, i.e., up to an elastic strain of 12,000 microin/in. These strain magnitudes determine the desirable measuring range of a photoelastic strain gage.

Sensitivity Requirements. An accuracy of 1% of the full range generally meets the technical requirements for strain gages. Thus, a photoelastic strain gage suited for measuring strains on a medium-strength steel and on aluminum under static-loading conditions should be designed such that its sensitivity is approximately 60 microin/in. In case of dynamic loading and in case of low-strength steel and of low-strength light metal subjected to static load, the requirement on sensitivity might raise to approximately 30 microin/in. In case of concrete, the requirements on sensitivity are still greater, as dictated by the lower strain at which fracture occurs in this material.

Gages of the same fundamental design as treated here but of an increased size can meet these latter requirements.[4]

Strain-optical Data. Epoxy resin (Araldite 6020, for instance)—if properly hardened—displays linear stress-strain-optical relations up to at least 7000 psi (E = 500,000 psi). The maximum linear strain which this resin can undergo at normal temperature is therefore 14,000 microin/in. This is more than required in investigations on steel, aluminum or other commonly used metals in the elastic range.

The strain-optical sensitivity of a $^1/_{10}$-in. thick epoxy plate was determined by calibration in tension as one fringe per 800 microin/in. strain. Consequently, the requirements on sensitivity of this photoelastic strain gage amount to a readability of at least one-twelfth of a fringe order. The displacement of a fringe can be read on the gage scale to this accuracy and the requirements on sensitivity are fulfilled.

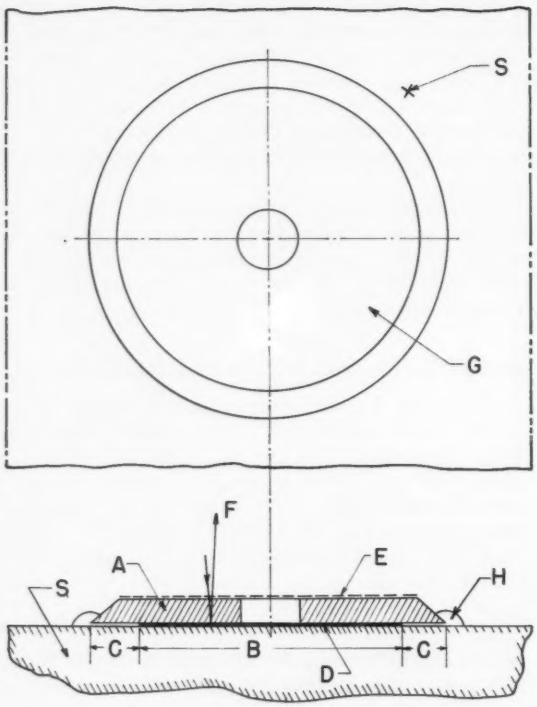

Fig. 7—Biaxial gage. Design diagram. G—gage, S—specimen, A—circular gage with circular hole at center, B—silvered area at rear face of gage plate, C—gluing area, D—rubber sheet, E—circular-polarizing compound film, H—glue

Bonding. Photoelastic strain gages used for measurements at room temperature are rigidly fixed to the specimen or to the structural part by gluing. A cold-setting two-component glue which consists of an epoxy resin and an appropriate hardener is used for this purpose. The hardening takes 3 to 6 hr when a controlled heating device is used. In cases where this time is not available, a so-called contact glue—hardening in a few seconds—may be applied.

The Biaxial Photoelastic Strain Gage

Another type of photoelastic strain gage is the biaxial gage having the form of a circular plate. The main purpose of this gage is to indicate the directions of the principal strains and stresses by photoelastic fringe patterns, in which the axes of symmetry of such patterns coincide with the principal directions.

Three gages of the biaxial type are shown by Fig. 6. The gages were bonded to a plate clamped along one edge and loaded by a concentrated force which was exerted by hand. The lines of symmetry (marked by arrows) of the three fringe patterns coincide with the principal directions at the respective locations. The fringe patterns displayed by such gages undergo immediate changes in orientation as the location of load application is changed.

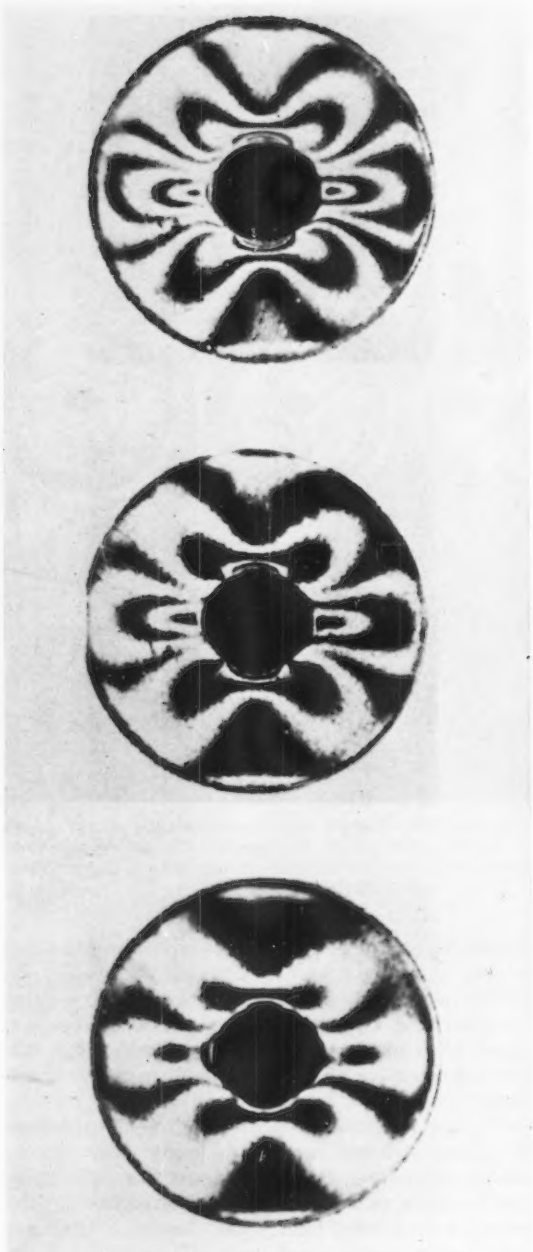

Fig. 8—Biaxial gage. Effect of increasing the load in tension

Furthermore, the number of fringes visible in the gage is a measure of the magnitude of stress and of strain to which the gage and the structural part are subjected.

Details of the design of the biaxial photoelastic strain gage are shown in the diagram of Fig. 7. The circular gage plate (*A*) of uniform thickness has a circular hole at its center. The hole acts as a stress raiser and causes a stress concentration effect

in its surroundings. A rubber sheet (*D*) covers the center part (*B*) of the gage plate and prevents the gage from being rigidly bonded to the structural part in this region. The gage plate is, therefore, free to deform at its hole. The boundary (*C*) of the gage plate serves as the gluing area. A circular polarizing film (*E*) attached to the front face of the gage plate renders a self-contained biaxial photoelastic strain gage.

When subjecting this gage to a state of uniaxial tensile stress, fringe patterns of the type shown by Fig. 8 originate. Increasing the tensile stresses maintains the character of the fringe pattern but increases the number of fringe lines.

Subjecting the gage to torsion causes another type of fringe pattern. The type of fringe pattern displayed by the gage, therefore, depends upon the ratio of the principal stresses acting in the biaxial gage. This effect can easily be explained by a calculation of the lines of constant maximum shearing stress which corresponds to the lines observed in a photoelastic fringe pattern. The mathematical calculation uses the theoretical solution developed by G. Kirsch[5, 6] in treating the effect of a circular hole on the stress distribution in a plate. This solution can be applied here as a close approximation, since the gage is free to deform at the hole like a hole in a large plate, and since the unbonded region of the gage is large in comparison to the hole.

Figure 9A illustrates the shearing stress distribution as found by calculation at a circular hole in a plate which is subjected to uniaxial tension. The axes of symmetry of the calculated shearing stress pattern at the hole can be seen to coincide with the directions of the tensile stress and of the principal strains in the plate. If uniaxial tensile stress directed differently from that in Fig. 9A is applied to the plate, for example inclined at 15 deg to the former direction, then the pattern at the hole has its axes of symmetry rotated correspondingly (Fig. 9B). Since in the case considered here the second principal stress was zero, the stress ratio S_{II}/S_I may be designated as being zero. Other stress ratios applied to the plate alter the calculated stress pattern at the hole, as shown in Figs. 9C, D, E, and H. These patterns state, furthermore, that the axes of symmetry of the pattern always coincide with the directions of principal strains and principal stresses.

In case of equal biaxial tensile or compressive stress, however, there exists no preferred direction, since the measurable shearing stresses in the plate remote from the hole are zero. The calculated pattern in this case consists of concentric circles (Fig. 9E).

In the case of pure shear applied to the plate, the calculated shearing stress pattern at the hole admits two rectangular crosses of symmetry 45 deg to each other. The cross cutting the shearing stress minima coincides with the directions of the principal stresses and strains in the plate(Fig. 9H).

Two general rules derived from the calculations indicated above are stated:

(*a*) The rectangular cross of the principal stress and strain directions coincides with the axes of symmetry of the fringe pattern and cuts the minima of the shearing stresses which exist in the surroundings of the hole.

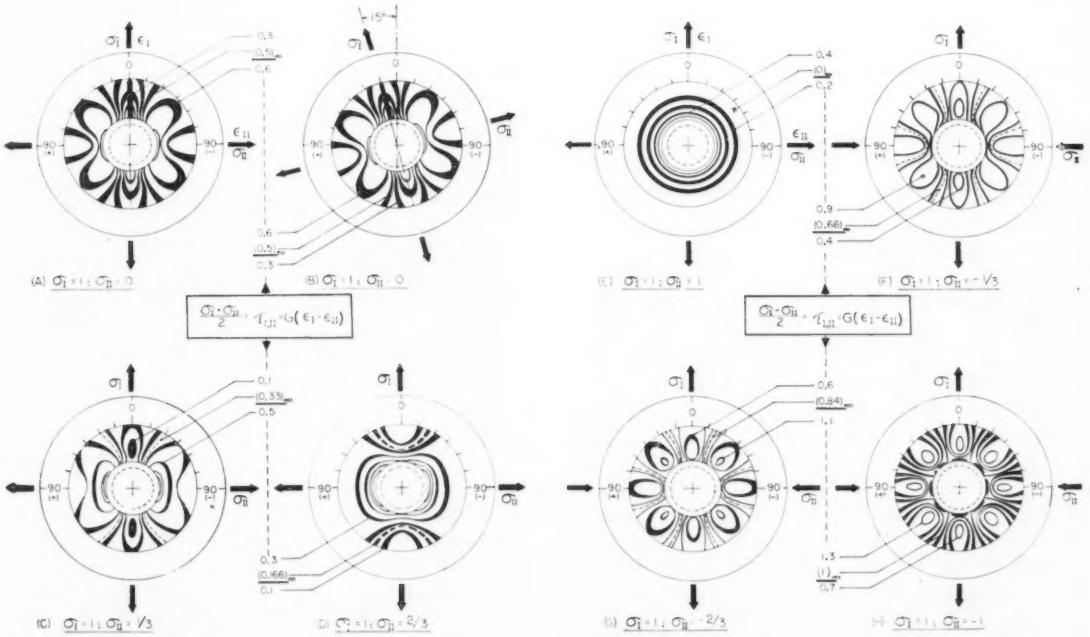

Fig. 9—Biaxial gage. Theoretical shearing stress distribution for different stress ratios

(*b*) The disturbances caused by a circular hole in a plate become negligible outside an area having a diameter three or four times the diameter of the hole.

If, therefore, a biaxial gage designed as shown by Fig. 7, and having an outer diameter equal to four times the diameter of the circular hole, is attached along its boundary to the surface of a structural part, then the gage will undergo at its boundary the same deformations as the structural part. The gage will react at its hole like a large plate with a hole. The gage will indicate strains and stresses acting in the region of the structural part to which the gage is bonded.

The isochromatic fringe lines visible in the gage will correspond to lines of constant shearing stress. The fringe patterns shown in Fig. 10 A–E were obtained from tests conducted with gages which were bonded to a plate and then subjected to various stress ratios. Comparison of the actual patterns with the calculated ones show full similarity for corresponding stress ratios. The directions of the principal strains and stresses are therefore indicated by the axes of symmetry of the fringe pattern displayed by the gage.

The stress ratio, on the other hand, can also be obtained by comparison of the type of the actual fringe pattern with the calculated one. A more exact procedure, however, is to be based upon a comparison of the actual fringe pattern with calibrated ones. In cases of different Poisson's ratios of the gage material and the structural material, a correlation diagram (Fig. 11) can be used for correcting the stress ratio as apparent in the gage in order to obtain the true stress ratio which is acting in the specimen.

The magnitudes of the stresses acting at a certain region at the surface of a structural part can also be evaluated from the biaxial gage. This is done by multiplying the fringe order observed at a particular point of the gage—for example, at a point *B* as marked in Fig. 11—with a modified gage factor and the stress ratio. The determination of the magnitudes of the stresses by aid of the biaxial strain gage is more complicated than a determination by aid of the uniaxial gage. The latter is therefore preferable for this purpose. The biaxial photoelastic strain gage, however, is extremely well suited for the determination of the directions of the principal strains and stresses and also useful for a fast approximate determination of the stress ratio.

Special Advantages of Photoelastic Strain Gages

Photoelastic strain gages have numerous advantages over other strain gages. The most remarkable one is that these gages do not require any complicated and expensive or troublesome additional equipment for conducting strain measurements. The gage provides quick information.

The magnitude of the strain can be read directly from a scale attached to the uniaxial gage. The gage also indicates instantaneously; i.e., changes in strain are indicated practically without any inertia effect.

A number of gages can be observed or photographed at the same time. The variation of strain in a structural part due to periodic loading can be observed by aid of photoelastic strain gages if a stroboscopic light source is used.

For the same condition of loading, a multichannel electronic computer would be necessary if electric-resistance strain gages were employed for immediate determination, for example, of the principal strain directions. Even very small biaxial photoelastic strain gages ($^1/_4$ in. in diameter) provide an accurate means to find the principal strain directions. Unlike the electric-resistance strain gages, photoelastic strain gages can be used in explosive atmosphere where high-voltage equipment—as required with

Fig. 10—Biaxial gage. Actual fringe patterns for different stress ratios. (A, B) $S_{II}/S_I = 0$, (C) $S_{II}/S_I = {}^1/_3$, (D) $S_{II}/S_I = {}^2/_3$, (E) $S_{II}/S_I = 1$, (F) $S_{II}/S_I = -{}^1/_3$, (G) $S_{II}/S_I = -{}^2/_3$, (H) $S_{II}/S_I = -1$

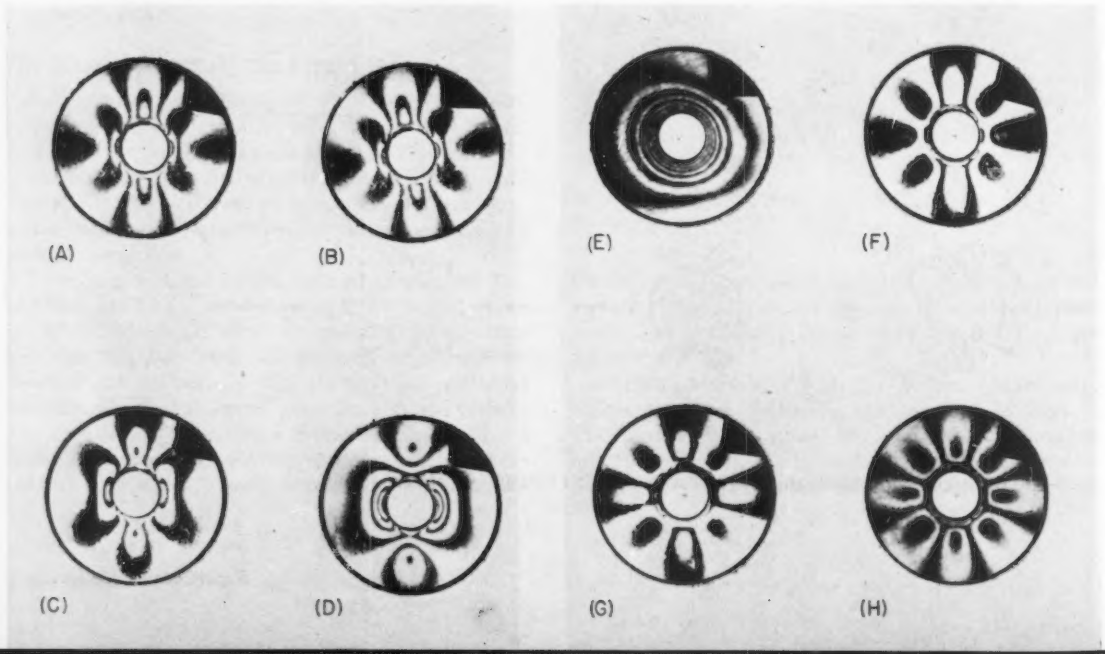

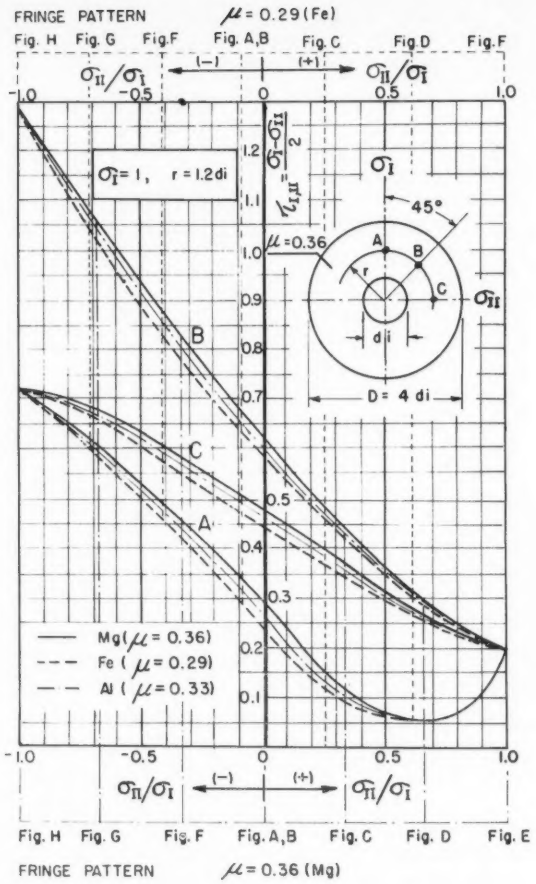
FRINGE PATTERN
μ = 0.29 (Fe)
Fig. H Fig. G Fig. F Fig. A,B Fig. C Fig. D Fig. F
σII/σI
(−)
(+)
σI = 1, r = 1.2di
45°
μ = 0.36
D = 4 di
Mg (μ = 0.36)
Fe (μ = 0.29)
Al (μ = 0.33)
Fig. H Fig. G Fig. F Fig. A,B Fig. C Fig. D Fig. E
FRINGE PATTERN
μ = 0.36 (Mg)

Fig. 11—Biaxial gage. Stress ratio correlation diagram for different structural materials

electric-resistance strain gages, electric-capacitance gages or inductance strain gages—is not permissible.

Telemetering of strain sensed by photoelastic strain gages can also be done in an explosive atmosphere since the photoelastic telemetering device can be completely encased. The ease of setting up a test using photoelastic strain gages results, in general, in considerable saving of time over measurements with other types of strain gages, for instance, rosette gages.

Photoelastic strain gages can withstand rough handling without being disturbed. That signifies another advantage over other strain gages such as mechanical, optical, acoustical and pneumatical strain gages.

With the birefringent-coating method,[7] as well as with an older type of photoelastic strain gage,[8] continuous strain readings for continuous changes in loading at a certain point can be obtained only by employing additional optical compensating devices. Continuous readings with these newly developed photoelastic strain gages do not require additional equipment since these new gages apply

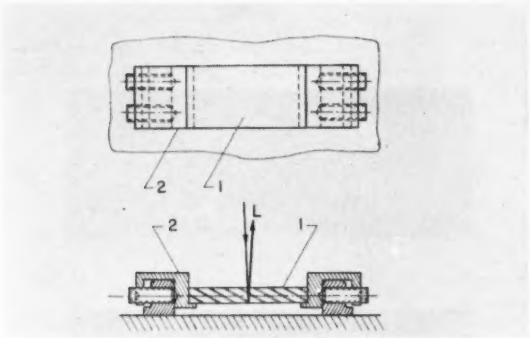

Fig. 12—Design diagram of a high-temperature uniaxial photoelastic strain gage

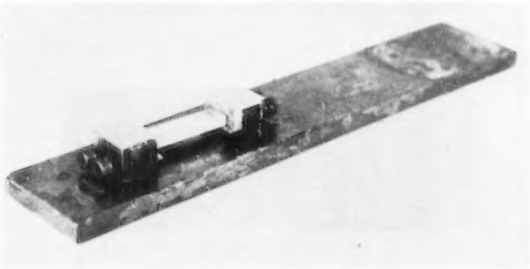

Fig. 13—High-temperature uniaxial strain gage

the frozen-stress method* and the stress concentration effect for obtaining continously moving fringe lines and continuity in indication.

The same photoelastic strain gage can be used for measuring strains at different locations by repeated removal of the gage, if due care is taken in this procedure. The advantages of the photoelastic strain gage over X-ray stress analysis and brittle-lacquer stress analysis—which latter method requires repeated preparation of the specimen for determining stresses caused by different types of loading—are obvious.

Imperfect bond of the photoelastic strain gage, as well as faulty load applications, can easily be detected by aid of the fringe pattern. There is no equivalent method for detecting such sources of error in the case of electric-resistance strain gages.

Further Developments

A promising field for future applications of photoelastic strain gages are strain measurements at high and at extremely high temperatures. Measurements of this kind are becoming more and more important.

The principle of the photoelastic strain gages can be extended to high and to extremely high temperature by virtue of the strain-optical and the physical properties of certain photoelastic materials. Those

** The author proposed the application of the frozen-stress method besides to uniaxial gages also to biaxial photoelastic strain gages in his US-patent application Serial No. 816 918 May 29, 1959.*

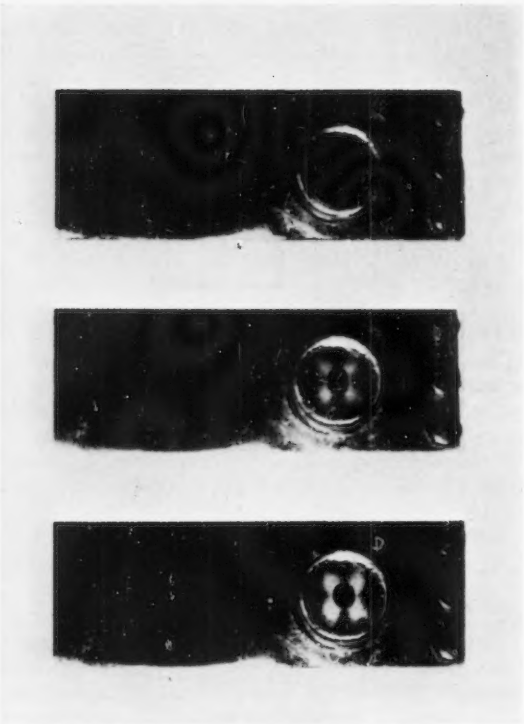

Fig. 14—High-temperature biaxial photoelastic strain gage. Effect of increasing the load

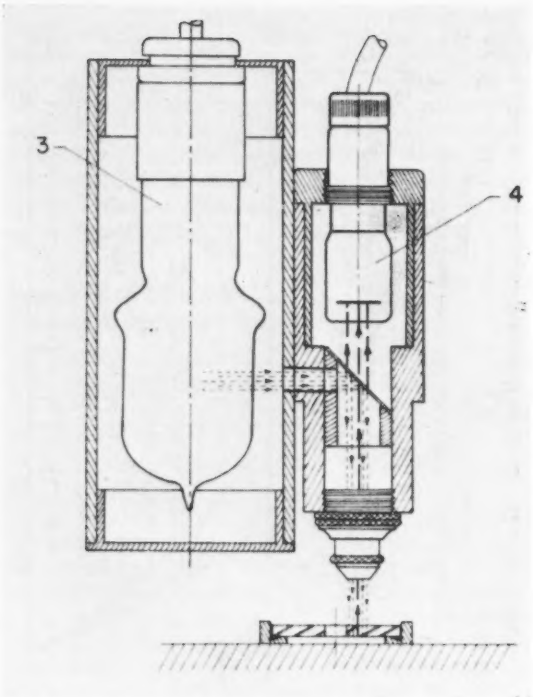

Fig. 15—Photoelectronic micro-telemeter for photoelastic strain gage measurements (design diagram). 3—monochromatic light source, 4—phototube

materials suited for extremely high temperatures are diamond and synthetic gems such as sapphire and corundum, for example. Heat-resistant glass is suited for high-temperature applications of photoelastic strain gages.

The strain-optical constants of glass and of diamond are approximately equal. These constants and the elastic properties (Young's modulus) which influence the characteristic behavior of a photoelastic strain gage change little in wide temperature ranges up to close to the softening and melting points of these materials. The melting point of heat-resistant glass is approximately 1400° F, the limitations for diamond are at 6000° F and those for synthetic gems lie in between, while stainless steel and tungsten have melting points of 2500 and 6150° F, respectively.

Since Young's modulus of stainless steel drops from 28×10^6 psi at room temperature to approximately 20×10^6 psi at 1000° F, and since its yield strength diminishes in almost the same ratio, the elastic strains obtainable and, therefore, the requirements on sensitivity are almost the same as those discussed for normal temperatures.

Figures 12 and 13 show a design sketch of a uniaxial high-temperature photoelastic strain gage and also an actual gage brazed to a steel specimen. A simple reading device facilitates strain readings with this uniaxial strain gage.

Besides the uniaxial high-temperature strain gage, a biaxial photoelastic high-temperature strain gage was developed. This type of gage utilizes the stress concentration effect and consists of a transparent circular plate having a hole at its center and a metal plate holder. Such a gage using pyrex glass as a photoelastic strain indicator is demonstrated in Fig. 14, showing the optical effect displayed by the gage in the unloaded state as well as under load which was increased in two steps. The heat-resistant glass gage can be used up to temperatures of 1200° F.

For the purpose of remote strain measurements, a photoelectronic micro-telemetering device (Fig. 15) has been developed. This device was designed for connection to the terminals of an oscilloscope. Further efforts, however, have to be made for a thorough development of the high-temperature photoelastic strain gages.

As another development, the application of spectroscopic methods to photoelastic-strain-gage measurements might be mentioned. A white light source supplying a continuous spectrum is used to illuminate the strain gage and a spectroscopic device is used for analysis of the light emerging from the gage. When changing the strain acting on the gage, a dark line indicating the phase difference in the gage is displaced in the spectrum visible on the screen of the instrument. Since a strain of 1000 microin/in. applied to the uniaxial gage (Fig. 1) produced a displacement of one fringe order, and since there are approximately 5000 Å units per wave length, a meas-

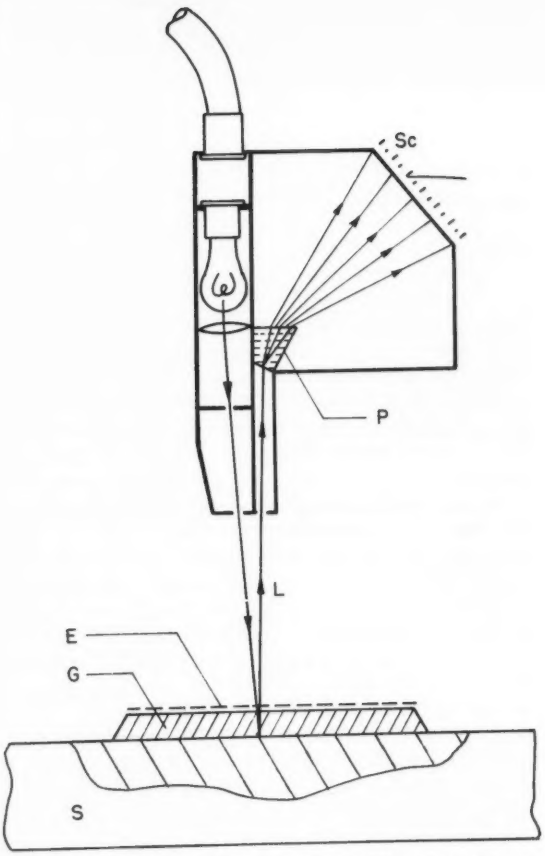

Fig. 16—Reflection-spectroscope for photoelastic strain gage measurements (schematic diagram). S—specimen, G—photoelastic strain gage, E—polarizing film, L—beam of light, P—prism, Sc—scale on spectrum screen

urement with an accuracy of 5 Å units corresponds to an accuracy in strain of approximately 1 microin/in. This accuracy in Angstrom units was obtained in practical measurements, whereas a greater accuracy could be obtained by employing a high-quality spectrometer. Figure 16 shows a schematic diagram of a reflection-spectroscope which was designed for facilitating precision measurements with photoelastic strain gages. From the results thus far obtained, it is concluded that great requirements on accuracy can be met by photoelastic strain gages.

For recording oscillating strain, a bridgelike photoelastic strain gage has been developed (Fig. 17). A frozen-in fringe line, L, is made visible at the rear face, R, of the gage plate, G, by attaching polarizing film to the rear as well as to the front face of that plate. The trace, T, of the oscillating fringe line as caused by oscillating strain is recorded by simple contact printing without any other photographic equipment than a light sensitive film, F, or a contact-printing paper moved through the gap left between gage and specimen, a suitable casing and a common means of transportation of the film and some light source.

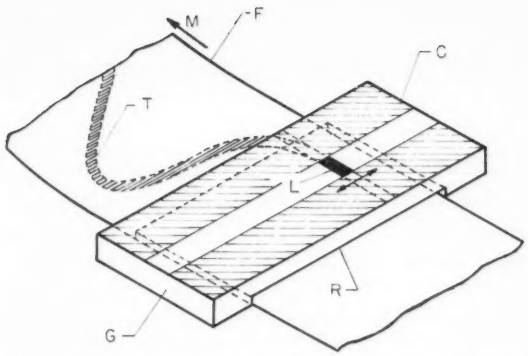

Fig. 17—Schematic diagram of a photoelastic strain gage for recording oscillating strain. G—gage plate, L—fringe line, R—rear face of gage plate, F—photographic film, M—direction of transportation of film, T—trace of fringe line, C—lightproof covering material

Conclusions

Two new types of photoelastic strain gages have been developed. The fundamentals of these gages are treated and their advantages—direct indication of strain magnitudes and of strain directions—are demonstrated. The application of photoelastic strain gages to high and extremely high-temperature strain analysis is promising and in progress.

Acknowledgments

The development of the photoelastic strain gages as described in the foregoing has been supported by the David Taylor Model Basin, Washington, D.C., especially by J. S. Brock of that institution.

The Department of Engineering Mechanics of The Pennsylvania State University, University Park, Pa., headed by J. Marin, gave facilities for the investigations. The assistance of the following collaborators in the work is acknowledged: J. Schwaighofer, P. H. Dehoff, W. L. Bingham, U. Rimrott, and Y. C. Lee. The development of these photoelastic strain gages was started at the end of 1956.

References

1. *Oppel, G.*, "*Photoelastic Strain Gages for Strain Analysis on Structural Parts and Machines*" (*Spannungsoptische Messelemente fuer die Bean spruchungsermittlung an Bauteilen und Maschinen*), Industrie-Anxeiger *No. 96, 1449–1451 (1958).*

2. *Hetenyi, M.*, Handbook of Experimental Stress Analysis, *Drucker, D. C., "Three Dimensional Stress Analysis, pp. 924–950, John Wilev & Sons, New York (1950).*

3. *Oppel, G., "The Photoelastic Investigation of Three-dimensional Stress and Strain Conditions," National Advisory Committee for Aeronautics, T. M. No. 824, 1–17 (1937).*

4. *Schwaighofer, J., "Applications of Photoelastic Strain Gages," Paper No. 575, SESA Meeting, Detroit, Mich. (Oct. 21–23, 1959).*

5. *Kirsch, G., "Die Theorie der Elasticitaet und die Beduerfnisse der Festigkeitslehre,"* Z. VDI, 42, *No. 29, 709, 805, 806 (1898).*

6. *Timoshenko, S., and Goodier, J. N.*; Theory of Elasticity, *McGraw-Hill Book Co., New York, particularly pp. 78–82 (1951).*

7. *Oppel, G., "The Photoelastic Lacquer and Surface Layer Method for Stress and Strain Analysis at the Surface of Metal Parts,"* Z. Ver. deut. Ing., ZVDI, 81, *803–804 (1937).*

8. *Mabboux, G., "Process and Device for the Application of Elasticimetry Particularly of Photoelasticimetry," U. S. Pat. 2,014, 688 (1935).*

9. *Oppel, G., "Direct Indicating Photoelastic Strain Gages for Strain and Stress Analysis on Structural Parts,"* Z. Ver. deut. Ing. (ZVDI), 101, *No. 20, 809–816 (1959).*

Effects of the Thickness of Birefringent Coatings

Experimental procedure is suggested for evaluating an unknown distribution of strain at the metal surface on the basis of the observed photoelastic pattern

by J. Duffy

ABSTRACT—It is known that birefringent coatings are a powerful experimental technique for the determination of surface strains of metals or other opaque bodies. In this paper the complete state of strain in such a coating is determined for an arbitrary one-dimensional variation of the displacement at the metal surface. It is shown that strain gradients or curvature of the surface have a pronounced effect on the observed birefringence, and must be taken into consideration. This can be done by means of two correction factors derived in the paper which take into account the elastic properties of the coating and its thickness. An experimental procedure is outlined for determining an unknown distribution of strain at the metal surface on the basis of the observed photoelastic pattern.

Introduction

The strain on the surface of a metallic body can be determined by the use of a reflection polariscope and a birefringent coating on the polished metal surface. This method was originally conceived by Mesnager.[1] Recently, it has been developed into a practical tool for stress analysis by D'Agostino, Drucker, Liu and Mylonas, who performed an extensive study of the photoelastic properties of epoxy resins and of the behavior of birefringent coatings.[2, 3] It was found that the strain-optical sensitivity of the epoxy resins is sufficiently high so that, even with a thin coating, an appreciable birefringence is obtained for elastic or plastic strains in metals. (The resin with the highest sensitivity had a strain optical coefficient of 1.5×10^{-4} strain difference per fringe per inch thickness.)

An important advantage of the birefringent coating over other means of strain measurement is that the strain is obtained over the entire coated area in a single picture. On the other hand, the observed birefringence is directly proportional to the surface strain at a point only as long as the strain is uniform over the surface or changes little over distances comparable to the coating thickness. In such cases, it is relatively easy to determine the strain. However, in the presence of strain gradients at the metal surface, the deformation of the coating will vary across its thickness and the observed birefringence will depend on the magnitude of the strain and also on the intensity of its gradient. In addition, the photoelastic pattern will be affected by any curvature of the metal surface occurring under load. In this paper, a study of the effects of coating thickness and surface curvature is presented. Its purpose is to extend the application of the coating technique to the determination of arbitrary surface strains. Fourier or power series are used to approximate the strains over the region of the surface which is of interest. For the present, however, the method is limited to one-dimensional variations in the displacement at the metal surface.

J. Duffy is Associate Professor of Engineering, Brown University, Providence, R. I.

Paper presented at 1958 SESA Annual Meeting held in Albany, N. Y., on November 12–14.

The results presented in this paper were obtained in the course of research sponsored by the Ballistic Research Laboratories of Aberdeen Proving Grounds under Contract DA-19-020-ORD-798.

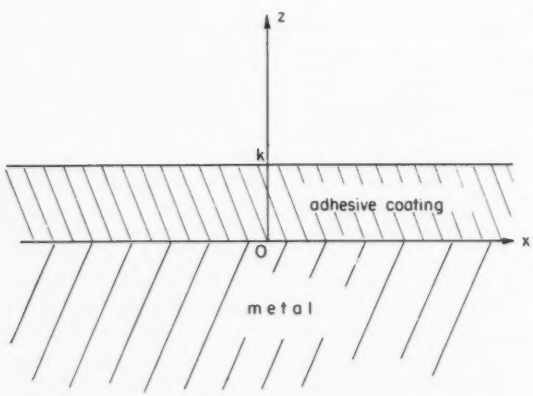

Fig. 1—Section through coating and metal

Statement of the Problem

When the metal is under strain, the adhesive coating, in general, will undergo elastic deformation even for plastic strains in the metal of the order of several percent. Under these conditions, the problem of finding the state of stress in the adhesive is one of elasticity. Figure 1 shows an infinite adhesive strip of thickness k with a given displacement on the metal side and zero traction on the other. The boundary between metal and plastic is the plane of x and y, and the normal to the coating is the z-axis of a rectangular coordinate system. Rectangular components of displacement are designated by u, v and w.

In the plane of the interface between metal and coating, v is set equal to zero, and a solution is sought for which

$$u = u(x, z)$$
$$v = 0$$
$$w = w(x, z) \quad (1)$$

represent the displacement at any point of the coating. The nonvanishing components of strain are

$$\epsilon_{xx} = \frac{\partial u}{\partial x}, \qquad \epsilon_{zz} = \frac{\partial w}{\partial z}, \qquad 2\epsilon_{xz} = \frac{\partial w}{\partial x} + \frac{\partial u}{\partial z} \quad (2)$$

while σ_{xx}, σ_{zz} and σ_{xz} designate the corresponding stress components. At the interface, $z/k = 0$, the displacement components u_0 and w_0 are to be arbitrary functions of x. The requirement of zero traction across the free surface is met by setting

$$\sigma_{zz} = \sigma_{xz} = 0 \quad \text{at } z/k = 1 \quad (3)$$

Solutions are obtained for a displacement on the boundary $z/k = 0$ expressed either as a Fourier series or a power series in the x-coordinate.

Interface Displacement Expressed as Fourier Series

The solution first is established for a displacement at the interface given by

$$u_0 = A \cos px + B \sin px$$
$$w_0 = C \cos px + D \sin px \quad (4)$$

in which A, B, C and D represent amplitudes of displacement and the wave number $p = 2\pi/\lambda$, where λ is the wave length of the displacement. (For an arbitrary displacement at the interface, the solution of the elasticity problem is obtained by use of Fourier's theorem through a superposition of solutions based on the surface displacements which eqs. (4) provide.) For equilibrium it is necessary that the functions $u(x, z)$ and $w(x, z)$ satisfy the equations

$$2(1 - \nu)\frac{\partial^2 u}{\partial x^2} + (1 - 2\nu)\frac{\partial^2 u}{\partial z^2} + \frac{\partial^2 w}{\partial x \partial z} = 0$$
$$\frac{\partial^2 u}{\partial x \partial z} + (1 - 2\nu)\frac{\partial^2 w}{\partial x^2} + 2(1 - \nu)\frac{\partial^2 w}{\partial z^2} = 0 \quad (5)$$

where ν is Poisson's ratio. (If $\nu = {}^1/_2$, eqs (5) are equivalent to the condition of incompressibility of the material.) In addition these functions must satisfy the conditions at the boundary $z/k = 0$ of eq (4), and the requirement of zero traction across the free surface expressed by eq (3).

In order to simplify the mathematical expressions, the solution is presented in two parts, the complete solution being obtained by their superposition. In the first part, it is specified that $C = D = 0$ so that the interface undergoes no curvature as loading progresses. In the second part, on the other hand, C and D are arbitrary but interface strain is excluded by letting $A = B = 0$.

If $C = D = 0$ it may be shown that the biharmonic functions

$$u = (A \cos px + B \sin px)[(\Gamma_1 - \Gamma_3 pz)e^{pz} + (\Gamma_2 - \Gamma_4 pz)e^{-pz}]$$
$$w = (A \sin px - B \cos px)[(\Gamma_1 - \Gamma_3 pz)e^{pz} - (\Gamma_2 - \Gamma_4 pz)e^{-pz} + (3 - 4\nu)(\Gamma_3 e^{pz} + \Gamma_4 e^{-pz})] \quad (6)$$

are solutions of eqs (5) and will satisfy the boundary conditions for a proper choice of constants Γ_1, Γ_2, Γ_3 and Γ_4. For convenience, the Γ's are expressed in terms of a new set of constants φ_1, φ_2, φ_3 and φ_4 through the relations

$$\Gamma_1 = \varphi_1/(\varphi_1 + \varphi_2) \qquad \Gamma_3 = \varphi_3/(\varphi_1 + \varphi_2)$$
$$\Gamma_2 = \varphi_2/(\varphi_1 + \varphi_2) \qquad \Gamma_4 = \varphi_4/(\varphi_1 + \varphi_2) \quad (7)$$

from which it may be seen that only three of the φ's are independent and that

$$\Gamma_1 + \Gamma_2 = 1$$

as required by the first of eqs (4). The second boundary condition at $z/k = 0$ requires that there be no curvature of the interface. This condition is met if

$$\varphi_1 - \varphi_2 + (3 - 4\nu)(\varphi_3 + \varphi_4) = 0 \quad (8)$$

leaving only the conditions at $z/k = 1$ to be satisfied. Inserting the displacement given by eqs (6) into eqs (2) and using Hooke's law, one obtains for the stress components

$$\sigma_{xx} = -2p\mu(A \sin px - B \cos px)[(\Gamma_1 - \Gamma_3 pz)e^{pz} + (\Gamma_2 - \Gamma_4 pz)e^{-pz} - 2\nu(\Gamma_3 e^{pz} - \Gamma_4 e^{-pz})]$$
$$\sigma_{zz} = 2p\mu(A \sin px - B \cos px)[(\Gamma_1 - \Gamma_3 pz)e^{pz} + (\Gamma_2 - \Gamma_4 pz)e^{-pz} + 2(1 - \nu)(\Gamma_3 e^{pz} - \Gamma_4 e^{-pz})]$$
$$\sigma_{xz} = 2p\mu(A \cos px + B \sin px)[(\Gamma_1 - \Gamma_3 pz)e^{pz} - (\Gamma_2 - \Gamma_4 pz)e^{-pz} + (1 - 2\nu)(\Gamma_3 e^{pz} + \Gamma_4 e^{-pz})] \quad (9)$$

which satisfy the equilibrium conditions

$$\frac{\partial \sigma_{xx}}{\partial x} + \frac{\partial \sigma_{zx}}{\partial z} = 0, \qquad \frac{\partial \sigma_{xz}}{\partial x} + \frac{\partial \sigma_{zz}}{\partial z} = 0$$

for any value of Poisson's ratio. To satisfy the boundary conditions given by eqs (3) it is necessary that

$$(\varphi_1 - \varphi_3 pk)e^{pk} + (\varphi_2 - \varphi_4 pk)e^{-pk} + 2(1 - \nu)(\varphi_3 e^{pk} - \varphi_4 e^{-pk}) = 0$$
$$(\varphi_1 - \varphi_3 pk)e^{pk} - (\varphi_2 - \varphi_4 pk)e^{-pk} + (1 - 2\nu)(\varphi_3 e^{pk} + \varphi_4 e^{-pk}) = 0 \quad (10)$$

Eqs (8) and (10) constitute a system of three linear algebraic equations in the ratios of the φ's. It may be shown that they are satisfied for

$$\varphi_1 = 1 + 2(3 - 4\nu)e^{-2pk} + [2pk - (3 - 4\nu)]^2$$
$$\varphi_2 = 1 + 2(3 - 4\nu)e^{2pk} + [2pk + (3 - 4\nu)]^2$$
$$\varphi_3 = 2[2pk - (3 - 4\nu) - e^{-2pk}]$$
$$\varphi_4 = 2[2pk + (3 - 4\nu) + e^{2pk}] \quad (11)$$

which determine the constants Γ_1, Γ_2, Γ_3 and Γ_4 uniquely.

An arbitrary displacement u_0 at the interface can be expressed as the Fourier series

$$u_0 = {}^1/_2 A_0 + \sum_{n=1}^{\infty} A_n \cos p_n x + \sum_{n=1}^{\infty} B_n \sin p_n x \quad (12)$$

where

$$A_n = \frac{1}{c}\int_{-c}^{c} u_0(\xi) \cos \frac{n\pi\xi}{c}\, d\xi$$
$$B_n = \frac{1}{c}\int_{-c}^{c} u_0(\xi) \sin \frac{n\pi\xi}{c}\, d\xi$$

and $p_n = n\pi/c = 2\pi/\lambda_n$. In these expressions, n is a positive integer, and $2c$ is the interval of expansion of u_0. The displacement components $u(x, z)$ and $w(x, z)$ which fulfill equilibrium and boundary conditions are

$$u = {}^1/_2 A_0 + \sum_{n=1}^{\infty} (A_n \cos p_n x + B_n \sin p_n x) \times [(\Gamma_{n1} - \Gamma_{n3} p_n z)e^{p_n z} + (\Gamma_{n3} - \Gamma_{n4} p_n z)e^{p_n z}]$$

$$w = \sum_{n=1}^{\infty} (A_n \sin p_n x - B_n \cos p_n x)\,[(\Gamma_{n1} - \Gamma_{n3} p_n z) e^{p_n z} - (\Gamma_{n2} - \Gamma_{n4} p_n z) e^{-p_n z} + (3 - 4\nu)(\Gamma_{n3} e^{p_n z} + \Gamma_{n4} e^{-p_n z})] \quad (13)$$

in which the constants Γ_{nf} are given by eqs (7) with φ_{nf} replacing φ_f, and the constants φ_{nf} by eqs (11) where p_n replaces p.

If the interface undergoes a change in curvature under load but no extensional strain, the solution is obtained in a similar manner. The constants A and B in eqs (4) are set equal to 0 and C and D are allowed arbitrary values. It may be shown that the equilibrium conditions given by eqs (5) are satisfied if

$$u = (-C \sin px + D \cos px)\,[(\Gamma_1' - \Gamma_3' pz) e^{pz} - (\Gamma_2' - \Gamma_4' pz) e^{-pz} - (3 - 4\nu)(\Gamma_3' e^{pz} + \Gamma_4' e^{-pz})]$$

$$w = (C \cos px + D \sin px)\,[(\Gamma_1' - \Gamma_3' pz) e^{pz} + (\Gamma_2' - \Gamma_4' pz) e^{-pz}] \quad (14)$$

where

$$\Gamma_1' = \varphi_1'/(\varphi_1' + \varphi_2') \qquad \Gamma_3' = \varphi_3'/(\varphi_1' + \varphi_2')$$
$$\Gamma_2' = \varphi_2'/(\varphi_1' + \varphi_2') \qquad \Gamma_4' = \varphi_4'/(\varphi_1' + \varphi_2') \quad (15)$$

and the φ's, found in the same way as before from the boundry conditions, are given by

$$\varphi_1' = 1 + 2(3 - 4\nu) e^{-2pk} + [2pk + (3 - 4\nu)]^2$$
$$\varphi_2' = 1 + 2(3 - 4\nu) e^{2pk} + [2pk - (3 - 4\nu)]^2$$
$$\varphi_3' = 2[2pk + (3 - 4\nu) + e^{-2pk}]$$
$$\varphi_4' = 2[2pk - (3 - 4\nu) - e^{2pk}] \quad (16)$$

It may be noted that

$$\varphi_1 + \varphi_2 = \varphi_1' + \varphi_2' = 8[(pk)^2 + (3 - 4\nu)\cosh^2 pk + (1 - 2\nu)^2]$$

For an arbitrary curvature of the interface the expressions for $u(xz)$ and $w(xz)$ in terms of Fourier series are given by expressions which can be obtained in the same way as were eqs (13).

Example of a Displacement Expressed as a Trigonometric Function

The behavior of the plastic coating under load will be illustrated by a simple example. Suppose the displacement at the interface is

$$u_0 = A \cos px$$
$$w_0 = 0$$

then eqs (6) with $B = 0$ give the displacement at any point of the coating. The magnitude of the displacement obviously depends on the value of the ratio λ/k. In Fig. 2 such displacements are plotted for three thicknesses of coatings given by λ/k = 1, 2, and 10. In each case, Poisson's ratio is equal to one half. Consider the coating in Fig. 2(*a*) for which $\lambda/k = 10$. This coating may be considered thin since its thickness is only $^1/_{10}$ of the wave length of the applied strain. The displacement component u decreases in magnitude as z goes from the interface to the free surface (except at $x = \lambda/4$ where it vanishes across the whole thickness). However, within any one cross section, it always has the same sign. At the free surface, for instance, the value of the strain is reduced to about 42% of its value at the interface, and the average strain across the thickness

$$\frac{1}{k}\int_0^k \frac{\partial u}{\partial x}\,dz$$

is about 65% of the strain at the interface. On the other hand, for $\lambda/k = 2$ as may be seen in Fig. 2(b) the strain decreases much more rapidly with thickness, vanishes at about $z/k = 0.4$, and from there to the free surface has a reversed sign. The average strain is only about 8% of the strain at the interface. Finally, if $\lambda/k = 1$, Fig. 2(c), the strain dies down very rapidly and reverses sign at about $z/k = 0.2$. In this case, the average strain across the thickness is only about 0.4% of the interface strain.

From a study of this simple example, one anticipates a result derived more fully in the next section; namely, for a surface not subjected to curvature, the birefringence measured with a reflection polariscope does not increase linearly with the thickness of the coating, and even decreases for a coating of sufficient thickness. In other words, for a given λ there is a coating thickness k for which the fringe order is a maximum. It is important to know what this

Fig. 2—Displacement in coating for interface displacement $u_0 = A \cos px$

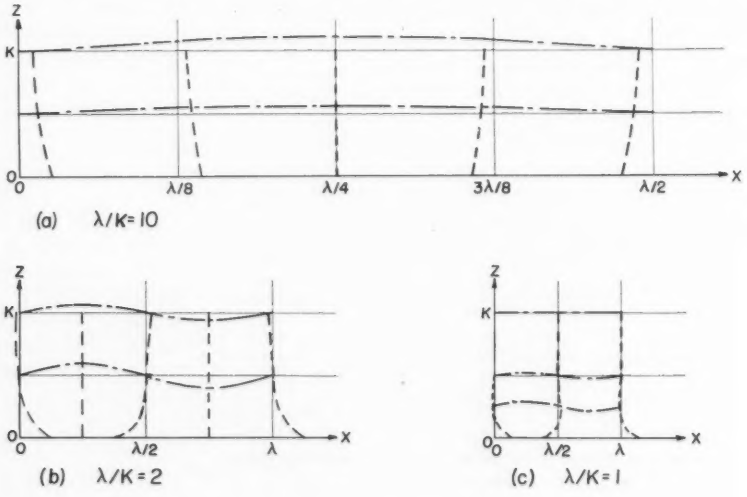

thickness is for any experiment, since even with the most sensitive materials available, fringe orders obtained in the reflection polariscope are not high.

On the other hand, it may be shown that for an interface displacement given by

$$u_0 = 0$$
$$w_0 = C \cos px$$

TABLE 1—VALUES OF CORRECTION FACTORS F AND G

Poisson's Ratio	λ/k	F	pk F	G
0.3	0.5	..	..	0.555
	1.0	0.0719	0.451	0.545
	1.5	..	..	0.503
	2.0	0.1626	0.510	0.447
	2.5	..	..	0.398
	3.0	0.2594	0.542	0.362
	4.0	0.3506	0.550	0.310
	6.0	0.5116	0.535	0.231
	8.0	0.6357	0.499	0.1751
	10.	0.7251	0.455	0.1325
	12.5	0.8012	0.403	0.0961
	15.	0.8515	0.356	0.721
	20.	0.9096	0.286	0.440
	25.	0.9399	0.236	0.293
	30.	0.9573	0.200	0.0208
	40.	..	..	0.01232
	50.	0.9841	0.1236	0.01197
	100.	0.9959	0.0625	0.00774
	400.	0.9997	0.01258	0.001965
0.4	0.5	..	..	0.713
	1.0	0.0475	0.299	0.697
	1.5	..	..	0.624
	2.0	0.1320	0.413	0.525
	2.5	..	..	0.440
	3.0	0.2318	0.485	0.378
	4.0	0.3218	0.505	0.302
	6.0	0.4771	0.499	0.219
	8.0	0.6003	0.471	0.1650
	10.	0.6925	0.435	0.1262
	12.5	0.7738	0.389	0.0925
	15.	0.8290	0.347	0.0698
	20.	0.8945	0.280	0.0432
	25.	0.9293	0.234	0.0290
	30.	0.9494	0.199	0.0206
	40.	..	..	0.01190
	50.	0.9811	0.1233	0.00771
	100.	0.9952	0.0624	0.001960
	400.	0.9997	0.0157	0.0001232
0.5	0.5	..	..	0.999
	1.0	0.0037	0.0234	0.971
	1.5	..	..	0.842
	2.0	0.0804	0.252	0.669
	2.5	..	..	0.517
	3.0	0.1928	0.404	0.414
	4.0	0.2863	0.449	0.300
	6.0	0.4375	0.458	0.205
	8.0	0.5586	0.438	0.1537
	10.	0.6528	0.410	0.1188
	12.5	0.7392	0.371	0.0881
	15.	0.79991	0.335	0.0672
	20.	0.8743	0.274	0.0421
	25.	0.9149	0.230	0.0284
	30.	0.9390	0.1968	0.0204
	40.	0.9647	..	0.01182
	50.	0.9770	0.1228	0.00768
	100.	0.9941	0.0624	0.001958
	400.	0.9996	0.05172	0.0001232

the fringe order obtained is always greater for a thicker coating.

The Photoelastic Effect

In a reflection polariscope, the fringe order N at any point may be obtained from

$$N = (\epsilon_1 - \epsilon_2)2k/C\epsilon$$

where $C\epsilon$ is the strain-optical coefficient for the coating material and ϵ_1 and ϵ_2 are the secondary principal strains in the plane of the wave front, which in the present instance is the plane of the interface between coating and metal. These strain components can be obtained from the displacement by a summation of strain across the thickness, i.e.,

$$\epsilon_1 = \frac{1}{k}\int_0^k \frac{\partial u}{\partial x}\,dz$$

while $\epsilon_2 = 0$, since $v = 0$. The expected fringe order therefore is given by

$$N = \frac{2}{C\epsilon}\int_0^k \frac{\partial u}{\partial x}\,dz$$

It is convenient to express N in terms of the extensional strain at the interface, $\partial u_0/\partial x$, and the displacement of the interface normal to its plane w_0. If correction factors F and G are defined by

$$F = \frac{1}{k}\int_0^k \left(\frac{\partial u}{\partial x}\right)_1 dz \Big/ \frac{\partial u_0}{\partial x} \tag{17}$$

and

$$G = \int_0^k \left(\frac{\partial u}{\partial x}\right)_2 dz \Big/ w_0 \tag{18}$$

where $(\partial u/\partial x)_1$, is the strain at any point of the coating due to the longitudinal strain at the interface, and $(\partial u/\partial x)_2$ is the strain due to the curvature of the interface, then

$$N = 2[Fk\,\partial u_0/\partial x + Gw_0]/C\epsilon \tag{19}$$

gives the fringe order at any point. The correction factor F is found by inserting u from eqs (6) into eq (17) and making use of eqs (7) and (11) while G is found from eq (18) by inserting u from eqs (14) and making use of eqs (15) and (16). In this way, one can show that

$$\left.\begin{aligned} F &= \frac{2\nu pk\cosh pk - 2\nu(1-2\nu)\sinh pk + (1-2\nu)(2pk + \sinh 2pk)}{pk[(pk)^2 + (3-4\nu)\cosh^2 pk + (1-2\nu)^2]} \\ G &= \frac{4\nu(1-\nu)(1-\cosh pk) - 2\nu pk\sinh pk + (pk)^2 + \sinh^2 pk}{(pk)^2 + (3-4\nu)\cosh^2 pk + (1-2\nu)^2} \end{aligned}\right\} \tag{20}$$

These factors are given in Table 1 for various values of λ/k and are plotted in Figs. 3 and 4.

From these figures, it is apparent that the correction factors are not particularly sensitive to changes in the value of Poisson's ratio for the range of values of this parameter generally encountered in birefringent plastics. The only exception occurs for thick coatings, i.e., for a coating thickness approaching the wave length of the displacement at the interface.

As mentioned above, it is to be expected that the birefringence in a coating under load will be small.

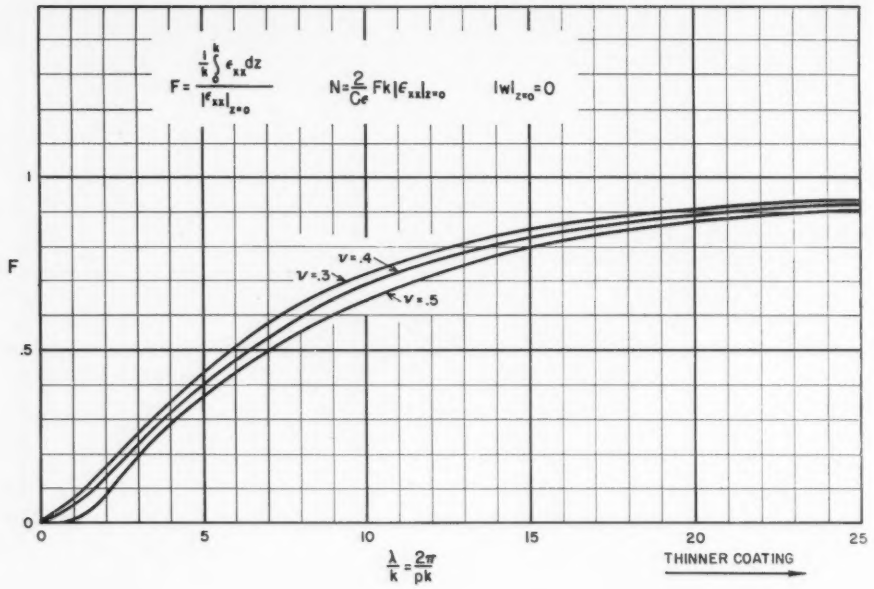

Fig. 3—Dependence of correction factor, F, on coating thickness

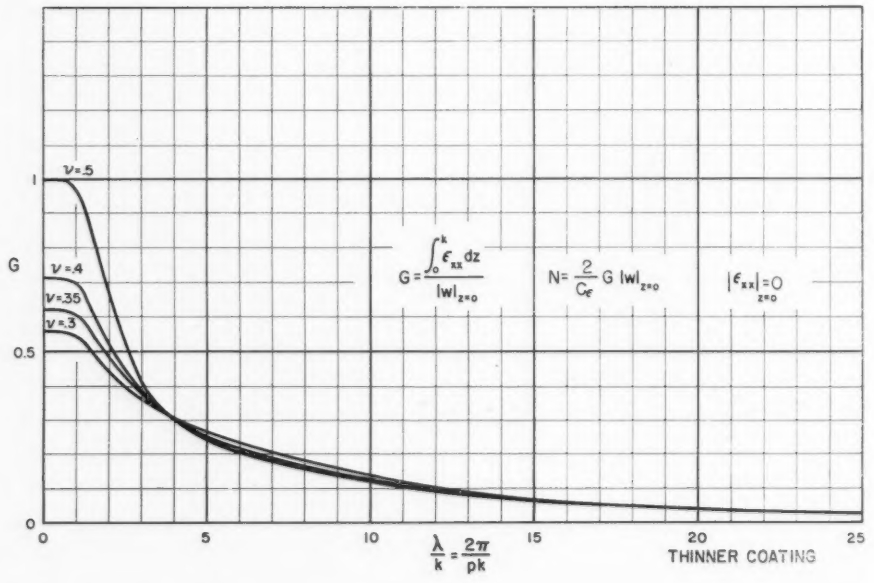

Fig. 4—Dependence of correction factor, G, on coating thickness

Hence, it is important to choose a coating thickness giving the greatest possible fringe order consistent with other requirements. If $u_0 = 0$, it is evident from Fig. 4 that the fringe order is greater for a thicker coating, and that the highest fringe order is obtained when the coating thickness is equal to or greater than the wave length of the displacement. In particular, for a Poisson's ratio of one half (epoxy adhesives at an elevated temperature) and a sufficiently thick coating, the correction factor G approaches unity and the fringe order is given by $N = 2W_0/C\epsilon$ directly.

The situation is not the same for an interface displacement given by u_ϵ. From Fig. 3 it is evident that the factor F is greater for thin coatings. However, fringe order depends on the product of F and coating thickness k. This product is plotted in Fig. 5. It may be seen that an optimum thickness exists which is dependent on the value of Poisson's ratio of the coating material. This can be explained by

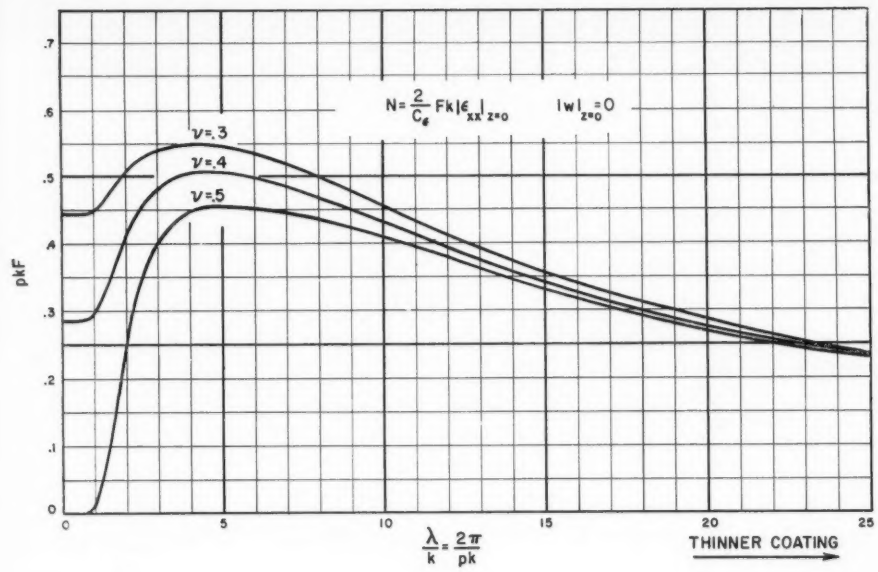

Fig. 5—Dependence of pkF on coating thickness

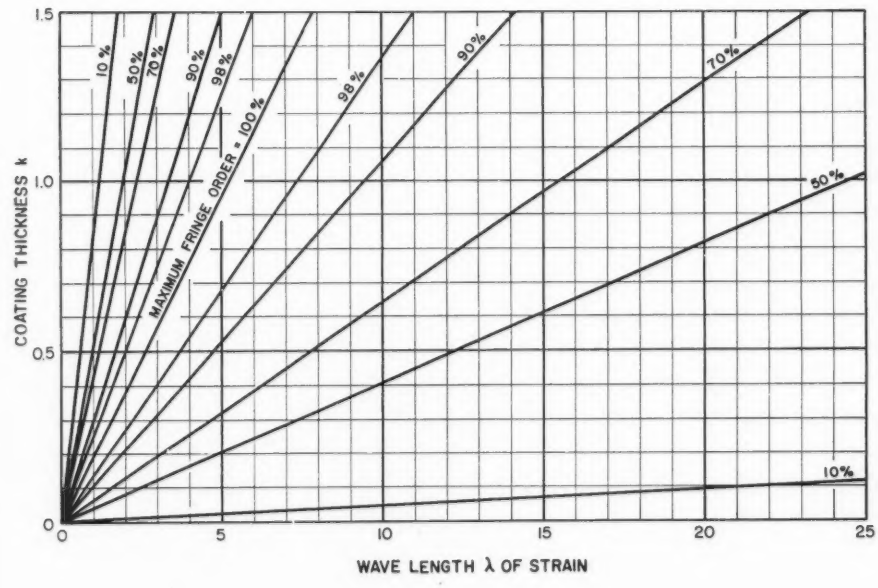

Fig. 6—Variation of fringe order with coating thickness for interface displacement $u = A \cos px$ and $v = {}^1/_2$

referring to the examples illustrated in Fig. 2. In all three cases the strain component $\partial u/\partial x$ is a minimum at the point $x = \lambda/4$ of the interface. The material in the neighborhood of this point is in compression and the coating must "bulge out," i.e., there will be a positive displacement w at points not on the interface. *Per se* this produces no visible photoelastic effect. However, a thick coating offers a resistance to "bulging out" and has a region not far from the interface where the sign of $\partial u/\partial x$ is reversed. This occurs in Fig. 2(c) in the neighborhood of $z/k = {}^1/_4$, in Fig. 2(b) near the free surface, and does not occur in the example of Fig. 2(a) where the thinner coating offers a smaller resistance to "bulging out." It is obvious that this whole effect is more pronounced for a higher Poisson's ratio. Indeed, a displacement $u_0 = A \cos px$ would produce no visible birefringence if the coating were sufficiently thick and its material incompressible. It is expected that departures from conditions of plane

strain would modify these results and increase the values of pkF for thick coatings. Figure 6 is meant as a guide in choosing the thickness of coating to give most fringes when the wave length of surface displacement is known approximately.

Fringe Order in Terms of Fourier Series

The Fourier series solution is particularly useful in finding the fringe pattern for arbitrary (one dimensional) displacements at the interface. For example, suppose that u_0 is given by eq (12). The strain at the interface is

$$|\epsilon_{xx}|_0 = -\sum_{n=1}^{\infty} A_n p_n \sin p_n x + \sum_{n=1}^{\infty} B_n p_n \cos p_n x \quad (21)$$

and the observed fringe order, N, from eq (17) will be given by

$$N = \frac{2}{C\epsilon}\left\{\sum_{n=1}^{\infty}(p_n k F_n)A_n \sin p_n x + \sum_{n=1}^{\infty}(p_n k F_n)B_n \cos p_n x\right\} \quad (22)$$

where F_n is given by the first of eq (20) with p_n replacing p. The factor pkF is plotted in Fig. 5. For a displacement normal to the plane of the coating

$$w_0 = {}^1/_2 C_0 + \sum_{n=1}^{\infty} C_n \cos p_n x + \sum_{n=1}^{\infty} D_n \sin p_n x \quad (23)$$

and from eq (17) the fringe order will be

$$N = \frac{2}{C\epsilon}\left\{\sum_{n=1}^{\infty} G_n C_n \cos p_n x + \sum_{n=1}^{\infty} G_n D_n \sin p_n x\right\} \quad (24)$$

where G_n is given by the second of eqs (20) with p_n replacing p. The reason fringe order is obtained from the Fourier series simply by weighting properly the coefficients is, of course, that the factors F and G do not vary with the x-coordinate. This, in turn, goes back to the separation of the independent variables in the solution given by eqs (6) and (13).

Interface Displacement Expressed as Power Series

A solution of the problem can be found also by the use of polynomials or of power series. However, since the algebra involved is somewhat tedious, only results are presented. The displacement components at any point in the coating are given by the power series in x and z

$$u = \sum_{n=0,1,2\ldots}^{\infty} u_n(x, z) \qquad w = \sum_{n=0,1,2\ldots}^{\infty} w_n(xz) \quad (25)$$

where $u_n(xz)$ and $w_n(xz)$ are functions which satisfy equilibrium and boundary conditions for each separate value of n. At the interface $z/k = 0$, these functions reduce to the following series which involve only the x-coordinate

$$u_0 = \sum_{n=0}^{\infty} U_n (x/k)^n \qquad w_0 = \sum_{n=0}^{\infty} W_n (x/k)^n$$

where U_n and W_n are arbitrary constants. (For a polynomial solution, U_n and W_n are set equal to 0 for values of n greater than the degree of the polynomial.)

The solution is simplified by presenting it in two parts. If the interface undergoes no curvature, all W_n vanish, and it may be shown that

$$u_n = \sum_{p=0,2,4,\ldots}^{n} U_n \frac{n!}{p!(n-p)!}\left(\frac{x}{k}\right)^{n-p} A_p$$

$$w_n = -\frac{z}{k}\sum_{p=0,2,4,\ldots}^{n-1} U_n \frac{n!}{p!(n-p-1)!}\left(\frac{x}{k}\right)^{n-p-1} B_p \quad (26)$$

where the summation is extended only over even integer values of p, including 0, independently of whether n is odd or even. In these equations

$$A_p = \sum_{q=0,1,2,\ldots}^{p} a_{pq}\left(\frac{z}{k}\right)^q$$

$$B_p = \sum_{q=0,1,2,\ldots}^{p} b_{pq}\left(\frac{z}{k}\right)^q \quad (27)$$

where a_{pq} and b_{pq} are determined on the basis of equilibrium and boundary conditions. Certain of these coefficients have been determined as follows:

$a_{00} = 1$

$$\begin{aligned} a_{20} &= 0 \\ a_{21} &= 4/(1-\nu) \\ a_{22} &= -(2-\nu)/(1-\nu) \\ a_{40} &= 0 \\ a_{41} &= 16(2+\nu)/(1-\nu)^2 \\ a_{42} &= -6/(1-\nu)^2 \\ a_{43} &= -4(3-2\nu)/(1-\nu)^2 \\ a_{44} &= (3-\nu)/(1-\nu) \end{aligned}$$

$b_{00} = \nu/(1-\nu)$

$$\begin{aligned} b_{20} &= -(1-2\nu)/(1-\nu)^2 \\ b_{21} &= 1/(1-\nu)^2 \\ b_{22} &= -(1+\nu)/3(1-\nu) \\ b_{40} &= -2(5+2\nu)(1-2\nu)/(1-\nu)^2 \\ b_{41} &= 4(2+\nu)/(1-\nu)^3 \\ b_{42} &= -4\nu/(1-\nu)^2 \\ b_{43} &= -2/(1-\nu)^2 \\ b_{44} &= (2+\nu)/5(1-\nu) \end{aligned} \quad (28)$$

which are valid for $0 \leqslant \nu \leqslant {}^1/_2$.

On the other hand, if surface strain is eliminated by letting $U_n = 0$ for all n, it may be shown that

$$u_n = -\frac{z}{k}\sum_{p=0,2,4,\ldots}^{n-1} \frac{W_n n!}{p!(n-p-1)!}\left(\frac{x}{k}\right)^{n-p-1} C_p$$

$$w_n = \sum_{p=0,2,4,\ldots}^{n} \frac{W_n n}{p!(n-p)!}\left(\frac{x}{k}\right)^{n-p} D_p$$

where

$$C_p = \sum_{q=0,1,2,\ldots}^{p} c_{pq}\left(\frac{z}{k}\right)^q$$

$$D_p = \sum_{q=0,1,2,\ldots}^{p} d_{pq}\left(\frac{z}{k}\right)^q$$

and the c_{pq} and d_{pq} are determined from equilibrium and boundary conditions. Some of these coefficients have been evaluated as follows:

$c_{00} = 1$

$$\begin{aligned} c_{20} &= 2/(1-\nu) \\ c_{21} &= 0 \\ c_{22} &= -(2-\nu)/3(1-\nu) \\ c_{40} &= 4(5+2\nu)/(1-\nu)^2 \\ c_{41} &= -4/(1-\nu)^2 \\ c_{42} &= -2(3-2\nu)/(1-\nu)^2 \\ c_{43} &= 0 \end{aligned}$$

$$c_{44} = (3 - \nu)/5(1 - \nu)$$

and

$$d_{00} = 1 \qquad d_{20} = 0$$
$$d_{21} = 0$$
$$d_{22} = \nu/(1 - \nu)$$
$$d_{40} = 0$$
$$d_{41} = -8(1 - 2\nu)/(1 - \nu)^2$$
$$d_{42} = 6/(1 - \nu)^2$$
$$d_{43} = 0$$
$$d_{44} = -(1 + \nu)/(1 - \nu)$$

The above solution is useful in predicting fringe order over limited regions of the coated metal surface. (For a derivation of the coefficients, reference is made to Technical Report DA 798/34 of the Division of Applied Mathematics, Brown University.) The series solution may be used also to demonstrate that fringe order is influenced in every case by the variation in strain across the thickness of the coating, unless the strain is constant along the interface or varies linearly with distance.

Example of Use of Power Series

As an illustration of the behavior of the coating, suppose it is known that the strain at the surface of the metal vanishes at the origin of the coordinate system and increases as the square of the distance x/k. In this case, all the coefficients U_n are 0 except for $n = 3$. In addition, if there is no curvature of the metal surface, $W_n = 0$. On the basis of the above solution it may be shown that the displacement at any point is given by

$$u = U_3 \left\{ \left(\frac{x}{k}\right)^3 + 3\left(\frac{x}{k}\right)\left[\frac{4}{1-\nu}\frac{z}{k} - \frac{2-\nu}{1-\nu}\left(\frac{z}{k}\right)\right] \right\}$$

$$w = -3U_3 \frac{z}{k} \left\{ \frac{\nu}{1-\nu}\left(\frac{x}{k}\right)^2 - \frac{1-2\nu}{(1-\nu)^2} + \frac{1}{(1-\nu)^2}\frac{z}{k} - \frac{1+\nu}{3(1-\nu)}\left(\frac{z}{k}\right)^2 \right\}$$

This displacement is plotted in Fig. 7 for $\nu = 1/2$ and for $U_3 = 1/4$. In this figure, the dotted lines represent the horizontal displacement of lines originally straight and normal to the interface at $x/k = \pm 1, \pm 2$, the dot-and-dashed line represents the vertical displacement of the free surface. The observed fringe order, based on eqs (27), is

$$NC\epsilon/U_3 = 6(x/k)^2 + 2(4 + \nu)/(1 - \nu)$$

in which the second term is the correction resulting from the effect of thickness. It is obvious that this term cannot be neglected in the neighborhood of the origin.

Determination of Surface Strains by Means of Birefringent Coatings

General

The problem considered so far in this paper is that of predicting the fringe order obtained with a birefringent coating for a given strain distribution at the interface. Of greater interest, however, is the inverse problem, namely, the determination of an unknown state of strain at the metal surface from a study of the fringe pattern in the coating. It has already been demonstrated that birefringent coatings yield a good measure of the interface strain for both elastic and plastic deformation of the metal part.[3] The present analysis provides a means of obtaining more precise results and extending the method to include sharp strain gradients at the metal surface.

The most general one-dimensional deformation at the interface involves gradients in both u_0 and w_0. These gradients may or may not occur in the same region and will have different intensities and magnitudes. The birefringence in the coating is due to the superposed effects of u_0 and w_0, eq (5). These effects must be separated to obtain either the surface strain or the curvature. Usually, it is the surface strain and, hence, u_0 which is of greater interest. Furthermore, w_0 can often be found by some other means, its effect calculated using the results of the present theory and subtracted from the measured values of birefringence. In this way, the effects of curvature can be eliminated and the problem reduced to a determination of surface strain from its photoelastic pattern.

Determining Surface Strain When Curvature is Known

Let us presume that w_0 has been determined, so that its photoelastic effect can be subtracted, and that the coating is to be used to find the surface strain. It can be shown, by using the power-series solution, that fringe order is directly proportional to

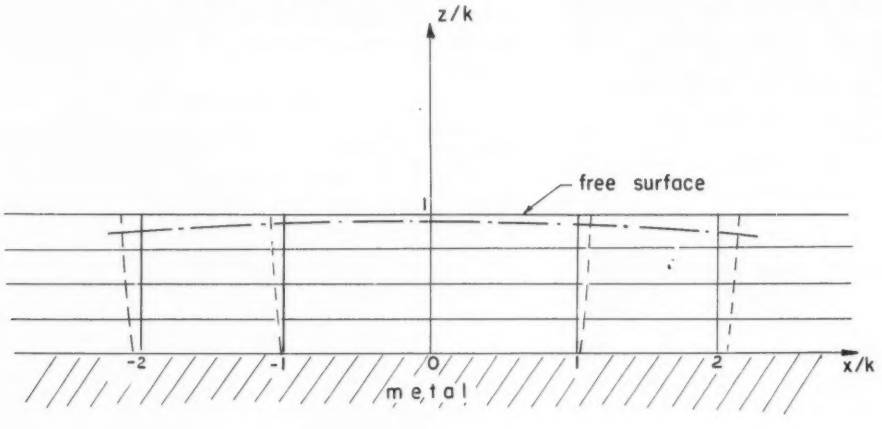

Fig. 7—Deformation of coating for strain at the interface varying as the square of the distance. (Example 1)

surface strain, i.e., that

$$NC\epsilon = 2kF\partial u_0/\partial x \qquad (29)$$

only if the strain is uniform or varies linearly with distance. In all other cases, the use of eq (29) to determine the surface strain will lead to errors which may easily be of significant magnitude. Thus, even for the example shown in Fig. 2(a), in which the coating is quite thin, eq (29) would give an error of 35% in the surface strain. It is also evident that the same correction factor F cannot be employed for the entire surface: its value must be adjusted in accordance with variations in the wave length of the strain gradient. However, if the coating is sufficiently thin, the value of F approaches unity and the fringe order, from eq (19), approaches the value given by eq (29) which may be used to determine surface strain. This method, while correct theoretically, has a serious disadvantage in that an extremely thin coating has a very small birefringence which in turn implies large experimental errors. On the other hand, a somewhat thicker coating may give a value of the correction factor F sensibly less than unity over regions having larger strain gradients. One way of overcoming this difficulty is to apply first a very thin coating to give approximate results which are used only to determine reasonable values of λ at the points of interest. Values of F can now be established for a second and thicker coating which will yield more accurate results.

The value of $\partial u_0/\partial x$ can be obtained with still greater precision within a particular region if the coating thickness k is such that the value of pkF from Fig. 5 is near its maximum. One possible procedure to obtain such a value of k is first to apply a very thin coating which is used to find λ for the region in question. Then k is chosen such as to make pkF a maximum and a second coating of this thickness applied. Measurements of birefringence will give the highest fringe order that can be obtained for this region. Obviously, a small error in the value of λ will not greatly affect results since the slope of a curve near its maximum is small.

Use of Coating to Determine Both Surface Strain and Curvature

There are two instances when the birefringent coating can be used to give both u_0 and w_0. In the first, the geometry and loading of the metal part must be such that the expected strain gradients, though perhaps very sharp, are quite short. The displacement w_0 is found first by applying to the metal surface a coating whose thickness exceeds the lengths of the expected gradients in u_0 and w_0. By conducting the test at an elevated temperature, the coating material becomes nearly incompressible and the fringe pattern observed is due almost entirely to w_0 (see Figs. 4 and 5). Furthermore, in this case, the fringe order at each point varies directly with w_0. This can be demonstrated by referring to the theoretical solution. Suppose w_0 were represented by a Fourier series. The length of its interval of expansion $2c$ need not exceed the coating thickness k. Hence $F \backsimeq 0$ and G $\backsimeq 1$ for the first term in the series. Succeeding terms in the series have progressively shorter wave lengths so that the value of λ/k becomes smaller for each term. Hence $F_n \backsimeq 0$ and $G_n \backsimeq 1$ for all terms of the series, so that $N = 2w_0/C\epsilon$ giving w_0 directly in term of N. There remains only the problem of finding u_0. (A procedure for doing this was given above. In following it, the effect of w_0 can be predicted easily for any thickness of coating, since w_0 itself has been determined.)

The limitation on the above method is the thickness of the coating. It is difficult to cast coatings much in excess of 1 in. thick, and, in addition, the reaction of a thick coating on the metal might sensibly change the deformation of the metal surface.

The effects of u_0 and w_0 can also be distinguished if the gradients in w_0 are extremely small. As may be seen in Fig. 4 a thin coating is almost insensitive to w_0, so that $G \backsimeq 0$. The value of N from eq (17) becomes

$$NC\epsilon = 2kF\,\partial u_0/\partial x$$

and the birefringence is due principally to u_0 which can be determined by the method outlined above. In this case it is not necessary to conduct the tests at an elevated temperature.

Conclusion

The ability of birefringent coatings to measure the strain on the surface of a metal part has been established by other investigators. However, experimental results are influenced considerably by two factors not previously investigated; namely, a gradient in the strain at the metal surface, and the curvature of this surface under load. Neglecting either of these factors may lead to large errors and, under certain circumstances, it is possible for one or the other to produce a greater birefringence than does the surface strain.

The results of the present theoretical investigation are applied to the problem of evaluating a strain whose distribution on the metal surface is unknown. An experimental procedure for doing this is suggested.

Bibliography

1. *Mesnager, M., "Sur la Determination Optique des Tensions Interieures dans les Solides a Trois Dimensions," Comptes Rendus, Paris 190, 1249 (1930).*
2. *D'Agostino, J., Drucker, D. C., Liu, C. K., and Mylonas, C., "Epoxy Adhesives and Casting Resins as Photoelastic Plastics" Proceedings of the Society for Experimental Stress Analysis* XII *(2), 123–128 (1955).*
3. *D'Agostino, J., Drucker, D. C., Liu, C. K., and Mylonas, C., "An Analysis of Plastic Behavior of Metals with Bonded Birefringent Plastic," Proceedings of the Society for Experimental Stress Analysis* XII *(2), 115–122 (1955).*

Two-dimensional Photoelastic Study of Turbine-shell Flanges

Five tests dealing with the stress distribution in the flange joint and the optimum width of flanges are reported upon by the author. All tests were conducted on a single model which was modified in successive tests

by P. D. Flynn

ABSTRACT—Results of a two-dimensional photoelastic study of turbine-shell flanges are reported. Equations of transition from model to prototype are given. A special loading jig for applying a uniform pressure to the boundary of a plane model is described. Pertinent aspects of the experimental technique are summarized.

Introduction

A turbine shell operating under today's high steam pressures and temperatures must withstand considerable mechanical and thermal stresses during both starting and continuous operation of the machine. Turbine-shell flanges must be designed to prevent both radial steam leakage and axial interstage leakage, and excessive permanent distortions of the shell must be avoided. As we go to even higher pressures and temperatures, these problems become more severe.

The Large Steam Turbine-Generator Department requested a photoelastic study of the stresses produced in turbine-shell flanges by the mechanical loading due to bolt forces and internal pressure. A turbine shell varies in diameter along the axis of the machine and is a complex three-dimensional structure. It could be analyzed by using three-dimensional photoelastic techniques, but the stress freezing and slicing procedure used in this method is destructive. The two-dimensional photoelastic method, however, is nondestructive, and the model can be re-machined and re-tested to simulate various configurations of interest. When performing a series of tests, this feature may result in a considerable saving of time and effort.

For this investigation, a two-dimensional approach was selected because it provided a convenient means for studying the influence of flange geometry on the stresses at the flange joint. All tests were conducted on a single model which was modified in successive tests. The results of five of these tests dealing with the stress distribution on the flange joint and the optimum width of flanges are given in this paper.

P. D. Flynn was formerly associated with General Engineering Laboratory General Electric Co., Schenectady, N. Y., and is now Associate Professor of Mechanics, Illinois Institute of Technology, Chicago, Ill.

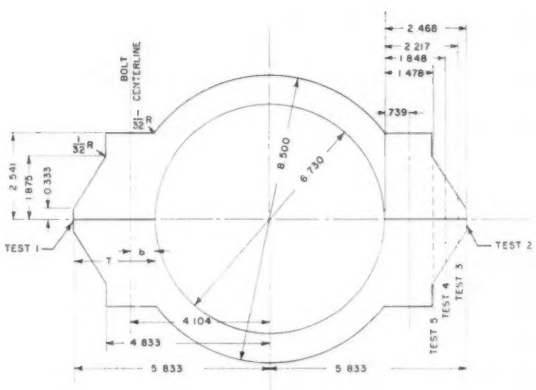

Fig. 1—Photoelastic model of turbine-shell flange and schedule of tests

Test Procedure

Photoelastic Model

A typical cross section through a high-pressure turbine shell was selected for the two-dimensional photoelastic study. The initial dimensions of the model and its subsequent modifications are shown in Fig. 1. The model was machined from a $^1/_4$-in. thick sheet of a thermosetting polyester resin used in photoelasticity.[1] The model was made in two halves in order to obtain a simple butt joint at the flange as in the prototype. Since the flange is solid (Fig. 1), the model corresponds to a cross section of the shell between bolt holes. In the prototype, there are no bolts acting in this cross section. External loads were applied to the model along the bolt centerlines in order to hold the model together and to simulate the effect of bolt forces on the flange joint.

Test 1 was used to determine the stress distribution on the flange joint. In this test the model was symmetrical about both the horizontal and vertical centerlines. Tests 2, 3, 4 and 5 were used to study the influence of the radial width of the flange on the stress at the inner boundary of the shell. It was found that changes in the geometry of the flange on one side of the model did not influence the stress

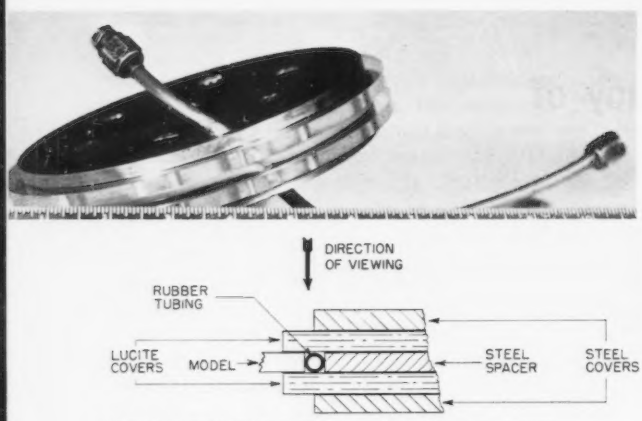

Fig. 2—Loading jig used to apply uniform pressure to interior boundary of model

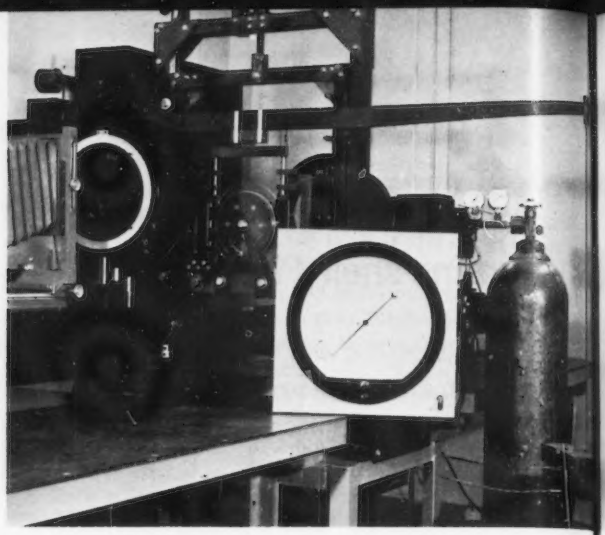

Fig. 3—Experimental setup for two-dimensional study of turbine-shell flanges

pattern on the other side. This fact was used in Tests 3, 4 and 5, i.e., the model was made symmetrical only with respect to the horizontal centerline in these tests.

Pressure-loading Device

A special loading jig for applying a uniform pressure to the boundary of a plane model was developed for this work. The loading device uses an inflatable rubber tube as did the one described by Durelli, *et al.*,[2] but the present design contains a number of improvements over their loading jig as discussed in Reference 3.

Figure 2 shows the uniform pressure-loading device used in the study of turbine-shell flanges. It consists of a continuous piece of rubber tubing which is placed in a groove formed by two Lucite covers separated by a spacer. Outer plates of steel hold the assembly together and permit the attachment of copper tubes. The ends of the rubber tubing are drawn into the copper tubes, one of which is closed off and the other serves as the inlet for gas pressure. The "piping," Fig. 2a, is arranged to minimize the discontinuity or gap in the rubber tubing. The operation of the uniform pressure-loading device can be visualized with the aid of the sectional view in Fig. 2b. As the rubber tubing is inflated, it expands and exerts a pressure on the model. Since Lucite is transparent and optically insensitive, the Lucite covers provide good boundary visibility of the model and confine the rubber tubing as the model deforms under load.

Experimental Setup and Typical Stress Patterns

Figure 3 shows the experimental setup with the photoelastic model and uniform pressure-loading device mounted in the straining frame of the polariscope. The effect of bolt forces was obtained by means of dead-weight loads applied to the flanges through the fixtures shown in the figure. The pressurizing system consisted of a nitrogen tank, regulator, bleeder valve and pressure gage. The lens-type polariscope has an 8-in. diameter field and can be set up readily for use with either a photometer or a camera.

Stress patterns of the flange under external load alone and under both external load and internal pressure are shown for comparison in Figs. 4a and 4b. The black core in each of these figures is produced by the opaque rubber tubing and the center of the jig, and the dark circle concentric with the core is obtained from the edges of the Lucite covers. It is seen that the Lucite covers provide good boundary visibility and do not affect the stress pattern in the model.

Transition from Model to Prototype

Let σ' be the stresses produced by concentrated loads, let σ'' be the stresses due to distributed loads or pressure and let σ be the stresses produced by both load and pressure. The model was made similar to the prototype, and since the structure is linear, it follows from dimensional analysis[4] that

$$\left(\frac{\sigma' Rt}{B}\right)_\alpha = \left(\frac{\sigma' Rt}{B}\right)_\beta \tag{1a}$$

and

$$\left(\frac{\sigma''}{p}\right)_\alpha = \left(\frac{\sigma''}{p}\right)_\beta \tag{1b}$$

where R, t, B, p are the characteristic length, thickness, force and pressure, respectively, in the model, α, and the prototype, β. By superposit o

$$\sigma = \sigma' + \sigma'' \tag{2a}$$

and

$$\frac{\sigma}{p} = \left(\frac{\sigma' Rt}{B}\right)\left(\frac{B}{Rtp}\right) + \frac{\sigma''}{p} \tag{2b}$$

It follows from eqs (1) and (2) that

$$\left(\frac{\sigma}{p}\right)_\alpha = \left(\frac{\sigma}{p}\right)_\beta \tag{3}$$

provided

$$\left(\frac{B}{Rtp}\right)_\alpha = \left(\frac{B}{Rtp}\right)_\beta \tag{4}$$

The ratio, B/Rtp, in eq (4) can be given a simple physical meaning. Let B be the bolt force, R the radius, t the thickness and p the pressure. Then

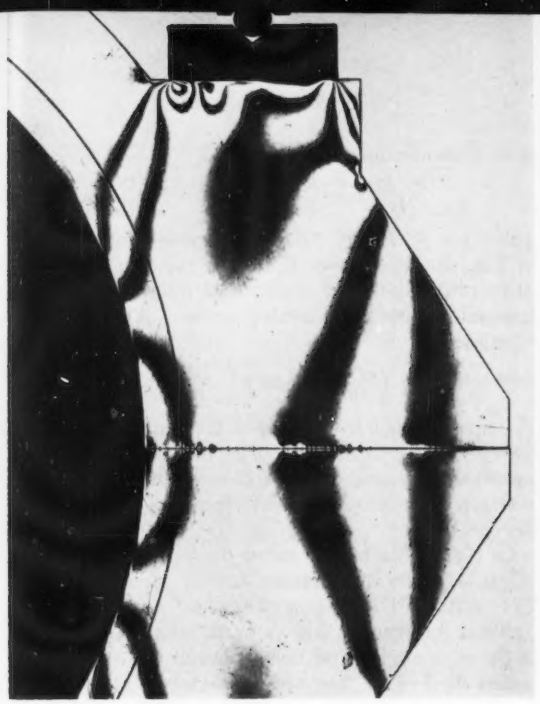

Fig. 4—Typical stress patterns of flange. (a) Test 2, B = 571 lb. p = 0 psi.

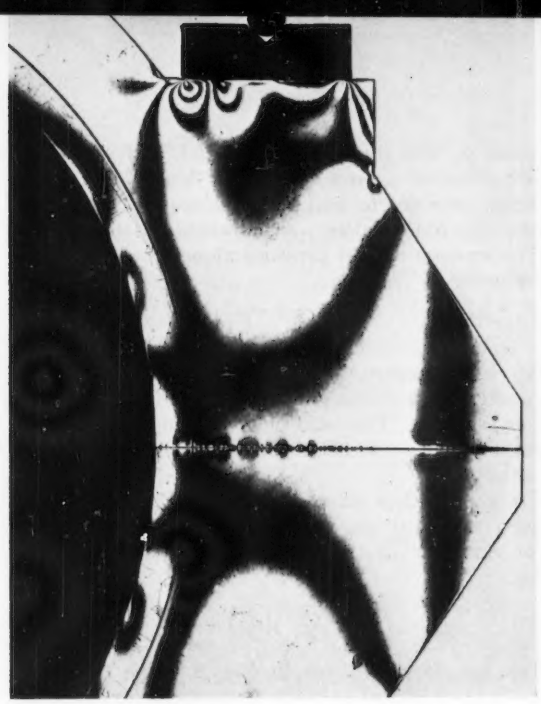

(b) Test 2, B = 571 lb, p = 180 psi, $F_c/F_0 = 3.70$

the forces holding the turbine shell closed are $F_c = 2B$, the forces tending to open the shell are $F_0 = 2Rtp$ and the ratio of the closing forces to the opening forces is

$$\frac{F_c}{F_0} = \frac{B}{Rtp} \tag{5}$$

The model was tested at values of F_c/F_0 equal to those in the prototype.

Experimental Results

Stress Distributions—Test 1

The effective pressure acting on the model was determined from the stresses on the vertical centerline. In this region, the stresses have polar symmetry, and only the fringe orders, n, were needed for the numerical integration of the equilibrium equation.[5] Figure 5 gives the radial and tangential stress distributions for the vertical centerline. The stresses computed from the Lamé solution for the thick ring[6] are shown for comparison. In the turbine shell, the tangential stress, σ_θ/p, is a maximum at the outer boundary, whereas in a thick ring, σ_θ/p is a maximum at the inner boundary. The average values of σ_θ/p are approximately equal, and the difference in the stress distributions is due to the bending stresses which are induced in the turbine shell by the restraining effect of the flanges.

Stresses were determined at the horizontal flange joint by using the shear-difference method.[7] A photometer and a compensator were used to make precision measurements of the directions of the principal stresses, θ, and the fringe orders, n, along auxiliary lines parallel to the joint as in Reference 8. The small disturbances at the joint (Fig. 4) were between the auxiliary lines, and hence the numerical

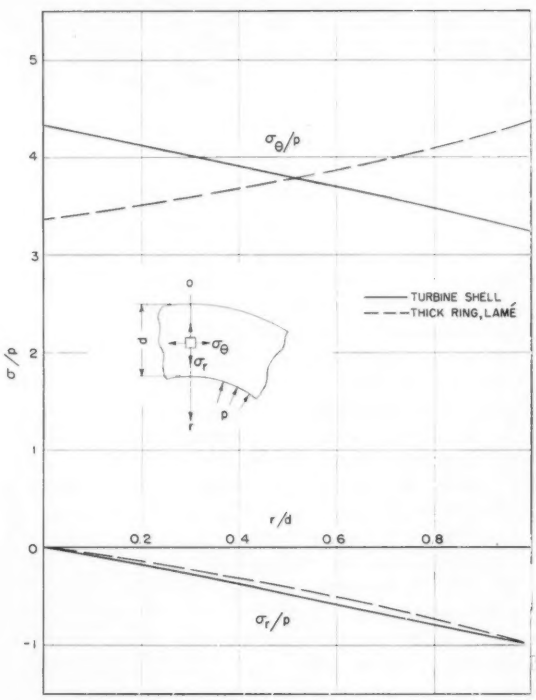

Fig. 5—Stress distributions on vertical centerline. Test 1, B = 571 lb, p. = 180 psi

integration for the horizontal stress component, σ_x, was not affected by the imperfections at the joint. In the calculation of the vertical stress component, σ_y, the fringe-order distribution at the joint was corrected to eliminate the small disturb-

ances on this line. Figures 6 and 7 give the distributions of σ_x and σ_y on the flange joint. The values of σ due to load and pressure and the values of σ' due to load alone were obtained experimentally. The stresses due to pressure alone were computed by using eq (2a), i.e.:

$$\sigma'' = \sigma - \sigma' \tag{6}$$

In order to check the stress distributions and the effective pressure, the quadrant of the model between the horizontal joint and the vertical centerline was isolated. The conditions for static equilibrium, namely, $\Sigma F_x = 0$, $\Sigma F_y = 0$, $\Sigma M = 0$, were satisfied within 2%.

Dimensionless stress ratios, $\sigma_y' Rt/B$ and σ_y''/p, were computed, and these values were superimposed for various F_c/F_0 ratios by using eqs (2b) and (5), i.e.:

$$\frac{\sigma_y}{p} = \left(\frac{\sigma_y' Rt}{B}\right)\left(\frac{F_c}{F_0}\right) + \frac{\sigma_y''}{p} \tag{7}$$

The results are shown in Fig. 8. The curve for $F_c/F_0 \doteq 3.70$ was actually obtained experimentally (σ_y curve in Fig. 7), and the other curves were derived from eq (7). These curves show the influence of stress relaxation of the bolts on the stress distribution at the flange joint. For this geometry, the stress at the inner boundary of the shell falls to zero at $F_c/F_0 = 1.44$, i.e., the closing forces have to be approximately 50% greater than the opening forces to just maintain a small compressive stress at the inner boundary.

Optimum Width of Flanges—Tests 2, 3, 4 and 5

The influence of the radial width of the flange, T, was determined from Tests 2, 3, 4 and 5. In these tests, attention was focused on the vertical stress component acting on the flange joint at the inner boundary of the shell (point A, Fig. 9). The basic data were obtained from two stress patterns of the model—one under external load, B, and the other under both load and pressure, B and p, e.g., Fig. 4. The σ_A and σ_A' stresses were calculated from boundary fringe orders, and σ_A'' was computed by using eq (6). The resulting dimensionless stress ratios are plotted in Fig. 9 with the ratio of flange width to bolt location, T/b, as the abscissa.*

It is seen that the compressive stress due to bolting, $\sigma_A' Rt/B$, is nearly constant for $T/b > 2.5$ but tends toward zero for $T/b < 2.5$. By considering a deep flange as a short column under eccentric load, the stress at point A in Fig. 9 due to bolting alone can be calculated from the expression

$$S_A' = -\frac{B}{Tt}\left[1 + 3\left(1 - \frac{2b}{T}\right)\right] \tag{8a}$$

or in dimensionless form

$$\frac{S_A' Rt}{B} = -\frac{R}{T}\left[1 + 3\left(1 - \frac{2b}{T}\right)\right] \tag{8b}$$

where $1.5 \leq T/b \leq 3.0$. This curve is also plotted in Fig. 9. It is seen that the experimental data corroborate both the shape and magnitude of the theoretical curve for bolting stress. A comparison shows that

$$\left(\frac{\sigma_A' Rt}{B}\right) \simeq 1.07\left(\frac{S_A' Rt}{B}\right) \tag{9}$$

The stress at the inner edge of the flange is approximately 7% greater than the value calculated by elementary means. This difference may be due to a stress-concentration effect from the curvature of the shell.

In Fig. 9, the tensile stress due to pressure alone, σ_A''/p, exhibits a minimum in the range of $2.5 < T/b < 3.0$. The trends of the σ_A' and σ_A'' curves combine to produce a maximum compressive value in the σ_A/p curve, and the optimum width of flange occurs at $T/b = 2.9$, approximately. Considering bolting alone, the optimum width of deep flanges is $T/b = 3$.

Conclusions

Two-dimensional photoelasticity proved to be a convenient method for studying the stresses in turbine-shell flanges subjected to external bolt forces and internal pressure.

On the basis of the static check, the use of photometric devices and numerical integration led to

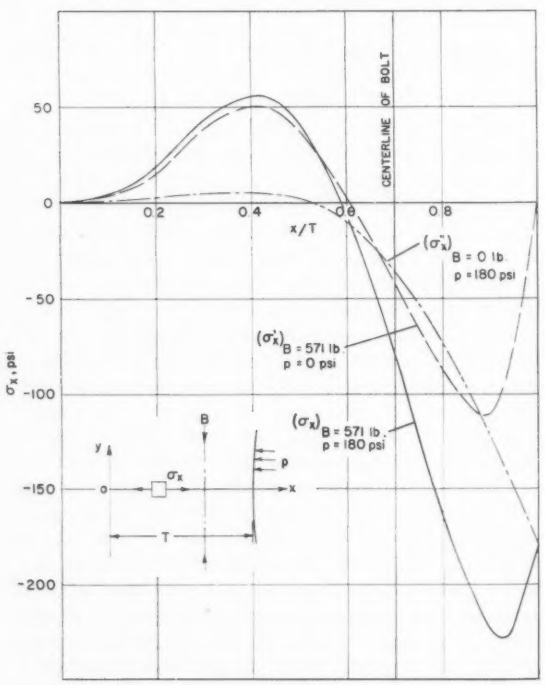

Fig. 6—Distribution of σ_x at flange joint, Test 1

For $F_c/F_0 = 3.70$ and $T/b = 3.34$, it may be noticed that the value of σ_A/p obtained in Test 2 (Fig. 9, $\sigma_A/p = -8.83$) differs from the value in Test 1 (Fig. 8, $\sigma_A/p = -7.36$), whereas these values should be equal. This difference is due to the fact that the stress pattern in Tests 1 and 2 was not perfectly symmetrical with respect to the vertical centerline even though the model was symmetrical, Fig. 1. The left-hand side of the model, Test 1, was used in a series of tests not reported in this paper. The right-hand side of the model was used throughout Tests 2, 3, 4 and 5 so that the curves in Fig. 9 are based on a consistent set of data.

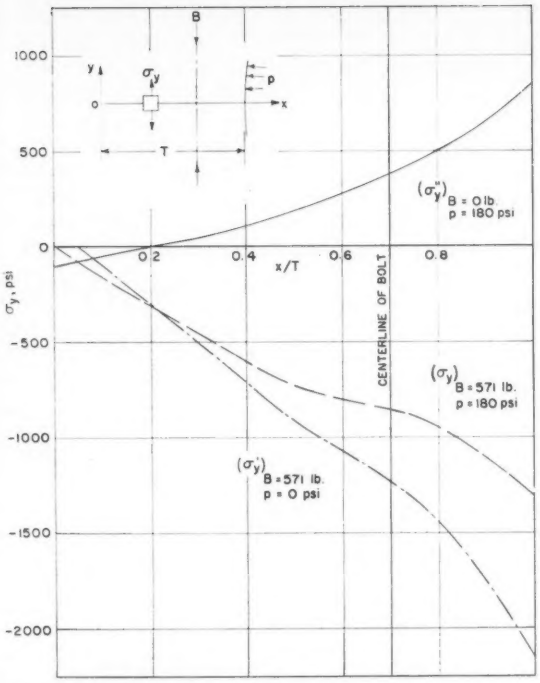

Fig. 7—Distribution of σ_y at flange joint, Test 1

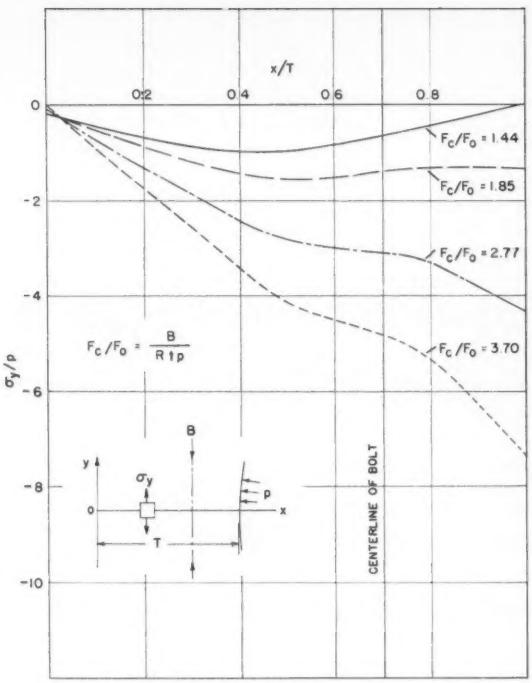

Fig. 8—Distribution of σ_y at flange joint for various F_c/F_0 ratios, Test 1

accurate values of the effective pressure and interior stresses.

For the flange geometry tested, the minimum ratio of closing forces to opening forces to just maintain compressive stresses over the entire joint is $F_c/F_0 = 1.5$, approximately. The optimum ratio of flange width to bolt location for a maximum compressive stress at the inner boundary of the shell is $T/b = 2.9$, approximately.

Acknowledgments

The author is grateful to the General Electric Co. for permission to publish this paper. The investigation was carried out in the General Engineering Laboratory (GEL) and was supported by the Large Steam Turbine-Generator Department (LST-G). Thanks are due to S. B. Coulter and V. K. Sahakian of LST-G and R. Guernsey of GEL for many helpful discussions during the course of the work.

References

1. *Frocht, M. M., and Pih, H., "A New Cementable Material for Two- and Three-Dimensional Photoelastic Research,"* Proc. SESA, *Vol. XII, No. 1, 1954, pp. 55–64.*
2. *Durelli, A. J., Lake, R. L., and Tsao, C. H., "Device for Applying Uniform Loading to Boundaries of Complicated Shape,"* Proc. SESA, *Vol. XI, No. 1, 1953, pp. 55–61.*
3. *Flynn, P. D., Discussion of ASME Paper No. 57-A-4 by A. J. Durelli and A. S. Kobayashi.* J. Appl. Mech., Vol. 26, Series E, No. 1, March 1959, pp. 150-151.
4. *Goodier, J. N., "Dimensional Analysis," Appendix II of the* Handbook of Experimental Stress Analysis, *edited by M. Hetényi, John Wiley and Sons, Inc., New York, 1950, pp. 1035–1045.*
5. *Dolan, T. J., and Murray, W. M., "Photoelasticity, I. Fundamentals and Two-Dimensional Applications," Chapter 17 of the* Handbook of Experimental Stress Analysis, *edited by M. Hetényi, John Wiley and Sons, Inc., New York, 1950, p. 889.*
6. *Timoshenko, S., and Goodier, J. N.,* Theory of Elasticity, *McGraw-Hill Book Company, Inc., New York, 1951, 2nd ed., p. 60*

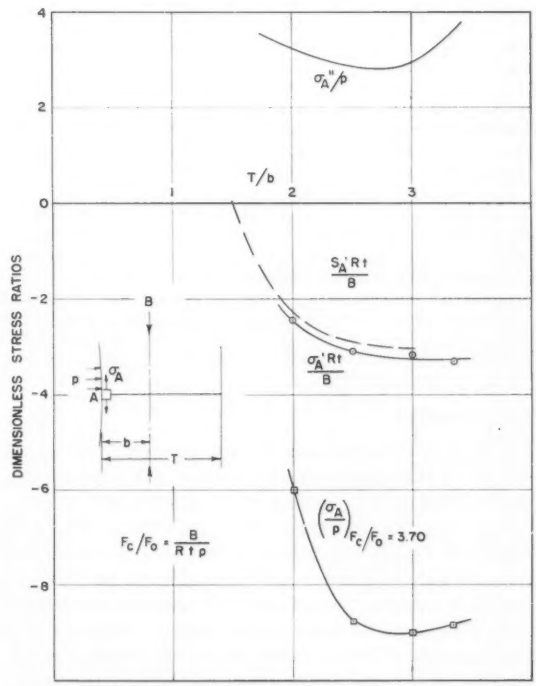

Fig. 9—Influence of width of flange, Tests 2, 3, 4 and 5

7. *Frocht, M. M.,* Photoelasticity, *Vol. I, John Wiley and Sons, Inc., New York, 1941, Chapter 8.*
8. *Frocht, M. M., Pih, H., and Landsberg, D., "The Use of Photometric Devices in the Solution of the General Three-Dimensional Photoelastic Problem,"* Proc. SESA, *Vol. XII, No. 1, 1954, pp. 181–190.*

Experimental Investigation of the Buckling Instability of Monocoque Shells

Authors present the results of two investigations conducted to determine the buckling instability of basic structural shapes considered for missile re-entry vehicle applications

by R. H. Homewood, A. C. Brine and Aldie E. Johnson, Jr.

ABSTRACT—Buckling of a series of thin-metal, shallow spherical shells under a uniform hydrostatic pressure has been investigated. Stress and deformation histories, as well as the critical buckling pressure and the post-buckling behavior, have been determined. Comparisons with theoretical analyses for buckling of spherical caps are given.

Results are presented for an initial phase of a stability study of truncated conical sections which have been subjected to combinations of axial load and lateral pressure. A series of roll-formed and butt-welded, truncated aluminum conical shells with a 75-deg base angle have been tested. Buckle modes for axial-load condition alone, lateral-pressure load alone and combinations of these loading conditions are described. Interaction curves for the conditions investigated are given.

Introduction

In the field of structural design, the optimization of weight is highly dependent on the accurate prediction of the stability limits of the shapes and configurations which constitute the structure. For the design of re-entry vehicles (in missiles, the so-called nose cones), it is essential to be able to predict the buckling modes and loads under the re-entry environments of temperature, aerodynamic pressure and inertial forces due to deceleration to obtain the optimum weight structure required for high performance. Thus, re-entry vehicle structural design requires a basic understanding of the shell structures which generally constitute the design.

Despite the basic nature of the problems and the considerable effort that has gone into stability investigations over the years, there exist, particularly for thin shells, incomplete theoretical analyses and limited experimental data or verification of theory. Unfortunately, it is in these areas that many of the shapes used on re-entry vehicles lie, and it has been necessary to substantiate designs with research on the buckling of three-dimensional bodies of revolution; e.g., cones and portions of spheres.

During the design and development of re-entry vehicles, information on the stability of conical, cylindrical and spherical cap structures was required. Some material was unavailable, and it was necessary to conduct tests to obtain the data required for the designs. Because of rapidly advancing technology in all areas of missile design, it was deemed advisable to perform general studies to include not only the geometric parameters of current thinking, but also, to extend the range of parameters as far as possible to include more-or-less drastic changes in configuration. The results of two investigations are discussed herein.

The first investigation is the buckling of thin spherical caps under a uniform external pressure. The buckling pressures, stresses and deflections have been determined for a considerable range of geometric parameter and, in particular, for a range of parameters which is not covered by known experi-

R. H. Homewood, A. C. Brine and Aldie E. Johnson, Jr., are associated with the Research and Advanced Development Division, Avco Corp., Wilmington, Mass.

Paper was presented at the 1959 SESA Spring Meeting held in Washington, D. C., on May 20–22.

mental data. Correlations with earlier experimental data are shown.

The second investigation is the determination of the combinations of loads that cause buckling of truncated conical sections which are subjected to combinations of axial load and external (lateral) pressure. The sections tested were designed to produce buckling over a wide range of membrane stress to study the buckle mode shapes for inclusion in a more comprehensive theoretical analysis.

Buckling of Spherical Caps

The use of blunt bodies for manned or unmanned reentry vehicles[1] may require that the supporting structure be relatively shallow and, probably (for other considerations), a body of revolution. To provide design data for one such configuration (namely, a spherical cap), an investigation was conducted to determine the buckling characteristics, deflections and stresses of a series of shallow spherical sections whose geometric properties covered a relatively wide range. Although considerable theoretical analysis was done[2-8] and some experimental work was performed,[2, 6, 9] the existing analytical work was not considered to be adequate for optimum design because of the general lack of agreement between existing theories and between theory and experiment.

The shells tested were considered to be "shallow" (although not all shells fell within the shallow-shell region which was somewhat arbitrarily defined as containing shells with a ratio of height to base radius of less than 1:8). It should be noted that there were no important differences in buckling characteristics or results which could be attributed to "nonshallow" shells.

Fabrication of Specimens

Twelve shells were formed by spinning from flat sheets of hot-rolled steel (SAE 1020) or wrought aluminum alloy (2024-T3). Inherent in the spinning process is a variation in finished thickness depending on the amount of stretching at the local area. After fabrication, the shell thickness at several locations was determined by ultrasonic means (Table 1). The thickness shown is the average of the measured values, and the deviations are given as a percentage of the average value. In all instances, the maximum thickness occurred at the center of the shells, and the minimum thickness occurred at the juncture of the spherical section and the flat attachment ring where the highest local stretching took place.

It was noted, after a few tests had been made, that buckling had occurred as a single asymmetric buckle in each shell. In an effort to determine whether the additional thickness in the central area of the shells due to the manufacturing process was responsible for the asymmetric buckling, three shells were machined after spinning. Unfortunately, two of the three machined specimens had material defects

TABLE 1—SPHERICAL-SHELL TEST DATA

SHELL No.	RADIUS, in.	THICKNESS, in.	THICKNESS VARIATION, %	MATERIAL	BUCKLING PRESSURE, psi	$\frac{q}{q_{cr}}$	λ	K	COMMENT
1	40	0.248	+8 −2	1020 H.R.S.	423	0.313	10.7	0.184	
2	40	0.165	+1 −2	1020 H.R.S.	191	0.319	13.1	0.194	Machined, this shell defective
3	40	0.110	+5 −4	1020 H.R.S.	115	0.432	15.0	0.258	
4	40	0.158	+3 −2	2024 Al	—	—	13.4	—	Machined, this shell defective
5	40	0.067	+4 −10	1020 H.R.S.	29	0.292	20.5	0.175	
6	78	0.235	+1 −3	1020 H.R.S.	166	0.516	7.7	0.314	Machined
7	78	0.260	+1 −7	2024 Al	77	0.544	7.3	0.336	
8	78	0.113	+1 −4	1020 H.R.S.	32	0.433	11.1	0.258	Nonpermanent buckle
9	78	0.370	+3 −4	2024 Al	110	0.387	6.1	0.238	
10	78	0.057	+6 −6	1020 H.R.S.	5.65	0.217	14.3	0.130	Nonpermanent buckle
11	78	0.070	+3 −6	1020 H.R.S.	8.2	0.289	14.0	0.170	Nonpermanent buckle
12	78	0.070	+3 −1	1020 H.R.S.	5.0	0.176	14.0	0.104	Nonpermanent buckle

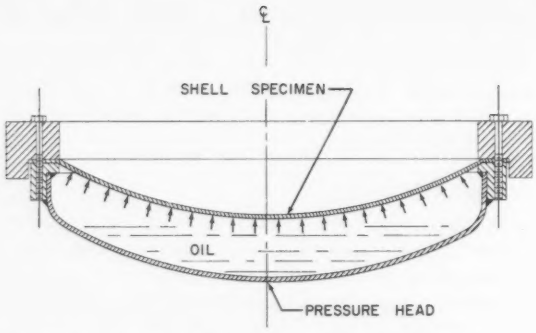

Fig. 1—Cross section of spherical-shell test fixture

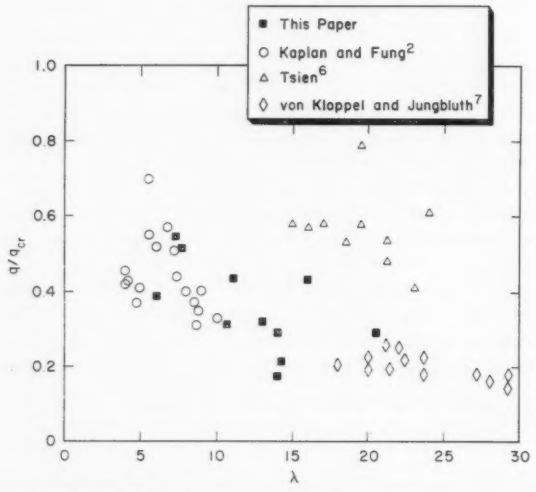

Fig. 2—Experimental buckling of spherical shells

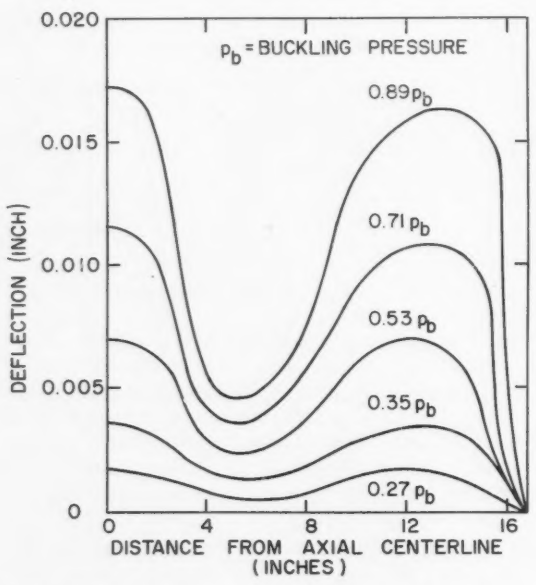

Fig. 3—Effect of pressure on the prebuckling deformation of a spherical shell ($\lambda = 14.0$)

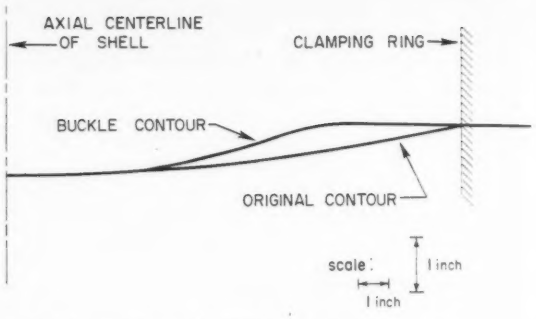

Fig. 4—Buckle profile for a spherical shell ($\lambda = 14.0$)

and, consequently, gave poor test results. The thickness variation in the third shell was less than in any other shell, but it also buckled asymmetrically.

The shells were formed into two basic spherical radii (40 and 78 in.) from plates of nominally $^1/_{16}$, $^1/_8$, $^3/_{16}$, $^1/_4$ and $^3/_8$ in. to produce ratios of radius to thickness in the range from 160 to 1250.

Loading Fixture

A uniform hydrostatic (oil) pressure was applied to the convex surface of the test shell in a pressure cell. The pressure cell (which is shown schematically in Fig. 1) consisted of a standard spun pressure head which was welded to a heavy-steel ring flange. The specimen was clamped to the flange by a second heavy-steel ring to effect a pressure seal. The inner diameter of the clamping rings was 34 in.

Instrumentation

Pressures were measured with Bourdon-tube pressure gages or electronic pressure transducers.

Deflections were measured with dial indicator-type gages along a meridional line on the exposed (concave) surface of the shell. In addition, pretesting and postbuckling contours of the shells were recorded autographically. A stylus pen, which was attached to a roller, traced the contour on a sheet of paper as the roller traversed a meridional line on the concave surface.

Selected specimens were instrumented with bonded-wire strain gages to determine meridional and circumferential strains in the shell, and to determine the effect of edge clamping on the uniformity of stress across the shell. Gages were applied to both concave and convex surfaces along a meridional line.

Testing Procedure

Loading was applied hydraulically in increments. After each increment of loading was applied, strain-gage and deflection readings were taken. Loading was continued until buckling occurred. In most instances, buckling occurred abruptly and, with the exception of shells 8, 9, 11 and 12, the buckles remained after the pressure was removed. For shells 8, 9, 11 and 12, the shells returned to their original

contour when the loading was removed. Subsequent reloading of these shells caused buckling to occur at the same location as before, and at approximately the same pressures.

Results

The buckling pressures for the shells are shown in Fig. 2 in terms of a geometric parameter, λ, and a load parameter, q/q_{cr}, where q_{cr} is the buckling pressure for the complete sphere, of which the shallow shell is a part (under uniform pressure), according to the classical solution which is based on linearized equations. The geometric parameter is defined as[2]

$$\lambda = 2[3(1 - \mu^2)]^{1/4}\left(\frac{h}{t}\right)^{1/2} \quad (1)$$

and the load parameter is[4]

$$\frac{q}{q_{cr}} = \frac{q}{2E}[3(1 - \mu^2)]^{1/2}\left(\frac{R}{t}\right)^2 \quad (2)$$

where:

E = modulus of elasticity, psi.
h = central height of shell above base plane, in.
q = external pressure at buckling, psi.
R = radius of middle surface of shell, in.
t = shell thickness, in.
μ = Poisson's ratio.

In addition, the experimental data[2, 6, 9] are shown on the figure.

The buckling data from the present experiments are also given in Table 1. Values of K in the table can be compared with the classical linear theory value of $K = 0.606$ when $\mu = 0.3$; i.e.,

$$K = \frac{\sigma_{cr}}{E}\left(\frac{R}{t}\right) \quad (3)$$

where σ_{cr} = critical buckling stress, psi.

Deflection curves were determined from dial-gage readings taken during loading. A typical curve is shown in Fig. 3 which indicates the growth of deformation prior to buckling. The ordinate is expanded to show more clearly the shape of the deformation mode. Part of the deformation which is shown, of course, is attributable to the general translation of the shell due to the increasing pressure; however, the wave deformation which has been superimposed on the over-all translation is the significant result.

For this same shell, the shell profile after buckling is shown in Fig. 4. It can be seen that the buckle occurs in the same region as the maximum deformation before buckling, but that the buckled deformation of the shell is considerably greater than the deformation prior to buckling.

It should be pointed out that this shell has buckled asymmetrically; that is, there is no buckle on the other side of the shell centerline or anywhere else in the shell. The buckle is symmetrical about an axial centerline through itself. If the pressure is increased after buckling, no additional buckles form but, rather, the existing buckle grows until eventually the shell becomes completely inverted.

From a comparison of the deflection curves which have been obtained during the loading of each shell, it is evident that there is a change of deformation mode as the geometric parameter λ increases. Typical of these curves are those shown in Fig. 5 for deformations slightly below the buckling value. For small values of λ (Fig. 5a), the deformation mode is a single half-wave across the shell with a maximum deformation at the center. As the value of λ increases slightly (Fig. 5b), the maximum deformation shifts to both sides of center with a slightly reduced deflection at the center. The center deflection is reduced considerably in the intermediate range of λ (Fig. 5c), to the point where the deformation mode is essentially two half-waves across the shell. For the larger values of λ (Fig. 5d), the deformation mode changes to three half-waves across the shell. It should be noted that, for the shells which are shown in Figs. 5c and 5d, the stresses in the buckled shell have not exceeded the yield strength of the material; that is, the shells have returned to their original shape upon unloading.

The deformation curves shown in Fig. 5 (and those for the remaining shells) appear to confirm the deformation mode concept of Reiss, *et al.*,[3] and are similar to those described by Kaplan and Fung[2] (which provided the substantiation given therein[3]).

One additional observation on deformations and buckling: all the shells which were tested (with the exception of numbers 2 and 4 which had known material defects at or near the center) buckled asymmetrically.

Thus, it is suggested that an asymmetrical buckle pattern is possibly more critical than a symmetrical buckle pattern. This may account in part for the unconservative theoretical results since all the referenced theories are based on symmetrical buckling. A series of frames from high-speed motion pictures are shown elsewhere[9] which indicate that, although the final buckle shape is symmetric, the intermediate stages of buckling were asymmetric.

The most reliable theoretical results on axisymmetric buckling of clamped shallow spherical shells, covering the largest range of λ, have been obtained independently, by very different techniques (see Budiansky[7] and Weinitschke[8].) (These results are in agreement with each other over a large range of λ, but differ markedly from the results of Reiss, *et al.*[3] and Archer[4] for λ greater than 5.) Budiansky's results, although indicating some degree of qualitative agreement with experimental results, show substantial lack of quantitative agreement for λ greater than 5, even when small initial axisymmetric imperfections are taken into account. Thus, Budiansky concludes that "a rational explanation of experimental results must incorporate consideration of nonaxisymmetric initial imperfections and deformations."

An investigation of the dynamics of buckling was made on shell number 10. This was one of the shells which, after buckling, returned to its original shape upon unloading. Outputs from bonded-wire strain gages and an electronic pressure transducer were

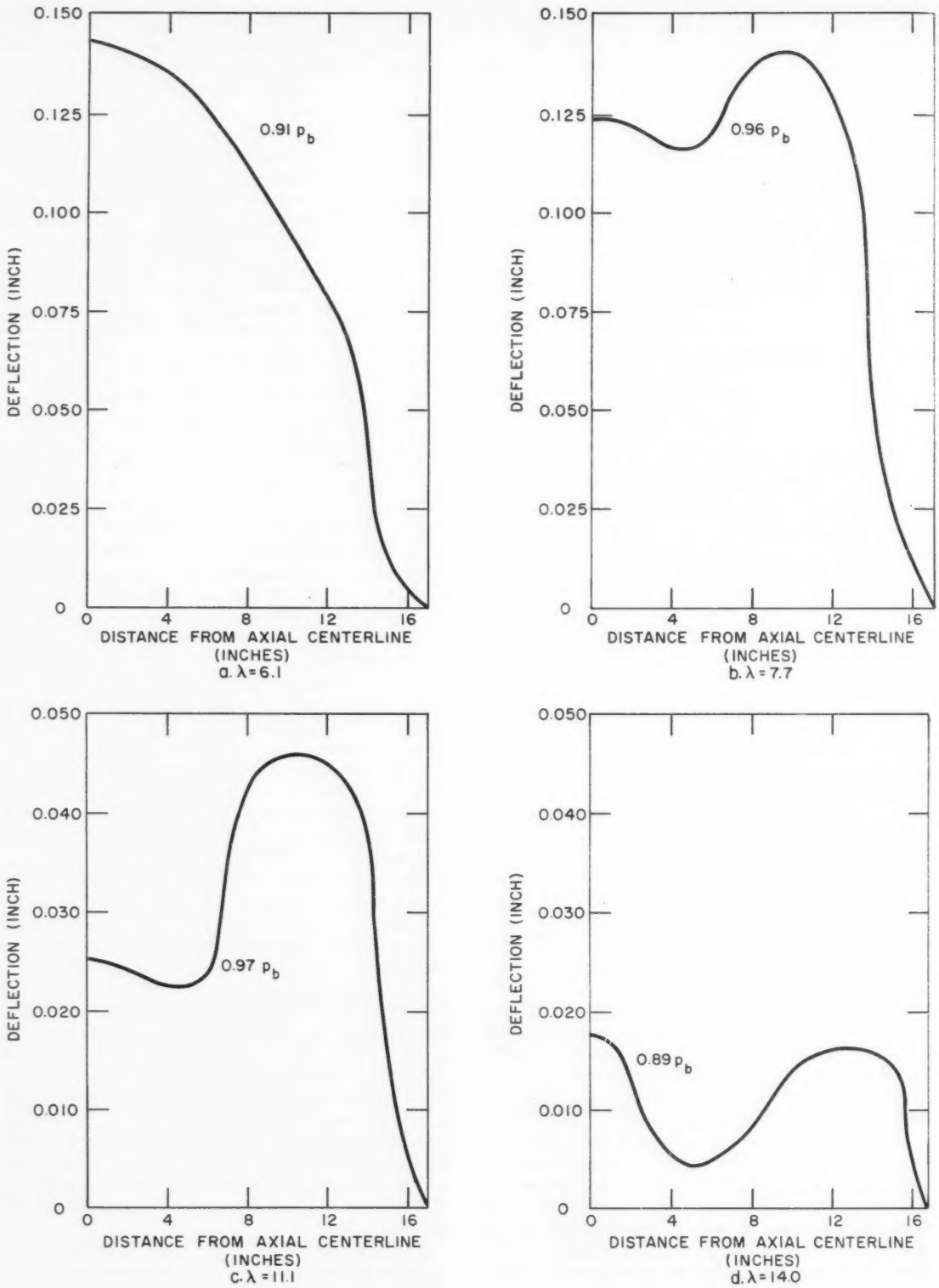

Fig. 5—Variation of prebuckling deformation shape with geometry for spherical shells (p_b=buckling pressure)

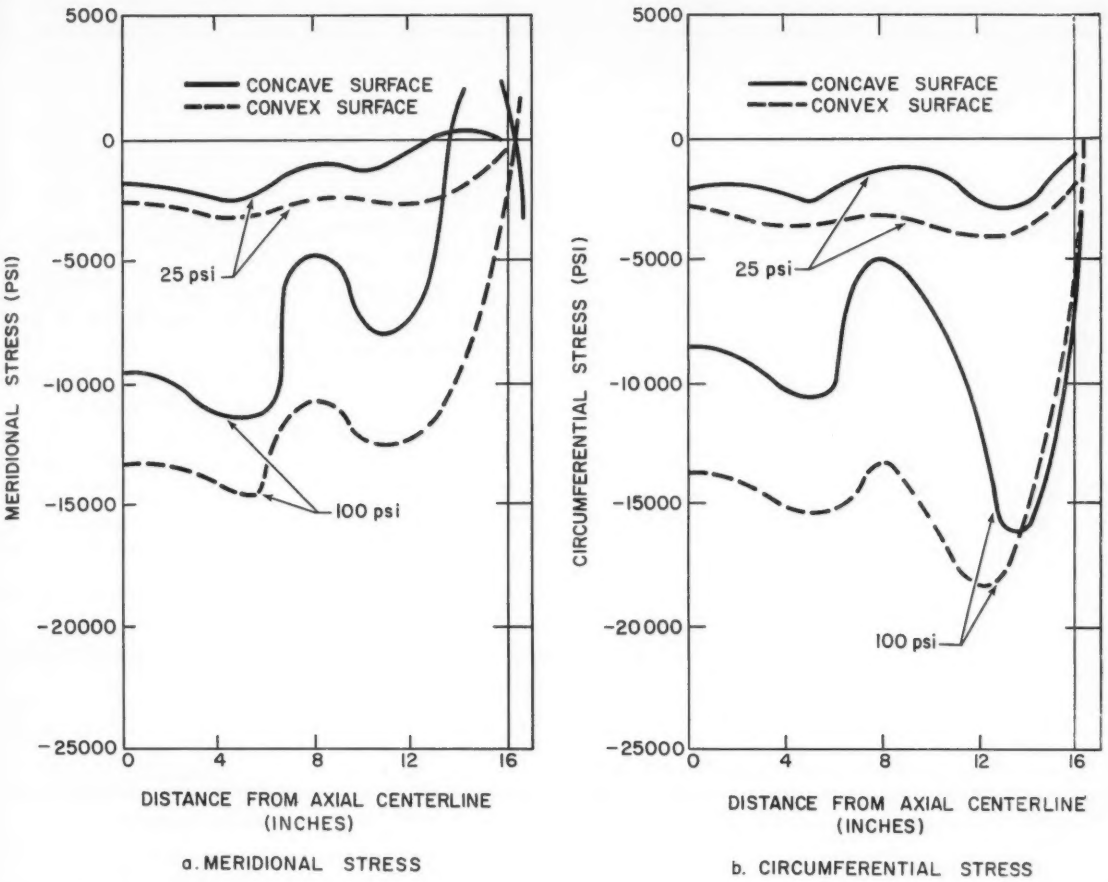

Fig. 6—Stress in a spherical shell ($\lambda = 6.1$)

recorded oscillographically to determine the extent and frequency of vibration of buckling. The significant results are that the buckling of the shell, under a slowly increasing hydrostatic pressure, caused the shell to vibrate at a frequency of 33.3 cps, and the vibration was damped out in approximately 0.4 sec.

Stress distributions for both meridional and circumferential stresses for a typical shell are shown in Figs. 6a and 6b. Stresses have been determined from strain-gage data for both concave and convex surfaces; however, stresses for only two pressures are shown. For the low pressure, the general shape is established which is maintained to the high pressure. The effect of edge restraint can be seen by the reversal of stress in the area immediately adjacent to the edge clamp.

Buckling of Truncated Conical Shells

Another shell-stability problem which is being studied is the determination of stability boundaries for conical sections subjected to combinations of axial load and lateral pressure. The initial phase of the investigation has been made on simple roll-formed metal, monocoque, truncated conical test sections.

Fabrication of Specimens

Conical shells were made from 6061-T6 aluminum alloy by rolling the developed shape of the truncated cone and butt welding the joint to produce cones with a 75-deg base angle. The shells were adhesive-bonded and riveted to heavy-steel loading flanges for testing. Figure 7 shows a dimensioned cross section of shell and loading flanges. Shells were made from 0.040-, 0.063- and 0.105-in. sheet material.

The butt-welded joint was ground smooth and tested for surface cracks by a fluorescent penetration method. Thickness variation in the vicinity of the joint and out of roundness of shell was determined (Table 2) before testing. The material thickness at locations other than the weld was found to be the standard sheet thickness for each cone. The shells were bolted to the loading flanges when out-of-roundness measurements were taken. Total

TABLE 2—PHYSICAL PROPERTIES OF CONICAL TEST SPECIMENS

CONE No.	THICKNESS, in.	OUT-OF-ROUNDNESS, in. TIR* (Top)	TIR (Middle)	TIR (Bottom)	THICKNESS VARIATION AT VICINITY OF WELD
1	0.040	0.059	0.045	0.043	Generally 0.039 in., but 0.033 in. in a small area
2	0.040	0.081	0.051	0.093	Generally 0.040 in., but 0.035 in. in some areas
3	0.040	0.069	0.032	0.025	Generally 0.040 in., but 0.038 in. in some areas
4	0.040	0.055	0.043	0.027	0.035 to 0.038 in.
5	0.040	0.070	0.034	0.066	Generally 0.039 in., but 0.036 to 0.038 in. in some areas
6	0.063	0.074	0.072	0.080	0.050 to 0.055 in., poor weld
7	0.063	0.037	0.035	0.078	0.050 to 0.060 in., fair weld
8	0.053	0.039	0.025	0.085	Generally 0.063 in., but 0.051 in. near buckle, fair weld
9	0.053	0.080	0.098	0.113	0.050 to 0.053 in., poor weld
10	0.063	0.074	0.050	0.054	Generally 0.045 in., but 0.053 in. in some areas, poor weld
11	0.063	0.044	0.042	0.025	0.040 to 0.050 in., fair weld
12	0.063	0.102	0.090	0.089	0.040 to 0.050 in., but 0.030 in. in some small areas, fair weld
13	0.105	0.037	0.053	0.050	0.085 to 0.090 in.
14	0.105	0.038	0.056	0.038	Generally 0.105 in., but 0.097 in. in some areas, good weld
15	0.105	0.037	0.030	0.041	Generally 0.099 in., but 0.090 in. in some small areas
16	0.105	0.040	0.061	0.036	Generally 0.100 in., but 0.090 in. in one area
17	0.105	0.110	0.123	0.085	Generally 0.095 in., but 0.090 in. in some small areas
18	0.105	0.102	0.084	0.055	0.080 to 0.090 in.

* TIR—total indicated reading.

TABLE 3—BUCKLING DATA FOR CONICAL TEST SPECIMENS

CONE No.	THICKNESS, in.	AXIAL LOAD,* lb	BUCKLING PRESSURE, psi	No. NODES in No. Degrees	DESCRIPTION OF BUCKLES
1	0.040	0	24.5	7 in 360	Full-length longitudinal buckles
2	0.040	−35,250	0	5 in about 225	Diamond-shaped buckles about 2 in. below bottom of top flange
3	0.040	−12,660	21.2	2 in about 102	Diamond-shaped buckles at midheight
4	0.040	−22,650	14.0	3 in about 150	Diamond-shaped buckles about midheight, indication of 2 rows of buckles
5	0.040	+12,460	25.2	7 in about 360	Full-length longitudinal buckles
6	0.063	0	67	1 in about 40	Full-length longitudinal buckle
7	0.063	−22,500	62	1 in about 40	Full-length longitudinal buckle
8	0.063	−40,000	29.5	1 in about 45	Almost diamond-shaped buckle about 2 in. above top of bottom flange, also, small diamond-shaped buckle 180 deg away
9	0.053	−57,500	0	5 in about 180	Diamond-shaped buckles about 2 in. below bottom of top flange
10	0.063	−63,000	0	3 in about 165	Diamond-shaped buckles about 2 in. below bottom of top flange
11	0.063	−38,800	35.5	4 in about 240	Diamond-shaped buckles at midheight
12	0.063	+12,230	59.3	1 in about 50	Full-length longitudinal buckle
13	0.105	−118,300	0	—	Full-circumference circumferential buckle
14	0.105	+900	232	—	Full-length longitudinal buckle
15	0.105	+29,600	195	1 in about 45	Full-length longitudinal buckle
16	0.105	−36,100	175	1 in about 45	Full-length longitudinal buckle
17	0.105	−76,800	136	1 in about 45	$^3/_4$-length longitudinal buckle from bottom flange to 3 in. from bottom of top flange
18	0.105	−39,600	150	2 in about 90	Full-length longitudinal buckles

* Tension is positive.

indicated readings (TIR) were recorded for circumferential lines which were located 2 in. below the top flange (top), at the mid-height of the shell (middle) and 2 in. above the bottom flange (bottom).

Loading Fixture

The shells, which were tested under axial load with no lateral pressure, were loaded in a testing machine.

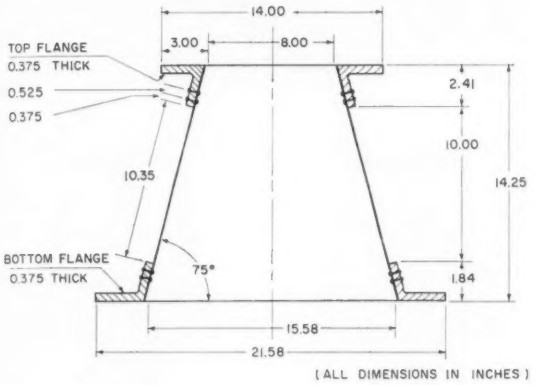

Fig. 7—Cross section of conical-shell specimen and loading flanges

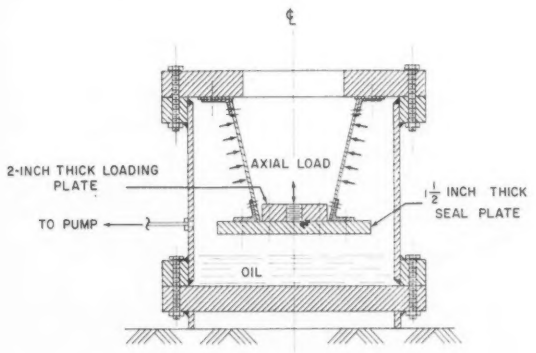

Fig. 8—Test setup for conical shells

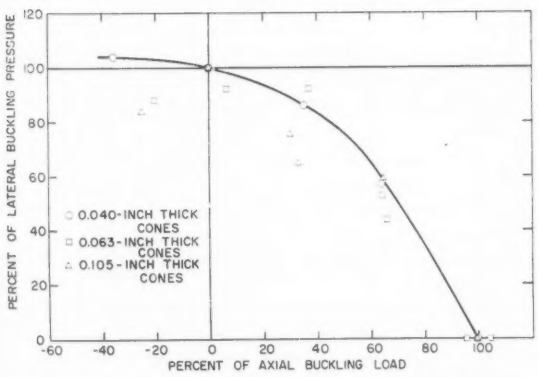

Fig. 9—Interaction curve for buckling of conical shells under combinations of axial load and lateral pressure. (Compressive loads positive—tensile loads negative)

The shells which were tested under lateral pressure, either singly or in combination with an axial load, were loaded hydrostatically in a modified pressure vessel. Figure 8 shows a cross section of the pressure vessel with a shell in place.

Instrumentation

Axial loads were weighed with electronic load cells, and the lateral pressure was measured with a Bourdon tube-type pressure gage.

Testing Procedure

For the shells which were tested under lateral pressure without axial load, a force was applied to the loading plate (Fig. 8) which was equal and opposite to the net force of the oil pressure on the seal plate. For this condition, therefore, there were no meridional membrane forces at the small diameter end of the shell. There were, however, meridional membrane forces at the large diameter end of the shell because of the conical shape.

For the tests with combined axial load and lateral pressure, the axial load was applied first and the lateral pressure was applied incrementally until buckling occurred. The axial load was monitored at each pressure increment, and the net oil pressure on the seal plate was considered when computing total applied axial load.

Results

The experimental buckling data are given in Table 3. Included in Table 3 are the number of experimental buckling nodes and a general description of the buckled shapes.

Also, the experimental data are given in Fig. 9 as buckling interaction curves (axial load at buckling as the abscissa, and lateral pressure at buckling as the ordinate). The data have been nondimensionalized in terms of load under combined loadings to cause buckling, and are expressed as a percent of the load required to buckle under single load. A curve faired through the data for the 0.040-in. thick cones is shown in the figure. The data of Table 2 indicate that more consistent and uniform shells were obtained in this thickness than in either 0.063- or 0.105-in. shells. This is also evident from the scatter of data on Fig. 9. The large variation in sheet thickness and out-of-roundness is attributed to poor welds at the butt joint and the local reduction of thickness by grinding of the welds to produce a smooth contour.

It is evident from Table 2 that, for the 0.063-in. thick cones, the welds are generally poor, and the thickness at the vicinity of the joint is generally about 0.050 in. This local weakness contributed to premature buckling in every instance except for the shells which were buckled under axial load alone. This was indicated since buckling occurred at the weld, or the buckle pattern showed definite evidence of being affected by the welded joint.

For the 0.105-in. thick series of shells, better welds were generally obtained, and the percentage

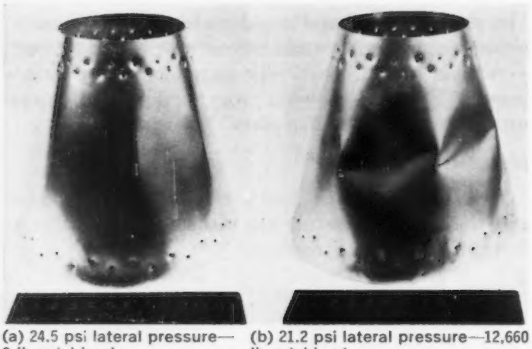

(a) 24.5 psi lateral pressure—0 lb axial load (b) 21.2 psi lateral pressure—12,660 lb axial load

(c) 14.0 psi lateral pressure—22,650 lb axial load (d) 0 psi lateral pressure—35,250 lb axial load

Fig. 10—Effect of axial compression on buckle mode for conical shells (0.040 in. thick cones)

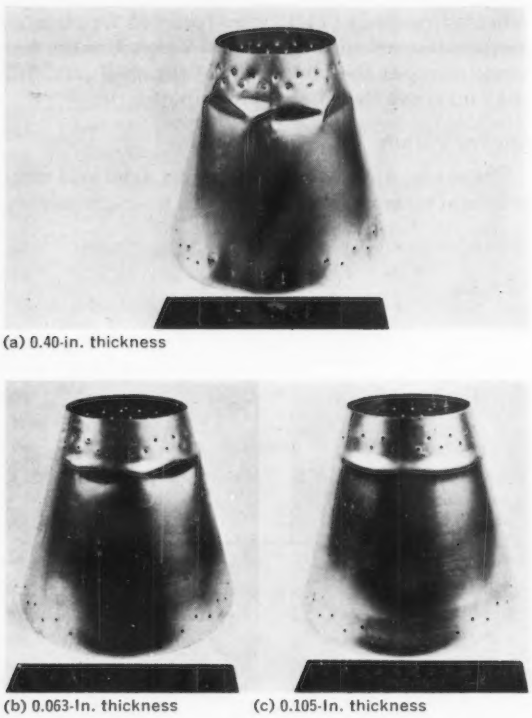

(a) 0.40-in. thickness

(b) 0.063-In. thickness (c) 0.105-In. thickness

Fig. 11—Buckle modes for conical shells subjected to axial loads

reduction of thickness at the weld due to grinding was less than for the 0.063-in. thick shells. However, the membrane stresses at buckling were considerably higher for the 0.105-in. than for the 0.063-in. thick shells. Tensile specimens which were cut from the buckled shells indicated that, because of welding, the yield strength of the material was reduced considerably in the vicinity of the butt joint. The higher stresses, together with the local weakness at the joint, contributed to premature failures as evidenced above.

In contrast to the thicker cones, the 0.040-in. thick series of shells had good welds generally and less thickness reduction at the weld (and buckled at relatively low membrane stress). Buckling occurred with more than one node and in a pattern which appeared to be relatively unaffected by the location of the welded joint.

Figure 10 shows the influence of type of loading on the buckle pattern for the 0.040-in. cones. When subjected to uniform lateral pressure, the buckle pattern consisted of full-length longitudinal buckles uniformly around the cone (Fig. 10a). For the cone which buckled under a small axial compressive load and a lateral pressure, long wave length diamond-shaped buckles occurred at mid-height (Fig. 10b). As the axial load was increased with a corresponding reduction in lateral pressure, the buckles became more pronounced and of a shorter wave length diamond pattern (Fig. 10c). For the shell which was buckled under axial load alone, very short wave length diamond-shaped buckles occurred immediately below the loading flange (where the net section is the smallest), as shown in Fig. 10d.

The influence of axial stress (with no lateral pressure) at buckling is shown by the comparison in Fig. 11.

The stress level at the buckle location was well below the proportional limit of the material for the 0.040-in. cone (Fig. 11a), at about the proportional limit for the 0.063-in. cone (Fig. 11b), and at the yield stress of the material for the 0.105-in. cone (Fig. 11c). The progression of instability from elastic to plastic buckling is apparent.

References

1. *Allen, H. J., and Eggers, A. J., Jr., "A Study of the Motion and Aerodynamic Heating of Missiles Entering the Earth's Atmosphere at High Supersonic Speeds," NACA TN 4047 (October 1957).*
2. *Kaplan, A., and Fung, Y. C., "A Nonlinear Theory of Bending and Buckling of Thin Elastic Shallow Spherical Shells," NACA TN 3212 (August 1954).*
3. *Reiss, E. L., Greenberg, H. J., and Keller, H. B., "Nonlinear Deflections of Shallow Spherical Shells," J. Aero. Sci. 24 (7), 533–543 (1957).*
4. *Archer, R. R., "Stability Limits for a Clamped Spherical Shell Segment under Uniform Pressure," Quart. Appl. Math. 15 (4), 355–366 (1958).*
5. *Weinitschke, H. J., "On the Nonlinear Theory of Shallow Spherical Shells," J. Soc. Ind. Appl. Math. 6 (3), 209–232 (1958).*
6. *Tsien, H. S., "A Theory for the Buckling of Thin Shells," J. Aero. Sci. 9, 373–384 (1942).*
7. *Budiansky, B., "Buckling of Clamped Shallow Spherical Shells," Technical Report 5, Contract Nonr 1866 (02), Harvard University. Presented at the IUTAM Symposium on the Theory of Thin Elastic Shells. Delft, Netherlands (August 1959), and to be published in the Proceedings of that meeting.*
8. *Weinitschke, H. J., "On the Stability Problem for Shallow Spherica Shells," to be published in the Journal of Mathematics and Physics.*
9. *von Kloppel, K., and Jungbluth, O., "Beitrag zum Durchschlag Problem dunnwandiger, Kugelschalen," Der Stahlbau 22, 121–130 (errata p. 288), Berlin Springer (1935) (in German).*

Photothermoelastic Analysis of Bonded Propellant Grains

A technique for the direct thermal loading of propellant-grain models has been developed and the results obtained for this loading have been compared with those obtained previously using pressure loading

by I. M. Daniel and A. J. Durelli

ABSTRACT—A two-dimensional model of the transversal cross section of a bonded rocket propellant grain was subjected to uniform and steady thermal loading and, alternatively, to mechanically applied uniform radial displacements on the outer boundary. The optimization of perforation contours (attained in previous research programs by applying uniform pressure on the outer boundary of the grain model) was confirmed for both types of thermal loading.

The concentration factor at the fillets of the inner contour was determined. An attempt was made to predict the maximum strain in the actual propellant subjected to the same thermal conditions.

The material used for the model was a urethane rubber. The thermoelastic properties of the model material were determined.

Introduction

A propellant grain is usually a thick-wall hollow cylinder bonded to the motor shell. The inner boundary of the grain cross section is usually star-shaped with sharp fillets at the points of the star. The outer boundary is sometimes irregular due to the presence of ducts next to the motor shell.

An important loading condition is the internal pressure produced by the burning, another is the change in temperature. The complete three-dimensional problem is too complicated to be analyzed effectively, mathematically or experimentally. If the effects of the ends are neglected, the middle portion of the grain can be considered to be under conditions of plane strain, but significant results can be obtained by analyzing a two-dimensional photoelastic model of the transversal cross section. The transversal stresses in the middle portion are the most significant and the concentration factor determined on the basis of the plane-stress approximation will not be appreciably different from the actual concentration factor in the three-dimensional propellant grain.

An extensive amount of work has been conducted on the experimental stress analysis of rocket propellant grains. The technique of effectively simulating the pressure loading in a propellant grain was developed by Durelli, Lake and Tsao.[1] The same technique has been used as an approximation in the analysis of propellant grains subjected to thermal loading, simulating the effects of uniform temperature changes by uniform external pressure. The effects of temperature gradients have been simulated by mechanically applying deformations at different points of the model by means of a deformeter.[2]

An important application of the experimental analysis of propellant grains is the optimization of contours. In previous research programs,[3-4] the inner and outer contours were optimized by studying the isochromatic fringe patterns obtained by loading the model by uniform pressure on the outer boundary, and several characteristic indices were defined as criteria for the merit of a design. It was found that a fillet design can be judged optimum if the maximum order fringe lies along or is parallel to the fillet contour.[5] While the uniform pressure loading is perfectly valid for the case of unbonded grains subjected to internal pressure, there were doubts as to how well it approximates the thermal loading of bonded grains.

The objectives of this program were to develop the technique of direct thermal loading of propellant-grain models and to compare results obtained for this loading with those obtained previously using pressure loading.

When the temperature of the motor shell is suddenly changed, a bonded grain is subjected to transient thermal stresses. It has been pointed out that, for the case of a thick circular cylinder, these thermal stresses will be monotonic functions of time and will reach a maximum either initially or finally when thermal equilibrium has been reached.[6] If this is also true for the star-shaped propellant, it is believed that the stresses on the outer boundary will reach a maximum initially and the stresses in the fillets of the inner boundary will reach a maximum finally, after thermal equilibrium has been reached but before appreciable viscous flow has taken place.

I. M. Daniel and A. J. Durelli are associated with Armour Research Foundation, Chicago, Ill.

Paper was presented at 1960 SESA Annual Meeting held in Berkeley, Calif., on October 19–21.

In this investigation only the case of uniform temperature changes were studied.

The grain subjected to a uniform drop in temperature tends to contract more than the motor shell and, as a result, it behaves as if it were subjected to radial displacements on the outer boundary, which are proportional to the radial distance. Thus, radial and circumferential tensile stresses are induced in the grain.

Two indices are used here for the evaluation of the grain design. One, $K_{\epsilon t}$, is the ratio of the maximum strain in the interior fillets of the grain at a given temperature to the uniform thermal strain produced in a stress-free body at the same temperature. The ratio K_{tu} between the maximum strain in the grain model and the maximum strain in a ring of width equal to that of the grain web is defined as the concentration factor for the inner fillets of the grain contour. (The web of the grain is defined as the radial distance between the center of the interior fillet and the outer contour.)

Two methods of studying the effects of thermal loading were used. The first one is a mechanical equivalent of thermal loading and consists of mechanically applying displacements to the outer boundary. The other method is the direct thermal loading in which the model is subjected to a drop in temperature.

Mechanical Equivalent of Uniform Thermal Loading

Test Procedures

A perforation in the shape of the outer contour of the grain model was made in a $^1/_2$-in. thick plexiglas plate. A grain model oversized by 1.2% relative to the perforation in the plexiglas plate was machined out of a soft urethane rubber identified as Hysol 8530 CH. The slightly oversized model was shrunk into the plexiglas mold and the resulting photoelastic pattern (Fig. 1) was viewed and photographed in the polariscope. The patterns show some irregularities along the outer boundary of the model due to small imperfections in the contact surfaces. However, this distortion does not extend to the fillets of the inner boundary and can be ignored in the determination of the stress concentration.

Results

It can be seen from the enlarged fringe patterns around the inner fillets of the grain model tested (Fig. 1), that no appreciable reduction in stress concentration can be effected by slight changes in the fillet contour. The maximum fringe order measured for 0.047 in. induced displacement at the outer boundary was:

$$n_{max} = 10.5 \tag{1}$$

The maximum fringe order present in a ring subjected to a given uniform radial displacement δ on the outer boundary is:

$$n_{ring} = \frac{E(\delta/b)}{(1 + \nu)m^2 + (1 - \nu)} \frac{t}{f_\sigma} \tag{2}$$

where

E = modulus of elasticity of ring.
δ = induced radial displacement at the outer boundary.
t = thickness of ring.
f_σ = material fringe value.
ν = Poisson's ratio.
b = outer radius or ring.
m = ratio of inner to outer radius.

For a ring of the same material as that of the grain model and width equal to its web, $E = 410$ psi, $\nu = 0.47$, $f_\sigma = 0.525$ psi/fringe, $t = 0.42$ in., $m^2 = 0.313$, $\delta/b = 0.012$ in/in. Then,

$$n_{ring} = 4.0 \tag{3}$$

and the concentration factor is

$$K_{tu} = \frac{n_{max}}{n_{ring}} = 2.63 \tag{4}$$

The maximum stress or strain per degree of temperature drop in the associated temperature problem can be determined from the concentration factor if the coefficient of thermal expansion and the material properties of the propellant grain are known at the desired temperatures.

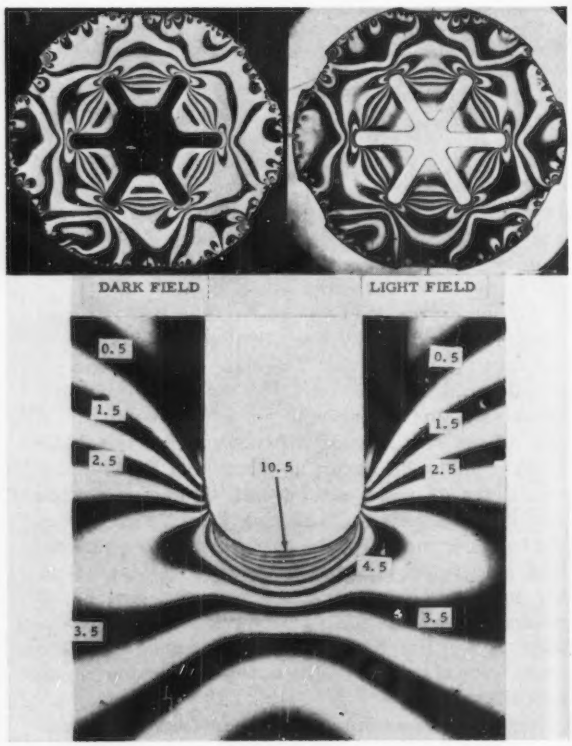

Fig. 1—Isochromatic fringe patterns of grain model subjected to mechanically applied radial displacements at the outer boundary. Enlargement of pattern around internal fillet. (Radial deformation applied was 1.2%. Fringe orders are indicated on the photograph)

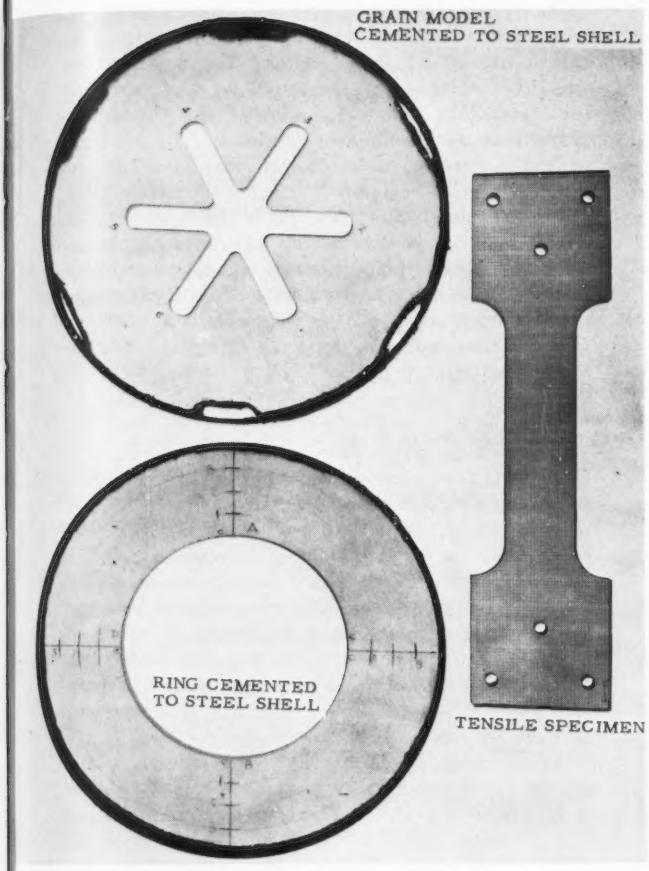

Fig. 2—Grain model and calibration specimens used in the experiments for steady uniform thermal loading. (Material is urethane rubber Hysol 8705)

Uniform Steady Thermal Loading of Propellant-grain Models

Test Procedure

A scaled steel model of the rocket-shell cross section with six alternate shapes of ducts was manufactured and a urethane-rubber model of the propellant-grain cross section was cemented to it. The model material was Hysol 8705. In addition to the grain model, a urethane-rubber ring of width equal to the web of the grain and cemented to a

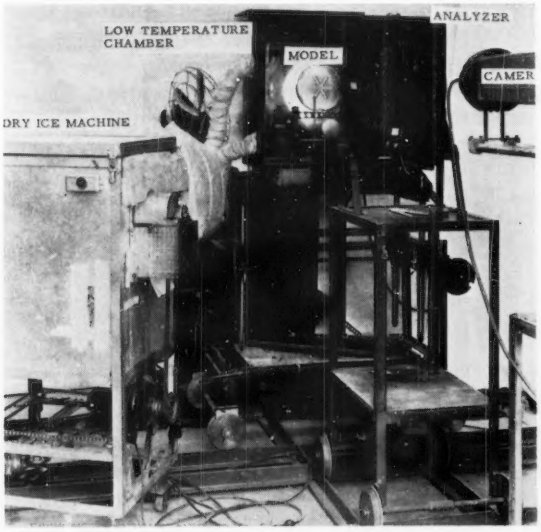

Fig. 3—Equipment and experimental setup for uniform thermal loading of grain model

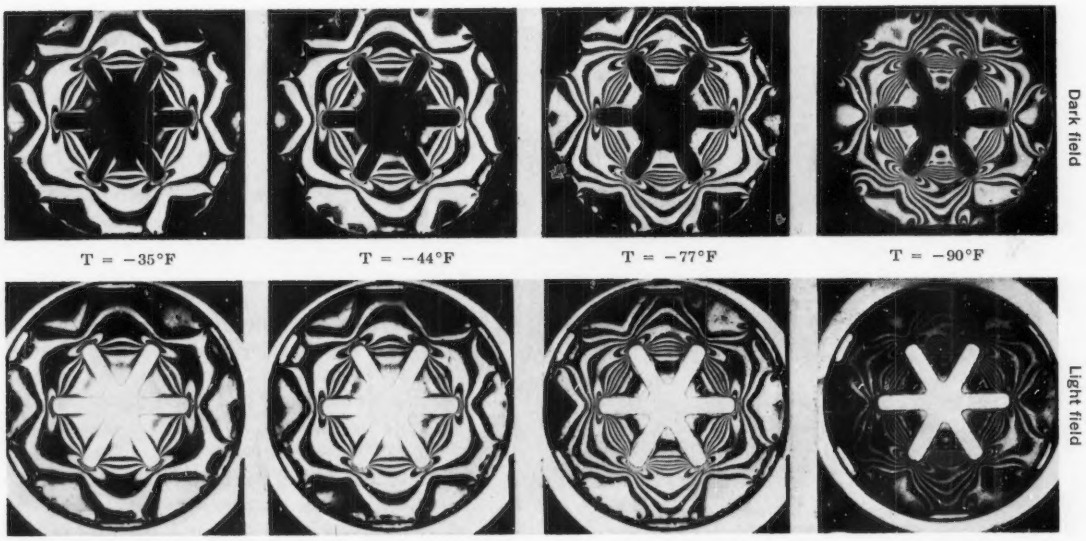

Fig. 4—Isochromatic fringe patterns of grain model obtained at several levels of temperature

steel ring was used. The urethane-rubber properties were determined from a tensile specimen and two disks. The model and calibration specimens tested are shown in Fig. 2.

A low-temperature chamber was built for the tests. It is a box with thermopane glass in the back and front faces, a side door and two openings for the inlet and outlet of the air. A dry-ice refrigerating machine with a variable-speed fan was used and its inlet and outlet hoses were connected to the two openings of the chamber (Fig. 3). Moisture condensation on the external faces of the thermopane was controlled by fans. The model and calibration specimens were placed in the chamber and the temperature was dropped to several low levels by varying the quantity of dry ice and the speed of the machine blower. Temperatures as low as $-90°$ F were reached in the chamber. The temperature recording was done by thermometers placed at various positions in the box. All results that follow refer to this environmental temperature and not to the actual model temperature. The temperature was dropped in steps. At every level of temperature, sufficient time was allowed for the fringe patterns in the specimens to stabilize. In this time interval, however, most of the retarded elasticity response and viscous flow of the model material took place. Although the viscoelastic behavior of the model material is a handicap in the study of an elasticity problem this is not necessarily disadvantageous in the present case, since the prototype material exhibits also some viscoelastic properties. (For the thermoelastic properties of Hysol 8705, see the Appendix.)

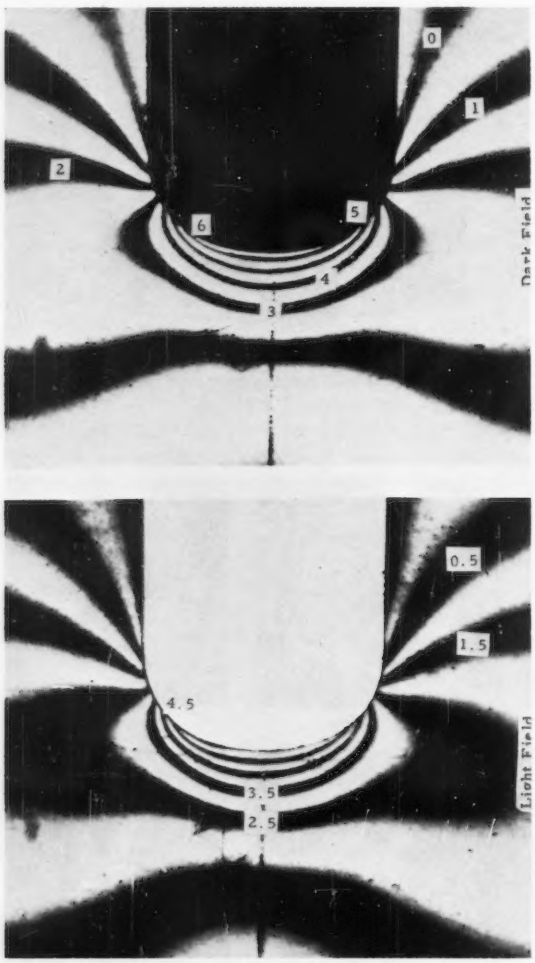

Fig. 5—Isochromatic fringe pattern around internal fillet of grain model at —25°F. (Fringe orders are indicated on the photographs)

Results

Isochromatic fringe patterns obtained for several levels of temperature are shown in Fig. 4. Figure 5 shows an enlargement of the fringe pattern around the inner fillet. The nature of these patterns indicates that no appreciable improvement can be effected by small changes in the fillet contour, which has already been optimized for a uniform pressure loading applied to the outer boundary.

The maximum fringe order in the grain model was plotted vs. temperature in Fig. 6. It can be seen that this fringe order does not increase in linear proportion to the drop in temperature. The fringe order increases faster at low temperatures. This can be attributed mainly to the viscoelastic nature of Hysol 8705 at low temperatures (see Appendix.) The retarded elastic response of the material becomes more pronounced as the temperature decreases. The coefficient of thermal expansion was found to increase with reduction in temperature and the strain fringe value was found to decrease with temperature.

The maximum strain in the fillet is:

$$\epsilon_{max} = \frac{2n}{t} \frac{f_\epsilon}{(1 + \nu)} \qquad (5)$$

where

n = fringe order.
f_ϵ = strain fringe value.
t = model thickness.
ν = Poisson's ratio.

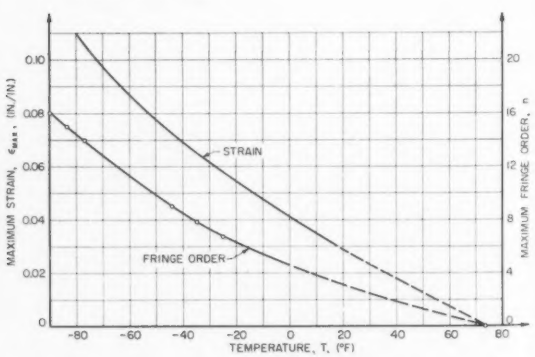

Fig. 6—Maximum fringe order and maximum strain in grain model versus temperature

Figure 6 depicts also the variation of ϵ_{max} with temperature.

The thermal strain in a stress-free body subjected to a uniform change in temperature T is

$$\epsilon_t = \int_0^T \alpha \, dT \tag{6}$$

If the coefficient of thermal expansion α is not a function of temperature

$$\epsilon_t = \alpha T \tag{7}$$

In the case of the propellant model cemented to the steel shell, this temperature strain will be defined as

$$\epsilon_t = \int_0^T (\alpha_1 - \alpha_0) dT \tag{8}$$

where

α_1 = coefficient of thermal expansion of the model material.
α_0 = coefficient of thermal expansion of steel.

The following index $K_{\epsilon t}$ is introduced as a criterion for the merit of a grain design from the standpoint of steady uniform thermal loading:

$$K_{\epsilon t} = \frac{\epsilon_{max}}{\epsilon_t} = \frac{\epsilon_{max}}{\int_0^T (\alpha_1 - \alpha_0) dT} \tag{9}$$

From the maximum strain ϵ_{max} and from measurements of thermal contraction (see Appendix), the index $K_{\epsilon t}$ was found to be:

$$K_{\epsilon t} \cong 5.9 \tag{10}$$

This is the average value of the index for a temperature range from 0 to $-80°$ F. The deviations from this value were less than 5%.

For the determination of the concentration factor present at the internal fillets, a ring was also tested. This ring has an inner radius equal to the radial distance of the center of the internal fillets of the grain and an outer radius equal to the outer radius of the grain model. The maximum strain at the inner boundary of the ring was obtained photoelastically for several levels of temperature. The ratio K_{tu} between the maximum strain in the grain and the maximum strain in the ring is defined as the concentration factor. This factor is independent of the temperature level and was found to be

$$K_{tu} = \frac{\epsilon_{max}}{\epsilon_{ring}} = 2.46 \tag{11}$$

Discussion

The values of the concentration factor K_{tu} obtained by the two methods of thermal loading differ by about 6%. This discrepancy is not very large and may be due to several factors. Slight variations in the material constants can affect it. The mechanical method may not duplicate thermal effects exactly, as it allows some circumferential displacements at the outer boundary of the model. Besides, in the thermal test there was evidence of a small thermal gradient in the radial direction of the ring. It is interesting to compare the values 2.63 and 2.46 for K_{tu} and the concentration factor $K_{\sigma'} = 2.63$, obtained for a uniform internal pressure in the propellant grain. ($K_{\sigma'}$ is defined in Reference 3 the same way as K_{tu}.)

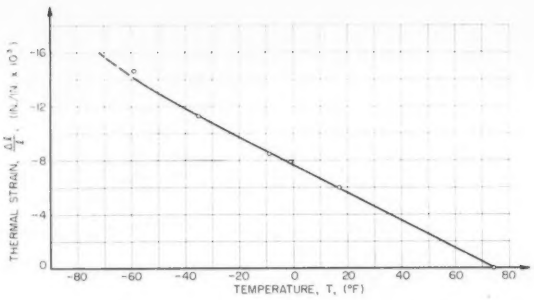

Fig. 7—Thermal strain versus temperature for Hysol 8705. (The slope of this curve gives the coefficient of thermal expansion)

Index $K_{\epsilon t}$ can be used in an attempt to predict maximum thermal strains in the actual propellant subjected to a drop in temperature. Neglecting three-dimensional effects and assuming similar viscoelastic behavior of the propellant and model materials, we get

$$\epsilon_p \cong K_{\epsilon t} \int_0^T (\alpha_p - \alpha_0) dT \tag{12}$$

where

ϵ_p = maximum strain in the propellant.
α_p = coefficient of thermal expansion for the propellant material.
α_0 = coefficient of thermal expansion for steel ($=7 \times 10^{-6}$ in/in/° F.)

The coefficient α_p depends on the type of propellant used. No reliable figure for α_p is known to the authors for the low temperatures considered. For a typical propellant it is known that

$$\alpha_p = 54 \times 10^{-6} \text{ in/in/° F} \tag{13}$$

Assuming this value to remain constant at temperatures below zero, it is found that, for a temperature drop from $+75$ to $-25°$ F,

$$\epsilon_p(@_{-25°\,F}) \cong 5.9 \times 47 \times 10^{-4} = 0.028 \text{ in/in} \tag{14}$$

An alternate method of estimating the maximum strain in the propellant, taking into consideration three-dimensional effects, is the following:

The stresses in a long hollow circular cylinder bonded to a steel case and subjected to a uniform change in temperature are:[6]

$$\sigma_r = \frac{E\epsilon_t}{1 - 2\nu + m^2}\left(1 - \frac{a^2}{r^2}\right)$$
$$\sigma_\theta = \frac{E\epsilon_t}{1 - 2\nu + m^2}\left(1 + \frac{a^2}{r^2}\right) \tag{15}$$
$$\sigma_z = \frac{E\epsilon_t}{1 - 2\nu + m^2}(1 + m^2)$$

where ϵ_t is defined as in eq (8).

The maximum strain in the cylinder is

$$\epsilon_{cyl} = (\epsilon_\theta)_{r=a} = \frac{\epsilon_t}{1 - 2\nu + m^2}\left[2 - \nu(1 + m^2)\right] \tag{16}$$

For a temperature drop from $+75$ to $-25°$ F and $\nu = 0.4$

$$\epsilon_{cyl}(@_{-25°\,F}) = 0.0135 \text{ in./in.} \tag{17}$$

Using the concentration factor K_{tu} (determined photoelastically), we obtain:

$$\epsilon_p = K_{tu} \quad \epsilon_{cyl} = 0.033 \text{ in/in.} \tag{18}$$

This strain could be compared with the ultimate strain of the propellant material determined for the particular level of temperature and for low strain rate. This comparison would give approximately an allowable temperature differential that the given grain design can withstand. It must be understood that all these conclusions are approximate and conditional on the assumptions made. They could be refined if the properties of the propellant were known better.

APPENDIX—THERMOELASTIC PROPERTIES OF HYSOL 8705

Introduction

Hysol 8705 is a soft urethane rubber very sensitive photoelastically. It is free from any measurable time-edge effects and does not exhibit viscous flow at room temperature. It has a high coefficient of thermal expansion and can be easily machined and cemented to other materials. For these reasons, it was chosen for the thermoelastic analysis of propellant grains.

The procedures followed for the determination of the coefficient of thermal expansion, modulus of elasticity, Poisson's ratio and material fringe values as functions of temperature are outlined below.

Coefficient of Thermal Expansion

A $^1/_4$-in. thick sheet of Hysol 8705 with a fine scribed grid on one face was suspended inside the cold chamber. Photographs were taken at room temperature and at several stabilized levels of low temperature. Photographic plates were used instead of film in order to avoid distortions due to film warping. The dimensional changes in the photographs were measured by means of a linear comparator. Using the room temperature of 74° F as a base temperature, the thermal strain was determined and plotted vs. temperature (Fig. 7). By differentiation of this curve, the coefficient of thermal expansion can be determined. This coefficient appears to remain constant down to about −30° F and then seems to increase a little. The value of the coefficient for the −30 to 75° F range is

$$\alpha(_{-30 \text{ to } 75}{}^\circ \text{ F}) = 104 \times 10^{-6} \text{ in/in/}^\circ \text{ F} \tag{19}$$

The values of α for lower temperatures cannot be determined with accuracy from the slope of a curve drawn through a few points. In the applications, however, the coefficient itself is not significant but the total unit contraction that takes place for a drop from room temperature to a given level of temperature. This is the thermal strain previously referred to in the section on "Uniform Steady Thermal Loading of Propellant-grain Models."

Polymers of the type of Hysol 8705 usually respond linearly to temperature within certain ranges of temperature. The coefficient of thermal expansion drops abruptly at a transition temperature, the "brittle point." There is no evidence in Fig. 7 that this point has been reached. The "brittle point" for urethane rubbers of the same group as given by Houghton Laboratories is below −80° F.

Modulus of Elasticity and Poisson's Ratio

These constants were obtained from a uniaxial specimen with a scribed grid on one surface. At room temperature (75° F) the material behaves elastically and it was found that

$$E = 430 \text{ psi} \qquad \nu = 0.467 \tag{20}$$

As the temperature decreases, the material becomes more and more viscoelastic exhibiting the phenomena of instantaneous elasticity, retarded elasticity and flow. The elastic constants are then functions of loading time and rate of loading. The mechanism of response of an idealized viscoelastic material can be represented by the mechanical model of Fig. 8. The instantaneous elasticity mechanism is represented by a spring of modulus G_1 (the instantaneous shear modulus of the material). The retarded elasticity mechanism is represented by a spring and a dashpot of modulus G_2 and viscosity η_2, respectively. Finally, the flow mechanism is represented by a dashpot of viscosity η_3.[7] The stress-strain relation is represented by eq[8]:

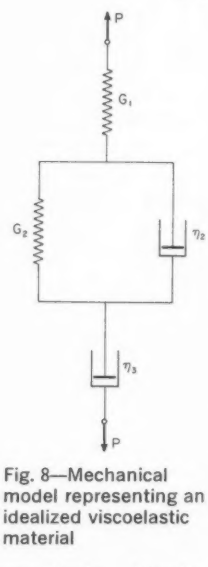

Fig. 8—Mechanical model representing an idealized viscoelastic material

$$\gamma = \tau \frac{1}{G_1} + \tau \frac{1}{G_2}(1 - e^{-G_2 t/\eta_2}) + \tau \frac{1}{\eta_3} t \tag{21}$$

where

γ = shear strain.
τ = shear stress.
G_1, G_2 = instantaneous and retarded shear moduli; $G_1 = E/[2(1 + \nu)]$.
η_2, η_3 = viscosities.
t = time.

At low temperatures, η_3 is very large and the flow is negligible. The instantaneous modulus G_1 increases as the temperature decreases and the elastic deformation becomes small. Retarded elasticity (or configurational elasticity) becomes more apparent as the temperature decreases, but the rate of the retarded elastic response decreases with temperature.[9] If the time of load application is sufficiently long, it is possible for almost all of the delayed elastic response to take place before the measurements are recorded. (This is often referred to as "cold flow.")

Thermal loading of a rocket propellant grain would

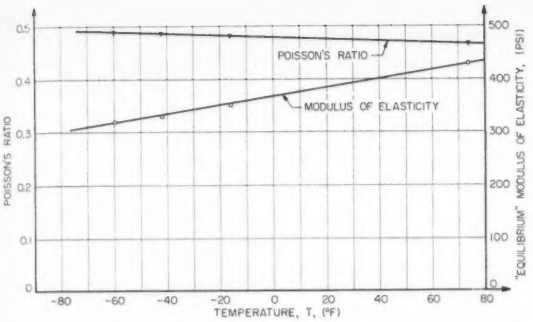

Fig. 9—"Equilibrium" modulus of elasticity and Poisson's ratio of Hysol 8705 versus temperature. (Values were obtained from a tensile specimen subjected to a constant load of long duration)

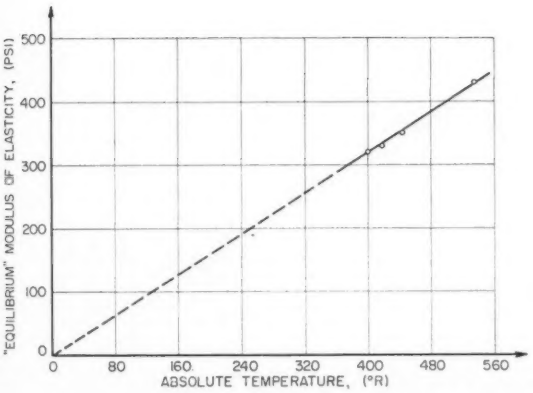

Fig. 10—"Equilibrium" modulus of elasticity of Hysol 8705 versus absolute temperature indicating the nature of "gas-like" elasticity of rubber-like materials. (Values were obtained from a tensile specimen subjected to a constant load of long duration)

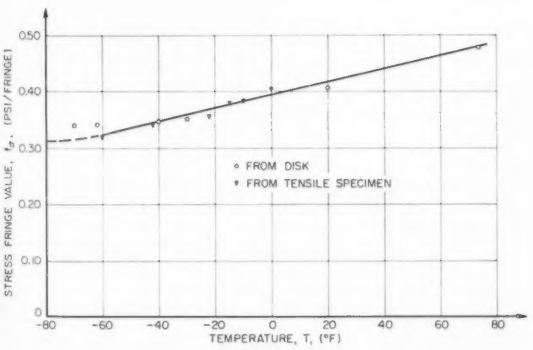

Fig. 11—Stress fringe value of Hysol 8705 versus temperature. (Values were obtained from a disk and a tensile specimen subjected to constant loads of long duration)

be a very slow loading over a relatively long period of time. The grain model was subjected to such a slow load of long duration. For this reason, the instantaneous elastic modulus of the model material is not the most significant one. The tensile specimen was loaded at room temperature and the load was left on throughout the period of the experiment. The temperature was dropped in steps and sufficient time was allowed for almost all the "cold flow" to take place. Photographs were taken at all stabilized levels of temperature and the strains measured by means of the comparator. In this manner, the "equilibrium" elastic modulus, and Poisson's ratio were determined and plotted in Fig. 9. It is interesting to note the linear variation of the modulus of elasticity with temperature. This is not surprising, however, since at the stage of complete equilibrium the elastic behavior of rubberlike materials is analogous to the elastic behavior of ideal gases.[9] In that case, the elastic modulus should be roughly proportional to the absolute temperature. Indeed, as can be seen in Fig. 10, this is true. The elastic modulus extrapolated at absolute zero would be zero. Poisson's ratio approaches soon the value of $^1/_2$, thus the material approaches the state of incompressibility.

Material Fringe Value

The prevalent point of view is Fresnel's hypothesis that birefringence of a photoelastic material is fundamentally a function of strain. For the two-dimensional state of stress in elastic materials, where the stress-strain relations are independent of time, one photoelastic constant is sufficient for the interpretation of fringe patterns. For materials that creep under load, the strain is not uniquely determined from the stress, and the stress-optic law must take both stress and strain into consideration. Coker and Filon[10] suggested that, for such a material, birefringence could be described as a linear combination of stress and strain and that two constants, a strain fringe value and a stress fringe value, are necessary for the interpretation of fringe patterns. This view was supported by Alfrey.[11] Mindlin[12] showed that, for a material exhibiting retarded elasticity but no flow, the relative birefringence is a linear function of stress and strain only.

The material used in this program exhibits appreciable retarded elasticity but negligible flow at low temperatures. The fringe patterns to be interpreted resulted from loads of long duration, which allowed most of the retarded elastic response to take place. This condition was simulated in the calibration tests. Fringe order readings were taken at the "equilibrium" state when the patterns were almost stabilized. At this state, the stress-strain relations of elasticity can be used since the time dependence of strains was almost eliminated. Thus, the material was treated as an elastic one and only one independent photoelastic constant was used.

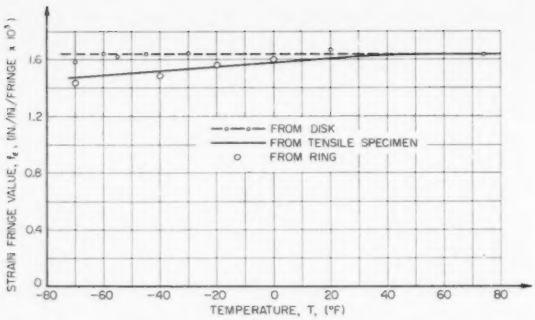

Fig. 12—Strain fringe value of Hysol 8705 versus temperature. (Values were obtained from a disk under constant deflection, a tensile specimen under constant load and a ring cemented to a steel ring. Readings were taken after delayed elastic response had taken place)

The stress fringe value was determined from a disk and a tensile specimen subjected to constant loads. The loads were kept on the specimens throughout the experiment and readings were taken at several levels of temperature. The "equilibrium" stress fringe value was plotted versus temperature in Fig. 11.

The "equilibrium" strain fringe value was obtained from three specimens: a tensile specimen under constant load, a ring cemented to a steel ring and a disk subjected to a constant (at room temperature) diametral deflection by means of a steel frame. Direct strain measurements in the tensile specimen were related to the fringe order readings at several levels of temperature. The strain fringe value from the ring was obtained from the following expression:

$$f_\epsilon = \frac{t}{n} \frac{\epsilon_t}{(1 + m^2) - \nu(1 - m^2)} (1 + \nu) \left(\frac{a}{r}\right)^2 \quad (22)$$

where

f_ϵ = strain fringe value.
t = thickness of ring.
n = fringe order at a point.
$\epsilon_t = \int_0^T (\alpha_1 - \alpha_0) dT$ = thermal strain as defined in eq. (8).
$m = a/b$ = ratio of inner radius to outer radius.
ν = Poisson's ratio.
r = radial distance of a given point.

The formula above was applied at the outer boundary of the ring, where $r = b$.

The strains at the center of the disk subjected to a given diametral deflection were calculated from the fringe order at room temperature and the strain fringe value at the same temperature. The diametral deflection was measured at room temperature and calculated at the other levels of temperature from the known differential contraction of the disk and the frame. It was assumed that the strains at the center of the disk are proportional to the diametral deflection. Thus, the strains at several low temperatures were calculated and related to the measured fringe orders.

The strain fringe value as determined from the three specimens above is plotted vs. temperature in Fig. 12. The values obtained from the ring and the tensile specimen are close to each other and show a small decrease of the strain fringe value with temperature. The values obtained from the disk are a little higher than the others and indicate a nearly constant (with temperature) fringe value. This discrepancy may be due to errors introduced by the indirect method used in the case of the disk.

Acknowledgment

The authors wish to express their appreciation to Thiokol Chemical Corp., Elkton, Md., for sponsoring the research program covered in this paper and permitting the publication of results. Thanks are also due to the Armour Research Foundation for supporting the publication.

Bibliography

1. *Durelli, A. J., Lake, R. L., and Tsao, C. H., "Device for Applying Uniform Loading to Boundaries of Complicated Shape,"* Proc. SESA, XI, *No. 1, 55–61 (1953).*
2. *Barriage, J. B., and Durelli, A. J., "Application of a New Deformeter to Two-Dimensional Thermal Stress Problems,"* Ibid., XIII, *No. 2, 97–106 (1956).*
3. *Durelli, A. J., and Hofer, K., "Photoelastic Studies of Stress and Strain Concentration Factors Associated with Rocket Propellant Grain Designs," Final Report, Armour Research Foundation, Project No. K165, Phase I, April 1959, to Thiokol Chemical Corp., Elkton Division, Elkton, Md.*
4. *Durelli, A. J., and Daniel, I. M., "Optimization of Outer Contour of Rocket Propellant Grain Designs," Final Report, Armour Research Foundation, Project No. K165, Phase 2, June 1959, to Thiokol Chemical Corp., Elkton Division, Elkton, Md.*
5. *Durelli, A. J., and Lake, R. L., "Determination of Optimum Geometry for Star-Perforated Propellant Grains," Final Report, Armour Research Foundation, Project K036-7, February 1953, to Thiokol Chemical Corp., Huntsville, Ala.*
6. *Zwick, S. A., "Thermal Stresses in an Infinite, Hollow Case-Bonded Cylinder,"* Jet Propulsion (*August 1957*).
7. *Alfrey, T.,* Mechanical Behavior of High Polymers, *Interscience Publishers, Inc., New York, p. 104 (1948).*
8. Ibid., *pp. 116–119.*
9. Ibid., *pp. 112–113.*
10. *Coker, E. G., and Filon, L. N. G.,* A Treatise on Photoelasticity, *Cambridge University Press, London, p. 273 (1932).*
11. *Alfrey T.,* loc. cit., *p. 224.*
12. *Mindlin, R. D., "A Mathematical Theory of Photo-Viscoelasticity,"* Jnl. Appl. Mech., **20**, *206–216 (February 1949).*

sesa news

Plant Tour and Ladies' Program Among Events Featured at Spring Meeting

Among the arrangements now definitely scheduled for the annual Spring Meeting to be held at the Benjamin Franklin Hotel, Philadelphia, May 10th–12th, are two that should prove a big drawing card. One is the plant tour scheduled for Thursday afternoon, May 11th, when the men will have a chance to stretch their legs and look around at what is probably one of the most modern coal-fired, high-pressure-steam electric generating plants in the country, now in operation. The other is probably the only good opportunity the "better halves" will find for avoiding a lot of unnecessary stresses and strains so important to their spouses. The Ladies' Program should prove to be a pleasant diversion.

Plant Tour Unusual

The Eddystone Station of the Philadelphia Electric Co. started operation in early 1960 with temperatures and pressures higher than had been previously used in the industry. Their No. 1 unit which operates in the supercritical region of 5000 psi and 1200° F was the result of a tremendous amount of research, investigation and testing. The more conventional No. 2 unit is designed for 3500 psi and 1050° F while each unit operates with reheats to 1050° F and is rated at 325,000 kw. Many innovations and engineering "firsts" have been incorporated in this 650,000-kw station. From coal handling details to the control of the two 18-ft, 6-in. diam stacks, the Eddystone installation, located on the Delaware near Philadelphia, should make an interesting tour.

Ladies Plan Sight-seeing Tours

A three-day program of activities scheduled for the ladies includes two days of sight-seeing in and around the Philadelphia area and one day of shopping. On Wednesday, a trip has been arranged around the points of historic interest in the City of Brotherly Love. Visits will be made to Independence Hall, Betsy Ross House and other places of colonial fame. On Thursday, after a "brunch" at the Hotel, the ladies will embark for a trip to Longwood Gardens, the fabulous estate built by Pierre S. duPont. Here will be seen one of the most complete and unusual horticultural displays in the country. Famous for its floral arrays in planting and for the landscaping of bushes, shrubs and flowers, Longwood is equally noted for its extensive orchid collection. On Friday, the ladies will have a day off to shop, each according to her pleasure.

Technical Paper Sessions

The main event of the three-day meeting, is shaping up to a five-session technical program. Four of the sessions are expected to develop from the 13 papers reviewed by the Papers and Proceedings Committee. One session will be arranged from the papers developed by the local Technical Papers Committee on the meeting theme: "Experimental Mechanics at High Temperatures." The tentative program arrangement of the papers and sessions will be made shortly and will appear in the April issue of EXPERIMENTAL MECHANICS. Papers selected by the Papers and Proceedings Committee will be published in E/M and will also appear subsequently in the bound volumes of SESA *Proceedings*. The papers for the theme session will also be considered for later publication in EXPERIMENTAL MECHANICS and the *Proceedings* after due review and approval by the Papers and Proceedings Committee members.

Computer Seminar Arouses Interest

On Wednesday evening a seminar titled, "The Role of Computers as a Tool in Experimental Mechanics" will cover two points of emphasis

---

SITE OF SPRING MEETING PLANT TOUR

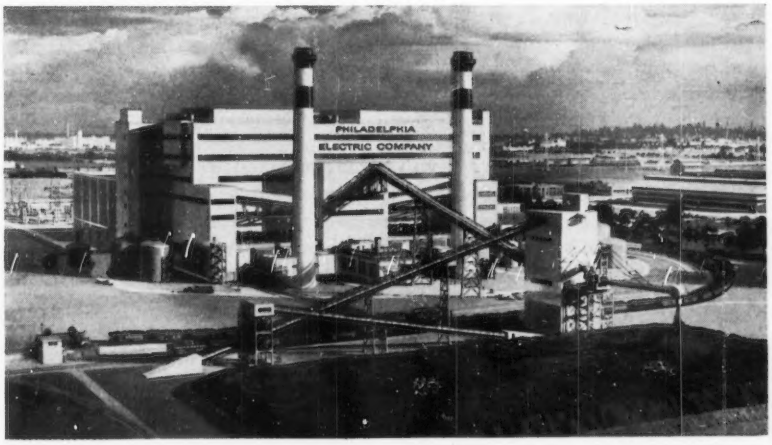

Aerial view of Philadelphia's Eddystone Electric Generating Station showing coal-handling equipment in the foreground. Plant-tour group will visit this installation during Spring Meeting, on May 11th

regarding the use of analog and digital computers. The first will be an introduction to the philosophy of computers: the basic differences between the type of analysis possible, the kind of mathematical functions inherent in the analog and digital circuitry. Fundamentals of programming will be discussed. The second part of the program will cover the solution of an actual problem in experimental mechanics. The digital installation at the University of Pennsylvania and the analog and digital machines at Drexel Institute are available for the seminar group and a visit is planned to one or both of these installations.

Banquet Scheduled

Scheduled for Thursday evening, a banquet, preceded by a cocktail hour, will feature a full-course hotel dinner and a prominent speaker of interest to the members. The details of this affair will become available for the next issue of EXPERIMENTAL MECHANICS.

... *SECOND THOUGHTS ON NSF GRANT*

There is some likelihood that the recent grant by The National Science Foundation to the SESA is not fully understood. Therefore, its nature and purpose can well be described in more detail. The specific purpose of the $45,000 grant is to help defray the expenses of organizing and producing the monthly journal, EXPERIMENTAL MECHANICS, for three years—at which time the magazine is expected to be self-supporting. As was well known, the financial resources of the SESA were not equal to the extraordinarily high cost of initiating a new journal, no matter how promising. With the aid of the NSF grant, the *Journal* has been able to make its debut in full dress and—although not perfect, to be sure—ready to take its place alongside other scientific and engineering publications.

The nature of the grant is related to the statutory responsibility of the NSF "to develop and encourage the pursuit of a national policy for the promotion of basic research and education in the sciences." The point is taken that science and technology in this country occupy a very important place, not only in our intellectual climate but in the future of our welfare and security. In this regard, the prompt and widespread publication of important technical papers becomes an urgent need. It is the duty of EXPERIMENTAL MECHANICS to help fill this need.

The importance of the fields in experimental mechanics today stems from the fact that modern developments in space, nuclear and rocketry technologies are asking questions never asked before and making ultimate demands upon the performance of materials and structures. Some of the older theories and assumptions, previously satisfactory, are now up for review and many new ones are needed. One of the most satisfactory means of obtaining the needed information—and in some cases the only means—is by studies in experimental mechanics.

Changes are sifting down from the new technologies to the older. The design and fabrication of structures—buildings, bridges, vehicles, machines—are moving in the direction of less weight, more strength, higher speeds, the use of new materials for reasons of economy, versatility, utility and esthetic demands. Again experimental investigation is needed.

Add to this the fact that the *Journal* should undoubtedly play a large part in the growth and development of the Society. The SESA has a tremendous educational potential, for, as most will agree, all is not learned at college. Herbert Hoover not long ago said, in speaking of engineering societies, "... they constitute a gigantic post-graduate course that continues all their professional lives."

ARE YOU PLANNING

to write a paper or a technical note for publication in Experimental Mechanics or for oral presentation at a national meeting?

DO YOU KNOW

how you can best organize and prepare your manuscript?

YOU CAN SAVE

time! Yours—the reviewing committee's—the editors'—and improve your chances for early publication;

YOU CAN INCREASE

the value of your presentation—its readability—its clarity—its appeal;

BY OBTAINING AND READING

SESA's instruction manual for authors. This booklet has dozens of helpful hints and suggestions for authors.

YOU WILL FIND

all the important instructions you will need—general information—arranging the contents of a paper—writing the paper—submission and publication—oral presentation—all important advice to aid in processing your paper.

YOU NEED ONLY

to write SESA headquarters, 21 Bridge Square, Westport, Conn. Ask for a copy of the booklet "An SESA Paper" and for the "Author's Check List."

WHEN COMPLETED

send 3 copies of your abstract and manuscript to: Dr. Roscoe Guernsey, Chairman, SESA Papers and Publications Committee, General Electric Co., Bldg. 37, Room 669, Schenectady 5, N. Y.

Two International Meetings Are Scheduled for 1961

Symposium on Photoelasticity Precedes Congress on Experimental Mechanics

This year, the calendar period starting Sunday, October 29th, and ending Friday, November 3rd, will witness in quick succession two international meetings of related importance to members of the SESA. The first meeting will present a number of significant advances made since 1954 in the specific field of photoelasticity. The second will cover the general field of experimental mechanics and, together with an industrial and educational exposition, will comprise the 1961 Annual Meeting of the Society. The timing—October 29–31 and November 1–3, respectively—is intended to bring both programs within the convenient scope of a single week. The arrangement will be of particular benefit to the many visitors from other countries who are expected to attend both meetings. The following are the details as developed to date.

Photoelastic Symposium

The International Symposium on Photoelasticity will be held on Oct. 29–31, 1961, at the Illinois Institute of Technology in Chicago. This Symposium is sponsored by the Office of Ordnance Research of the U. S. Army, IIT and the SESA, and has been coordinated with the SESA First International Congress on Experimental Mechanics scheduled for Nov. 1–3, 1961. Cosponsoring organizations include the ONR, OSR and the Applied Mechanics Division of the ASME.

This Symposium will embrace two- and three-dimensional photoelasticity, two- and three-dimensional photoplasticity, dynamic photoelasticity, birefringent coatings and photothermoelasticity.

The purpose of the Symposium is to provide a forum for the exchange of ideas in this important and rapidly expanding field. The only international meeting dealing with this subject was held in 1954 in Brussels, under the auspices of IUTAM. The advances made since 1954 are rather significant.

Some 30 scientists from England, France, Germany, Japan, Sweden, Switzerland and the United States have indicated their readiness to participate in this Symposium. Twenty-five abstracts have been received.

Inquiries should be addressed to Professor M. M. Frocht, Chairman, International Symposium on Photoelasticity, Illinois Institute of Technology, Chicago 16, Ill., U.S.A.

Experimental Mechanics Congress

The 1961 Annual Meeting of the SESA will become the first International Congress on Experimental Mechanics when it convenes on November 1–3, at the Hotel New Yorker in New York City. For this occasion the entire mezzanine floor of the hotel has been reserved for the purpose of conducting all the main events—registration, technical presentations, industrial and educational exhibits—in one suitably divided area. The Congress, local arrangements for which are being made by the New York Metropolitan Section, will feature technical presentations from a number of leading scientists from European countries—France, Germany, Italy, Netherlands, Portugal, Spain, Sweden and the United Kingdom. Outstanding representatives from this side of the Atlantic will also present papers on various theoretical and practical studies in the field of experimental mechanics.

The international aspect of the Congress and its location in New York City should help to make the 1961 meeting the best attended in SESA history. Equipment and instrumentation manufacturers are expected to take advantage of this situation by setting up displays in the exhibit area. In addition, a number of educational exhibits are being arranged to show typical examples of the latest work being carried on in governmental, private and university research laboratories.

Among the papers for which arrangements have been definitely made are the Murray Lecture award, this year made to Professor Egon Orowan of Massachusetts Institute of Technology, and the invitations extended to scientists abroad. All other papers intended for presentation must be submitted before May 31, 1961, to Dr. Roscoe Guernsey, Jr., Chairman, Papers and Proceedings Committee, Society for Experimental Stress Analysis, General Engineering Laboratory, General Electric Co., Schenectady 5, N. Y.

For other details concerning the meeting, inquiries should be addressed to SESA Headquarters, 21 Bridge Square, Westport, Conn.

ACKNOWLEDGING THE PLAUDITS . . .

Since the launching of EXPERIMENTAL MECHANICS *with the publication of the January issue, the congratulatory messages that have been coming in at headquarters indicate a most favorable reception. Members of SESA may well feel proud that their judgment on the need for this publication is so well supported on such a wide front. However, this is only the beginning for us. While much time and effort have gone into the initial preparation, the big job lies ahead—in the months and years to come. The future success of the Journal will surely depend on the concerted efforts of the membership as well as on how aptly it fills the need for publication of the information in its field.*

EXPERIMENTAL MECHANICS *will provide an earlier and a wider circulation for the research and the engineering papers of its members. Its publication is also expected to stimulate activity in the field of experimental mechanics.*

Many other benefits come from the Journal in the form of news coverage. Pertinent news in industry, new products, personnel changes, news in the universities, educational programs, research news, literature reviews, membership news, section activities, meetings, conferences—to name a few. To consistently organize the full area of readers' interests will take a little time and the full cooperation of the members. In the end, EXPERIMENTAL MECHANICS *will have truly played its part in the growth of the SESA.*

For the moment, on behalf of the staff and all the members who contributed their valuable time and effort, we extend our thanks for the many letters of congratulations received.

The Editors

section reports

Delaware Valley

New Officers Introduced

The Delaware Valley Chapter held a plant tour and a business meeting on Nov. 30, 1960. Sixty-one members and guests attended the plant tour at the Instrument Division of the Budd Co. where live demonstrations were given before interested groups.

After dinner at the Bull Tavern, Vice-chairman L. B. Moffett called the meeting to order and introduced the new officers for the 1960–61 term as follows: Chairman, L. B. Moffett; Vice-chairman, S. W. Sennett; Treasurer, T. C. Baumgartner; Secretary, R. R. Moser.

Chairman Moffett introduced S. W. Sennet as general chairman of the 1961 SESA Spring Meeting which will be held on May 10th–12th in Philadelphia. Mr. Sennet gave a brief rundown on the Spring Meeting including such details as: location at the Ben Franklin Hotel; theme of the meeting, "Experimental Mechanics at High Temperature;" and a general arrangement of events in a tentative schedule for the three-day period.

Mr. Sennet also named the chairmen of the various committees for the Spring Meeting, who are as follows: General Chairman, S. W. Sennet; Assistant Chairman, L. B. Moffett; Exhibits, A. Shore; Technical Sessions, H. M. Owens; Publications and Membership, H. Cook; Banquet, J. E. Scott; Seminars, R. J. Stone; Plant Tours, R. L. Stiles; Finance, P. Swartz; Advisers, L. Mains, F. Tatnall, J. Walmsley; Womens' Committee, Mrs. L. B. Moffett, Mrs. S. W. Sennet, Mrs. B. Sutton.

Following Mr. Sennet's discussion on the Spring Meeting, Mr. Mains and Mr. Walmsley both appealed to the membership for their all-out support and help in making this meeting a success.

(Report and photographs by R. R. Moser for the Delaware Valley Chapter)

Milwaukee

Fatigue in Chains

The first meeting of the 1960–61 season was held on Thursday, December 1, at Chain Belt Co. The meeting opened with a plant tour of the Chain Belt Co. facilities. Highlights of the tour were the Fatigue and Chain Dynamics Laboratory and the Material Handling Laboratory. Following the plant tour (attended by 46 persons), the group assembled for a social hour. Words of welcome were given by V. D. Petershack, past chairman, Milwaukee Section. A highlight of the program was the presentation of a new instrument recently developed by the company. The instrument, known as the "load-peak counter," is designed to record on electric counters random strain-gage load signals that are typical of those found in chain-drive systems.

The technical portion of the program was given in three parts. The

SESA Section Meeting Calendar

MARCH 6

NEW YORK METROPOLITAN Section. Joint meeting with ASME and IES. Dinner: call S. Black, PR 7-2900, Ext. 749, Woodridge, N. J. Talk: 8:00 P.M. Burchard Hall, Stevens Institute of Technology, Hoboken, N. J. "Statistical Methods Simplify Selection and Use of Experimental Data," by H. Gaffney, U. S. Testing Co., Hoboken, N. J.

MARCH 9

HUDSON-MOHAWK Section. Stanley Club, Pittsfield, Mass. Dinner: 7:00 PM. Talk: 8:00 P.M. "The Calculation of Elastic Displacement from Photoelastic Patterns," by Dr. H. Poritsky, General Engineering Lab., General Electric Co., Schenectady, N. Y.

MARCH 16

MILWAUKEE Section. Talk, "New Developments in Strain Gage Techniques," will be presented by a representative from Baldwin-Lima-Hamilton Corp.

APRIL 3

SALT LAKE CITY Section. Organizational meeting. Talk: "The Cause and Prevention of Fatigue Failures in Metal Parts," by C. R. Smith, General Dynamics Corp., San Diego, Calif. Contact: G. W. West, Eng. Lab., Thiokol Chemical Corp., Brigham City, Utah.

APRIL 4

DENVER Section. Organizational meeting. Talk, "The Cause and Prevention of Fatigue Failures in Metal Parts," by C. R. Smith, General Dynamics Corp., San Diego, Calif. Contact: M. Barrett, Ketchum Konkel & Hastings, Eng. Consultants, Denver, Colo.

APRIL 11

SEATTLE Section. Organizational meeting. Talk, "The Cause and Prevention of Fatigue Failures in Metal Parts," by C. R. Smith, General Dynamics Corp., San Diego, Calif. Contact: Prof. Emmet Day, Dept. Mech. Engr., Univ. of Washington, Seattle, Wash.

APRIL 27

HUDSON-MOHAWK Section. Rensselaer Polytechnic Institute, Troy, N. Y. Dinner: 7:00 P.M. Talk: 8:00 P.M. "Piezoresistive Strain Gages," by Dr. W. P. Mason, Bell Telephone Laboratories, Murray Hill, N. J.

EDITOR'S NOTE: Notices to be published in any one issue must reach SESA headquarters prior to the 15th of the second previous month. Give full information concerning date, time, place, topic and speaker for each meeting.

first part was presented by W. H. Bloedorn, research engineer, Chain Belt Co. The technical discussion dealt with the present system of dynamic load recording and pointed out limitations in that system which led to the development of the load peak counter.

The second portion of the program was given by Prof. T. I. Lyon, associate professor, Electrical Engineering, Milwaukee School of Engineering. Professor Lyon described the functional operation of the load-peak counter and described the main features embodied in its design. There followed a demonstration of the operation of the instrument.

The group then assembled for dinner in the company cafeteria. The third technical presentation of the evening followed. This was presented by W. F. Hofmeister, chief metallurgist, Chain Belt Co. Mr. Hofmeister's talk was entitled "The Cumulative Fatigue Damage Concept." This discussion showed how the dynamic load information once obtained, is used in predicting chain life.

The technical presentation was attended by 77 persons.

(Report and photograph by W. H. Bloedorn for the Milwaukee Section)

Effects of Vibration on Man

The January meeting of the Milwaukee Section was held at the ESM building on Jan. 12, 1961. Twenty-eight members were present.

The business meeting was brief out of consideration for the guest speaker. A proposal by the ESM to form an affiliate board won the SESA chapters' approval by voice vote. It was announced that the next meeting is scheduled for Thursday, March 16th. The speaker will be an engineer from Baldwin who will speak on "New Developments in Strain Gage Techniques."

Richard J. Hornick, Chief Research Psychologist, Bostrom Corp., spoke on the "Effects of Vibration on Man." He described some of the work being done by Bostrom and others to study the relationship of man to his environment, expecially when that environment is sharing.

Dr. Hornick pointed out that while people have been studied by sociologists and machines have been studied by engineers, it has only been since World War II that the man-machine has been studied to get optimum performance out of the pair.

Some of the factors which have been tested are:

1. Reaction Time—not affected by vibration during the test, but increased afterward.
2. Constant Foot Pressure—poor at the natural frequency of the body, $5^1/_2$ to $6^1/_2$ cps up and down, or $1^1/_2$ to 2 cps sideways. Affected by intensity of vibration.
3. Peripheral Vision—worst at the transverse natural frequency, affected by almost any intensity, but which strangely appears to be improved afterward.
4. Visual Acuity—mixed data, no conclusions.
5. Balance—not affected.
6. Blood Pressure—differs greatly with individuals, but shows immediate recovery after the vibration stops.
7. Disposition — severe vibration makes the subjects irritable during the test and for a few minutes afterward.
8. Body Position—even though acceleration can be withstood best when lying flat on the back, this is not the best position for vibration.
9. Physiological Damage—extreme vibration tests on monkeys show that breathing, coordination and jumping ability is affected, and death can result.

(Reported by Donald Niles for Milwaukee Section)

CHAIRMEN PLAN SESA 1961 SPRING MEETING

Committee chairmen express satisfaction over program format for the SESA 1961 Spring Meeting. The Delaware Valley members who met on January 3rd at Frank Tatnall's farmhouse are: (seated l. to r.) S. W. Sennet, general chairman; R. L. Stiles, plant tours; H. Cook, publications and membership; H. M. Owens, technical sessions; (standing) R. J. Stone, seminar; L. B. Moffett, assistant chairman; B. Sutton, general arrangements; J. E. Scott, banquet; Frank Tatnall, adviser

PLANT TOUR BY DELAWARE VALLEY

Members of the Delaware Valley Chapter form an interested audience during one of the live demonstrations at the Budd Co., Instruments Division on November 30th

MILWAUKEE GROUP AT CHAIN BELT PLANT

Members of the Milwaukee Section listen to Professor T. I. Lyon during their December 1st meeting held at Chain Belt Co. Plant

New York Metropolitan

Reduction of Resonance

First meeting of the 1960–61 season was held by the New York Metropolitan Section on November 23rd at the Hotel New Yorker. Following dinner, twelve members attended the meeting to hear a talk presented by Gerd Weissmann, member of the technical staff of the Bell Telephone Laboratories, Murray Hill, N. J. Mr. Weissmann's subject was, "Selection of Materials in Structures for the Reduction of Resonance." The talk was well illustrated with slides and the subject aroused considerable interest. Evidence of this was revealed in the lively one-and-a-half hour discussion period that followed.

(Reported by S. Black for N.Y. Metropolitan Section)

New Section Planned

The first meeting of the "Great Salt Lake" group was held Dec. 2, 1960, at the University of Utah in Salt Lake City. There were 23 in attendance at the time plans were laid for organizing and securing the necessary national membership required to petition for a charter.

C. S. Barton of Brigham Young University presided as the contact member and George West of Thiokol Chemical introduced the speaker. A. Newman Ormond of Ormond Instrumentation Center of California spoke on "Static Testing—Opening the Door into Space."

(Reported by Cliff Barton for Great Salt Lake group)

Representatives in Organizing Areas for SESA Sections

Atlanta	Prof. J. P. Vidosic 2851 Buford Highway, N. E. Atlanta 6, Ga.
Japan	Dr. Makoto Kikukawa Faculty of Engineering Osaka University Miyakojima-ku Osaka, Japan

ENGINEERS

...STRESS Responsible position requiring aircraft transmission experience in the determination of applied loads and the performance of stress analysis to insure structural integrity.

...STRUCTURAL TEST Senior level position for a man with group leader capabilities. Heavy experience in structural and fatigue test programs. **Model Design** • • • Familiar with static and dynamic wind tunnel model design techniques (electric model motors, force measuring systems and remote control apparatus). **Instrumentation** • • • A responsible position requiring experience in instrumentation for wind tunnel testing or associated fields.

Each of these positions requires an appropriate academic degree plus directly related experience and offers an attractive salary. Suburban location ten miles from Philadelphia. Forward resume, including salary requirements, in complete confidence to:

F. J. Skahill
Technical Employment Administrator

VERTOL DIVISION BOEING
MORTON PENNSYLVANIA

BOUND VOLUMES OF PROCEEDINGS AVAILABLE

Still available are a number of bound volumes of the series **Proceedings of the Society for Experimental Stress Analysis.** Published twice yearly, these volumes comprise the technical papers presented at national meetings and contain the results and descriptions of analytical and experimental investigations, as well as discussions of technique and instrumentation studies.

Price per copy: $7.00 to nonmembers and $6.00 to members; plus postage. Copies may be ordered through the Society for Experimental Stress Analysis, 21 Bridge Square, Westport, Connecticut.

from the campus

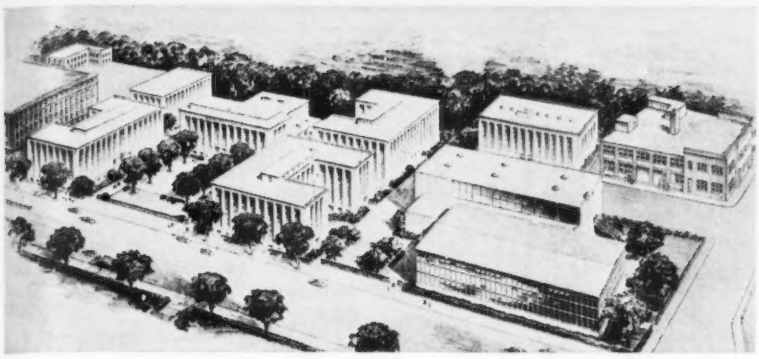

Northeastern University

NYU RESEARCH NEWS

The 1960 annual report of the Research Division of New York University, College of Engineering, contains several items of special significance in the field of experimental mechanics. Prepared under the direction of Dr. Harold K. Work, associate dean and director of the Division, the report mentions work under Dr. George Gerard, Herbert Tramposch and Professor Herbert D. Becker.

Dr. Gerard, during the past year and a half, has centered his attention on extending photothermoelastic techniques to three-dimensional problems. To accomplish this it was necessary to devise a new approach to the viewing of fringe patterns in large massive solids.

Herbert Tramposch developed a new sandwich technique that consisted of cementing a polariscope into the area of interest in a solid under investigation. The sandwich technique proved successful and is considered important in dealing with a number of thermal stress problems for which very few other experimental techniques are available.

Dr. Becker has been concerned with thermal stress analysis procedures in structures fabricated from corrugated sheets and with thermal stress in finite length rectangular plates and trimetallic strips. In the latter, a stress discontinuity has been observed. This condition is being investigated further.

Other work consists of studies of stresses at the intersection of a cone, a cylinder and a ring of a pressure vessel. To date, the simplest designs appear to develop the lowest stresses for configurations tested.

Dr. Gerard's group is also making experimental studies of the basic measure of ductility in regard to the manner in which ductility reduces stress-concentration factors. Another long-range study concerns the buckling of shell structures. Creep-buckling data on columns is being obtained by Ralph P. Papirno using precision techniques for the purpose of experimental evaluation of a number of different theories.

CORNELL ADOPTS NEW ENGINEERING CURRICULUM

All students entering the Cornell University College of Engineering in the fall of 1961 will be enrolled in a new Division of Basic Studies that will provide freshmen and sophomores with a program common to all engineering fields.

Continuing evaluation and development of the basic curriculum will be carried on by the Division in the future and coordination with upperclass programs, administrative procedures and operation of advising and counseling systems will be changed whenever necessary to keep abreast of the times.

Prof. Dale R. Corson, dean of the College of Engineering, said "A primary purpose of the change is to provide maximum opportunity for the student to become familiar with the range of professional programs available to him in the last three years of study in Cornell's five-year engineering program."

The student will be able to express a preference for one of the major fields on admission or during the following two years so that he can be assigned to appropriate advisers. He will not be committed to a particular field of engineering at the time of admission.

The courses in the two-year basic studies will include a strong concentration of work in mathematics, physics, chemistry, English and the fundamental engineering sciences. Special attention will be given to developing the concepts of engineering solutions through the application of the fundamental principles the student will be learning in his other courses.

A course on engineering methods and problems through which the student can become better acquainted with engineering and its various professional fields is expected to enable each student to develop a valid vocational objective.

Dean Corson pointed out that "In order to do this students must be trained on a broad base of fundamentals, and, at the same time their talents for the application of such fundamentals to solution of engineering problems must be developed."

Cornell broke from the traditional pattern of four-year engineering education in 1946 when all of its engineering curricula were extended to five years. This lengthened period of education for engineers provides the flexibility for the new basic studies program.

PLANS RESEARCH ON EFFECT OF CAVITATION

Prof. Ronald S. Brand, of the University of Connecticut, Department of Mechanical Engineering, has received a $11,500 one-year contract from the U. S. Navy to conduct research on the pressure waves radiated by a collapsing cavity from ship-propellor blades.

According to Professor Brand, the study, which is part of the Bureau of Ships' fundamental hydromechanics research program, will be mathematical. His primary tool will be the computers at Massachusetts Institute of Technology.

MARQUETTE MEASURES PROGRESS

A sharp increase in advanced degrees and published research provides a measure of the progress being made in the College of Engineering's faculty development program at Marquette University, Milwaukee, Wis. When Dean A. Bernard Drought outlined his objectives in 1956, three members of the engineering faculty had the doctor of philosophy degree, 18 faculty members had master's degrees and 21 teachers (nearly 50%), the bachelor's degree.

This fall, the total number of full-time faculty members is constant although there are now 12 graduate assistants where there was none in 1956. The significant change, however, is in the number of advanced degrees held by faculty members. There are now 17 men who have the Ph.D. or are writing a final dissertation. The number teaching with only the bachelor's degree has been reduced to seven, and 20 have the master's degree.

BIBLIOGRAPHY THREE-DIMENSIONAL PHOTOELASTICITY 1949–1959

Compiled by
Maurice H. Smith and Mary Lee

Continued from page 32A of February 1961 issue of Experimental Mechanics

PUBLISHED PAPERS AND RESEARCH REPORTS

Frocht, M. M. and Hill, H. N.
Stress - concentration factors around a central circular hole in a plate loaded through pin in the hole. ASME *Transactions*, v. 62, 1940, pp. A-5-9. (*Journal of Applied Mechanics.*)

Gerard, G., and Gilbert, A. C.
Photothermoelasticity: Exploratory Study. *Journal of Applied Mechanics*, v. 24, No. 3, September 1947, pp. 355–360.

Ghaswala, S. K.
Elements of the theory of photoelasticity. *Civil Engineering*, London, v. 45, No. 524, February 1950, pp. 107–109.

Gibson, J. E.
Stress distribution under foundations. *Engineering*, v. 180, No. 4680, October 1955, pp. 507–510.

Golubovic, G.
Different applications of photoelastic layers in the structural field. Translated from the French by M. H. S. Brown. *Gt. Brit. Royal Aircraft Establishment. Library Translation* No. 838, September 1959, 17 pp. (ASTIA AD 230,061.)

Hartman, J. B., and Leven, M. M.
Factors of stress concentration for the bending case of fillets in flat bars and shafts with central enlarged section. *Society for Experimental Stress Analysis. Proceedings*, v. 9, No. 1, 1951, pp. 53–62.

Helenelund, K. W.
Spannungsoptiken–en hjalpvetenskap for konstruktoren. *Tekniska Foreningens i Finland—Forhandlingar.*, v. 70, No. 8, August 1950, pp. 142–145.

Hetenyi, M.
The fundamentals of three-dimensional photoelasticity. *Journal of Applied Mechanics*, v. 5, December 1938, pp. 149–155.

Heywood, R. B.
Modern applications of photoelasticity. *Institution of Mechanical Engineers. Proceedings*, v. 158, No. 2, 1948, pp. 235–40; (discussion) 240–250, 8 supp. plates.

Hickson, V. M.
Errors in stress determination at free boundaries of "Frozen Stress" photoelastic models. *British Journal of Applied Physics*, vol. 3, No. 6, June 1952, pp. 176–181.

Hickson, V. M.
Photoelastic determination of free boundary stresses on frozen stress models by an oblique incidence method. *British Journal of Applied Physics*, v. 2, No. 9, September 1951, pp. 261–269.

Hiltscher, T.
Theorie und Anwendung der Spannungsoptik im elastoplastichen Gebiet. *VDI Zeitschrift*, v. 97, Jan. 11, 1955, pp. 49–58.

Hiltscher, R.
Photoelastic apparatus for research and industrial Laboratories. (In German.) *Instruments and Measurements Conference. Stockholm*, 1952, *Transactions*, 7 pp.

Ito, K.
On new materials for three-dimensional freezing photoelasticity and their application. (In Japanese.) *Scientific Research Institute. Reports*, v. 30, No. 4, July 1954, pp. 233–248.

Jessop, H. T., Snell, C., and Holister, G. S.
Photoelastic investigation on plates with single interference—fit pins with load applied (*a*) to pin only and (*b*) to pin and plate simultaneously. *Aeronautical Quarterly*, v. 9, May 1958, pp. 147–163.

Jessop, H. T.
A tilting stage method for three-dimensional photoelastic investigations. *British Journal of Applied Physics*, v. 8, No. 1, January 1957, pp. 30–32.

Jessop, H. T., and Stableford, W. H.
A method of correcting for initial stresses in frozen-stress observations. *British Journal of Applied Physics*, vol. 4, No. 9, September 1953, pp. 281–283.

Jessop, H. T.
Scope and limitation of photoelastic method of stress analysis. *Royal Aeronautical Society Journal*, v. 57, No. 507, March 1953, pp. 125–132; (discussion) pp. 132–140.

Jessop, H. T., and Snell, C.
Photoelasticity and aircraft design. *Aeronautical Quarterly*, v. 3, November 1951, pp. 161–172.

Jessop, H. T.
The scattered light method of exploration of stresses in two- and three-dimensional models. *British Journal of Applied Physics*, v. 2, No. 9, September 1951, pp. 249–260.

Jessop, H. T., and Wells, M. K.
The determination of the principal stress differences at a point in three-dimensional photoelastic model. *British Journal of Applied Physics*, v. 1, No. 7, July 1950, pp. 184–189.

Jessop, H. T.
The determination of the separate stresses in three-dimensional stress investigations by the frozen method. *Journal of Scientific Instruments*, v. 26, January 1949, pp. 27–31.

Johnson, R. C.
Three - dimensional photoelastic analysis of shafts in pure torsion and a comparison with results from relaxation. *Society for Experimental Stress Analysis. Proceedings*, v. 13, No. 2, 1956, pp. 107–118.

(*Continued next month*)

Based on Literature Search No. 17 published in April 1960 by the The James Forrestal Research Center Library, Princeton University, Princeton, N. J.

STRAIN GAGE INSTRUMENTS

NEW

BA-3 BAM-1 without large meter. In a case which racks 6 in an $8^3/_4$" x 19" panel. Or makes a neat package for individual use. Has own batteries. DC system—dc to 20,000 cps flat. Drives tape recorders and scopes directly. —$600

A-2 Output amplifier. Same case as BA-3. Own batteries. DC to 10,000 cps flat. Gain 2-20. Drives all galvos. Max. output ±60 ma into 50 ohms. Designed to be driven by BA-3, BAM-1, BAM-3. —$400

BA-3

A-2

REGULARS

BAM-1 General purpose box. Static on own meter. Dynamic with 'scope. DC bridge, dc transistor amplifier, 2 or 4 arm bridge. Battery operated. Low amplifier noise and drift. Frequency dc to 20,000 cps. Differential input cancels hum. —$525

B-1 Bridge. No amplifier. Operates off 115v 60 cycle line. 100 volts at 75 ma. max dc bridge power. 1% regulation. Line noise satisfactory on static indicators, differential input oscilloscopes and floating galvos. Not satisfactory on single sided scopes. Frequency dc to 20,000 cps. —$425

BA-12 Monitors fatigue tests. "Dynamic null balance" system gives wheatstone bridge accuracy to measurement of steady state dynamic signals including dc offset. Uses 'scope as indicator. 5 to 20,000 cps. —$650

BSG-6 6 channel switch and balance. Bridge power attenuation on each channel. 1, 2 or 4 external bridge arms. Any compensating gage can be connected into one or more channels. —$350

BSG-20 20 channel switch and balance. $8^3/_4$" x 19" rack panel size. —$900

BAM-1

B-1

BSG-6

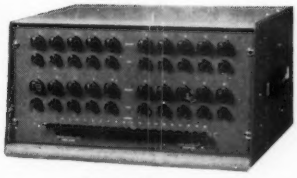

BSG-20

COMING

BA-13 New version of BA-12. Transistor amplifier. Frequency 1 to 20,000 cps. Variable SPREAD pot as well as fixed values. MEASURE zero at end of dial with + − switch. BAM-1 case. —around $800

BAM-3 Transducer box. Similar to BAM-1 but with minimum confusion of controls. 4 arm bridges only. Zero left meter. Definite ranges selected by switch. 'Scope connection. Frequency dc to 10,000 cps. —around $500

ELLIS ASSOCIATES

67 Lincoln Avenue, Pelham, New York • Telephone 914-PE 8-3360

SALES REPRESENTATIVES

Michigan
S. Sterling Company
15310 W. McNichols Rd.
Detroit 35, Michigan
Broadway 3-2900

Ohio
S. Sterling Company
5827 Mayfield Road
Cleveland 24, Ohio
Hillcrest 2-8080

Indiana
Pivan Engineering Co.
10302 N. College Ave.
Indianapolis 20, Ind.
Victor 6-1532

Illinois, Wisconsin
Pivan Engineering Company
3542 W. Peterson Avenue
Chicago 45, Illinois
Keystone 9-4838

Canada
Tatnall Measuring & Nuclear Systems Ltd.
17 Donway West
Don Mills, Ontario
Plymouth 5-5122

All other areas—Write or phone collect to home office.

For details, circle No. 7 on Reader Information Card

Sources of information on

STRAIN GAGES

STRAIN GAGE TECHNIQUES

by W. M. Murray & P. K. Stein

A comprehensive reference book on basic theory and experiments

669 pages, 8½ x 11, cloth bound, photo-offset from typewritten copy

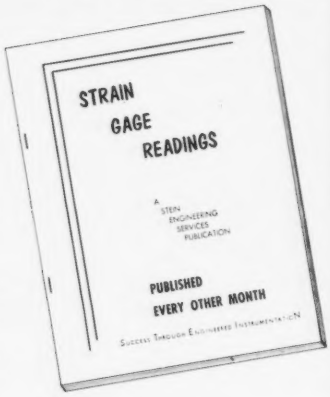

STRAIN GAGE READINGS

P. K. Stein, Editor

A bi-monthly journal devoted to new applications and techniques and reviews of current literature

THE STRAIN GAGE INSTRUCTOR

Aluminum stand and cantilever beam with mounted strain gages

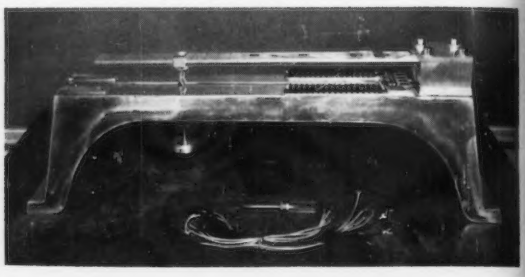

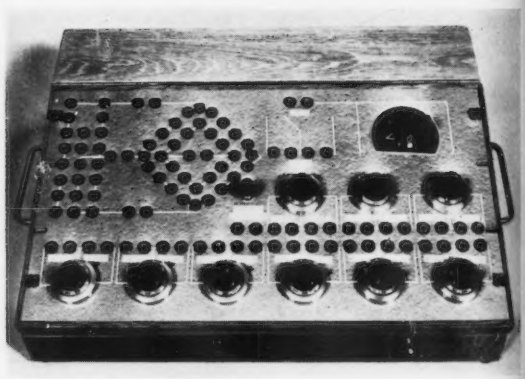

Plug board for strain gage & instrumentation circuits

EXPERIMENTAL EQUIPMENT

for demonstrating the theory and performing the laboratory experiments which are described in STRAIN GAGE TECHNIQUES and STRAIN GAGE READINGS
Available from

Stein Engineering Services, Inc.

5602 East Monte Rosa, Phoenix, Arizona

Write for prices and particulars

For details, circle No. 8 on Reader Information Card